PhD Thesis:
Control issues in oxy-fuel combustion

Dagfinn Snarheim*
Department of Engineering Cybernetics
The Norwegian University of Science and Technology

August 12, 2009

*Not original title page

Summary

Combustion of fossil fuels is the major energy source in todays society. While the use of fossil fuels is a necessity for our society to function, there has been an increasing concern on the emissions of CO_2 resulting from human activities. Emissions of CO_2 are considered to be the main cause for the global warming and climate changes we have experienced in recent years. To fight the climate changes, the emissions of CO_2 must be reduced in a timely fashion. Strategies to achieve this include switching to less carbon intensive fuels, renewable energy sources, nuclear energy and combustion with CO_2 capture.

The use of oxy-fuel combustion is among the alternative post- and pre-combustion capture concepts, a strategy to achieve power production from fossil fuels with CO_2 capture. In an oxy-fuel process, the fuel is burned in a mixture of oxygen and CO_2 (or steam), leaving the exhaust consisting mainly of CO_2 and steam. The steam can be removed by use of a condenser, leaving (almost) pure CO_2 ready to be captured. The downside to CO_2 capture is that it is expensive, both in capital cost of extra equipment, and in operation as it costs energy to capture the CO_2. Thus it is important to maximize the efficiency in such plants.

One attractive concept to achieve CO_2 capture by use of oxy-fuel, is a semi-closed oxy-fuel gas turbine cycle. The dynamics of such a plant are highly integrated, involving energy and mass recycle, and optimizing efficiency might lead to operational (control) challenges. In these thesis we investigate how such a power cycle should be controlled. By looking at control at such an early stage in the design phase, it is possible to find control

solutions otherwise not feasible, that leads to better overall performance. Optimization is used on a nonlinear model based on first principles, to compare different control structures. Then, closed loop simulations using MPC, are used to validate that the control structures are feasible. It is found that compared to a conventional gas turbine cycle, it is possible to change loads much faster. And if the right control structure is applied, it is possible to operate at part load with just a small loss in overall efficiency.

A central part in all gas turbines is the combustion chamber. It is well known that thermoacoustic instabilities can be a problem in combustion chambers, leading to large high frequency (up to several hundred Hz) pressure oscillations. Such pressure oscillations are unwanted, but their amplitude can be reduced by use of active control. The control problem is however challenging, due to the high frequencies involved. Experimental results have shown that the same problem is inherent to oxy-fuel combustion, possibly the instabilities are even worse.

In the thesis we present results on stabilization of a conventional combustion chamber by use of feed-forward microjet air injection. A look-up table is necessary to stabilize the process in this way, and the solution is not very robust. The use of feedback could probably improve the results.

To study thermoacoustic instabilities and control for oxy-fuel combustion, we developed a linear low order model of oxy-fuel combustion. The model is based on a modal discretization of the wave equation, combined with a flame model based on heat release from a thin wrinkled flame. Analysis on the model shows that injection of CO_2 is a promising actuator to stabilize the instabilities. The CO_2 should however be injected somewhere upstream of the flame, to allow the injected CO_2 to mix with the reactants before burning. Although the resulting time delay is small, it is a problem because of the high frequencies involved. We use a frequency domain method to include the time delay in the control analysis of a simple linear combustion model. An extension to the method is proposed and used to find a set of stabilizing controller parameters, and to analyze robustness of the controlled process. Extensive closed loop simulations on an advanced combustion simulator shows that the applied analysis is relevant, and provides useful information about how an oxy-fuel process should be controlled.

Preface

This thesis is submitted in partial fulfillment of the requirements for the degree Ph.D. at the Norwegian University of Science and Technology (NTNU), Department of Engineering Cybernetics. It is based on research done in the period August 2004 through April 2009, under the guidance of Professor Bjarne A. Foss and co-supervisor Dr. Ing. Lars Imsland. The research is funded by the Norwegian Research Council Strategic University Program: Process Systems Engineering - From Natural Gas to Energy Products, through the Gas Technology Center NTNU-SINTEF. Funds from SINTEF via the NFR BIGCO2 project are also acknowledged.

There are many people who deserves attention for their contribution to this research. I am grateful to my supervisor Professor Bjarne Foss, for the support and encouragement during my doctoral studies. His ability to make me see the larger picture and point out directions for the research, when I was stuck with details, has been very useful. My co-supervisor Lars Imsland also deserves attention. He has been helping me with everything from implementation to proof reading, and his general knowledge about control theory is impressive. I am thankful that he continued as a supervisor, even after changing job twice.

Further, I would like to thank Professor Ahmed F. Ghoniem for inviting me to the Reacting Gas Dynamics Laboratory at Massachusetts Institute of Technology. The work with a real combustion rig gave me valuable experience and knowledge. I also want to thank two of his Ph.D. students, Murat Altay and Ray Speth, for their way to make me a part of their group, and making the lab-work enjoyable.

Nils E. Haugen (Sintef Energy Research) deserves attention for writing the SINMA code and sharing it with me, and for all the useful discussions on the simulation results.

I want to thank my fellow PhD-students at the Department of Engineering Cybernetics for making a nice environment to do research. Especially Svein and Johannes for the coffee breaks and interesting discussions. The secretarial staff; Tove, Unni and Eva are appreciated for handling the administrative issues that arose during the PhD study.

Finally, I want to thank my girlfriend, Eirill, for all her love and support.

Contents

Chapter 1

Introduction

1.1 Motivation

Global warming and climate changes have received much attention in recent years. There is a broad consensus that the increase in CO_2 emissions is directly related to the climate changes we experience today. About 80% of the CO_2 emissions resulting from human activities are linked to the energy sector, IEA (2007b), and are mostly related to combustion of fossil fuels. As the world energy demand is increasing, it is a formidable task to achieve a reduction in CO_2 emissions. Alternatives to reduce CO_2 emissions from the energy sector includes switching to less carbon intensive fuels, renewable energy sources, nuclear energy and combustion of fossil fuels with CO_2 capture. However, to achieve a reduction within a reasonable timeframe, it is necessary to pursue several or all of these alternatives simultanously.

When it comes to CO_2 capture there are three main concepts to achieve this (Bolland and Undrum, 2003): Post combustion removal, pre combustion removal and oxy-fuel. Research and development is intense for all three concepts. Hence, studying control issues in oxy-fuel combustion makes sense as part of this larger effort. The oxy-fuel concept is based on that the burning of fossil fuels with pure oxygen will leave the exhaust consisting of mainly CO_2 and water. The water can easily be removed, leaving (almost)

pure CO_2 ready to be captured and stored. Among several alternatives for oxy-fuel combustion, one attractive concept is based on a semi-closed gas turbine cycle using CO_2 as a working medium. The concept is based on combustion of natural gas with O_2 in an (inert) CO_2 atmosphere. Some of the exhaust (CO_2) is recycled to reduce temperatures in the combustion chamber, while the rest is removed for storage. This mass and energy recycle creates interesting and challenging dynamics. By looking at the interplay between process design and control, one might find control solutions that results in better performance and overall power plant efficiency.

If one considers the combustion chamber alone, there exist dynamics on a much faster timescale. A phenomenon caused by coupling between the flame in the combustor and acoustics within the combustion chamber, can cause large high frequency (typically several hundred Hz) pressure oscillations. This is usually referred to as thermoacoustic instability, and is a well known problem for conventional combustion chambers. Obvious implications of these instabilities are vibrations and mechanical stress that might lead to structural damage and system failure. Alleviating the oscillations might allow for better energy utilization and less pollutant emissions.

When it comes to oxy-fuel, the literature on these instabilities is scarce. However, experimental results on a laboratory scale oxy-fuel combustion chamber published by Ditaranto and Hals (2006), indicates that similar instabilities occur in oxy-fuel combustion, possibly even more severe than in the conventional case. For conventional combustion chambers, it has been shown that the use of active control can reduce the pressure oscillations significantly, and herein we will work towards achieving the same for oxy-fuel combustion.

1.2 Contribution

The contributions of these thesis are:

Chapter 3 Control analysis on a nonlinear model of a semiclosed oxy-fuel gas turbine cycle.

- Offline optimization including constraints is used to compare power plant efficiency when operating at part load for four alternative control structures.
- Closed loop simulations using a MPC controller show that the control structures are feasible

Chapter 4 Experimental results on a conventional laboratory scale combustion chamber.

- Stabilization of thermoacoustic instabilities using micro-jet air injection.

The author of this thesis is not the first author of the paper in this chapter. Hence, there is a need to clarify his part in this work. The writer took part in rebuilding the lab for the new experiments. Especially in connecting new measurement devices and actuators, programming interfaces between actuators, measurement devices and Matlab, and programming a GUI to control the whole experiment from Matlab. The writer also took part in running the experiments and gathering data, and was responsible for presentation of the data (i.e creating figures for the paper).

Chapter 5 Modeling of oxy-fuel combustion.

- Developed a low order linear model to study thermoacoustic instabilities for oxy-fuel combustion.
- Propose CO_2 injection as a promising actuator to stabilize an oxy-fuel combustion process based on control analysis on the model.

Chapter 6 and 7 Control of oxy-fuel combustion using pre-flame CO_2 injection.

- Applied a frequency domain based method to analyse stability in the presence of time-delay.

- Proposed an extension to the frequency domain method to analyse stability and robustness for different controller parameters and perturbations in model parameters.

- Performed extensive simulations on an advanced nonlinear combustion simulator to validate the relevance of the method.

1.3 List of papers

D. Snarheim, L. Imsland, R. Ulfsnes, O. Bolland, and B. Foss, "Control design for a gas turbine plant with CO_2 capture capabilities," in *Proc. 16th IFAC World Congress, Prague, Czech Republic*, 2005. Also in *Modeling, Identification and Control*, vol. 27, pp. 57-66, 2006.

D. Snarheim, L. Imsland, and B. Foss, "Control-relevant modelling and linear analysis of instabilities in oxy-fuel combustion," in *Proc. 9th European Control Conference ECC'07*, 2007.

D. Snarheim, L. Imsland and BA. Foss, "Active control of oxy-fuel combustion using preflame CO_2-injection," *Accepted for European Control Conference ECC'09*, 2009.

D. Snarheim, N. E. Haugen, L. Imsland, , and B. A. Foss, "Control design and stability analysis of oxy-fuel thermoacoustic instabilities," *Submitted to IEEE Trans. Control System Technology*, 2009.

L. Imsland, D. Snarheim, R. Ulfsnes, O. Bolland, and B. Foss, "Modeling and control of a O2/CO2 gas turbine cycle for CO2 capture," *Proceedings of DYCOPS 2004*, 2004.

L. Imsland, D. Snarheim, B. Foss, R. Ulfsnes, and O. Bolland, "Control issues in the design of a gas turbine cycle for CO_2 capture," *International Journal of Green Energy*, vol. 2, no. 2, 2005.

M. Altay, R. Speth, D. Snarheim, D. Hudgins, A. Ghoniem, and A. Annaswamy, "Impact of microjet actuation on stability of a backward-facing step combustor," *Proceedings of 45th AIAA Aerospace Sciences Meeting and Exhibit*, 2007.

A. Ghoniem, H. Altay, R. Speth, D. Snarheim, and A. Annaswamy, "Novel hydrocarbon-flame anchoring strategies using highly reactive fuels," in *Proceedings of the 19th ONR Propulsion Meeting*, 2006.

1.4 Structure

This thesis is written mainly as a collection of papers. Chapter 2, however, provides background material on CO_2 capture. Further it gives an introduction to combustion and combustion modelling, and the topics of thermoacoustic instabilities and how they can be controlled are discussed.

In Chapter 3, which is based on Snarheim et al. (2005), we study control design for a proposed oxy-fuel gas turbine cycle to achieve CO_2 capture. Offline optimization is used on a nonlinear dynamic model of a complete power plant to asses four different control structures. The modelling of the power plant was a part of the master thesis (Snarheim, 2004), and therefore Imsland et al. (2005) is included in the appendix to make the model available to the reader.

In Chapter 4 we present experimental results on a laboratory scale combustor. Air injection is used to stabilize the combustor. The design of a microjet allows air injection at a much higher flowrate, and the effectiveness of such an actuator is compared to injecting with a conventional air slot. This chapter is based on Altay et al. (2007).

Chapter 5 covers a linear low order model suitable for studying thermoacoustic instabilities in oxy-fuel combustion. The content was published in Snarheim et al. (2007).

Chapter 6, which is based on Snarheim et al. (2009b), presents a method to analyse stability for an oxy-fuel combustion process controlled by use of preflame CO_2 injection. Because the injector is located upstream of the

flame, there will be a time delay due to transport of the injected gas to the flame. The time-delay is critical and must be included in the analysis. The same method is applied in Chapter 7. However, the resulting control design is tested on an advanced combustion simulator to validate the relevance of the applied analysis. The latter chapter is based on Snarheim et al. (2009a).

Since the body of this thesis contains a collection of papers there will be some repetition between chapters, in particular Chapter 5-7.

Chapter 2

Background

This chapter aims at giving the reader a brief overview of oxy-fuel combustion processes, thermoacoustic instabilities and how they can be controlled. The study of oxy-fuel processes is mainly motivated by the possibility to achieve close to zero CO_2 emission. In Section 2.1 we explain why CO_2 capture is important and how it can be achieved. The section will also show that the combustion chamber is a small (but important) part of a rather large and complex system to produce energy from fossil fuels.

In the rest of this chapter we will mainly consider the combustion chamber. In combustion processes it is well known that self-sustained pressure oscillations can occur. This happens due to a phenomena called thermoacoustic instabilities, which is the topic of Section 2.2.1. Modelling of combustion processes is an important topic, both to better understand and analyze thermoacoustic instabilities and for use in a model-based controller. This is the topic in Section 2.2.2. Section 2.3 is about how thermoacoustic instabilities can be controlled.

2.1 CO_2-capture

In IPCC (2005) we find the following statement: 'Emissions of CO_2 due to fossil fuel burning are virtually certain to be the dominant influence of the

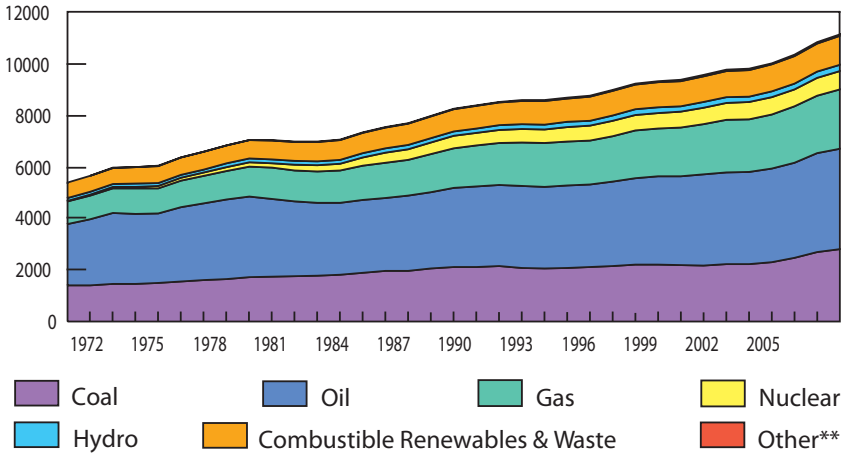

Figure 2.1: World energy usage based on different types of fuel (Mtoe) (IEA, 2007a).

trends in atmospheric CO_2 concentration during the 21st century.' CO_2 is considered to be the greenhouse gas that makes the largest contribution from human activities. With the ongoing debate on global warming and climate changes there is a clear incentive to investigate strategies to reduce the emissions of CO_2 to the atmosphere. One way to achieve this is to remove CO_2 from exhaust gases and store it away from the atmosphere, i.e CO_2-capture and sequestration.

Figure 2.1 shows how the world energy usage has been increasing in the last decades. As most of the energy is produced from fossil fuels, this also causes an increase in emissions. This can be seen clearly in Figure 2.2. According to IPCC (2005), the average yearly growth in CO_2 emissions during the period 1995-2001 was 1.4%, a number that was higher than

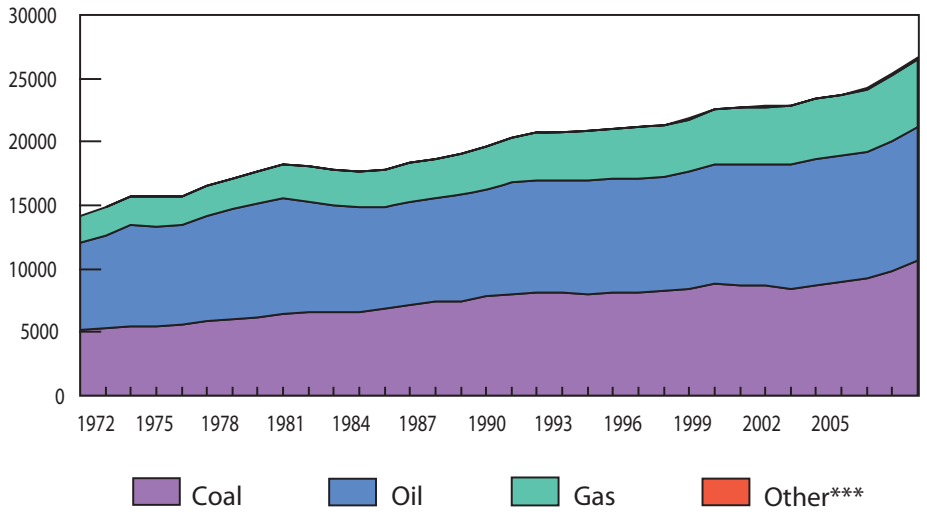

Figure 2.2: World CO_2 emissions from different fuels (Mt of CO_2) (IEA, 2007a).

the five year period before that. And from the figure, it seems like the growth has been even bigger in the last five years. To see what can be done to achieve a reduction in CO_2 emissions, it is useful to obtain an understanding of the major factors influencing CO_2 emissions. In (Kaya, 1995) the following relations is given for the total world CO_2 emissions;

$$CO_2 \text{ emissions} = \text{population} \times \left(\frac{\text{GDP}}{\text{Population}}\right) \times \left(\frac{\text{Energy}}{\text{GDP}}\right) \times \left(\frac{\text{Emissions}}{\text{Energy}}\right)$$

This means that the emissions are proportional to the population, the global wealth, the energy intensity of the global wealth and the emissions arising from production of energy. Both population and global wealth are increasing at the moment. Thus to achieve a reduction in CO_2 emissions we need to reduce the energy intensity and/or the emissions/energy ratio. As

two of the factors are increasing, the reductions will need to be significant. CO_2-capture from energy production using fossil fuels is one way to reduce the emissions/energy ratio. Other viable alternatives include switching to less carbon intensive fuels (for example gas instead of coal), renewable energy sources or nuclear energy.

In the literature CO_2-capture will often be referred to as CCS (Carbon Capture and Storage). When considering combustion of fossil fuels, it means that we need to separate the CO_2 from other gases and store it somewhere away from the atmosphere.

While capture of CO_2 is possible for all types of combustion, it is only considered to be viable for large power (or industrial) plants. To capture CO_2 from for instance a car engine would be very expensive, and it would also be a major problem to gather all the captured CO_2 and transport it for storage. Figure 2.3 shows four different concepts to achieve CO_2 capture. One is an industrial plant where CO_2 is separated from the flue gases in the process. The other examples are power plants, for which there are three different concepts; post combustion, pre combustion and oxy-fuel. These concepts will be discussed in more detail below. What all concepts have in common is the handling of the captured CO_2. To be able to transport the CO_2 it should be compressed to reduce its volume. Several options are available as storage sites, but only deep ocean and large geological formations are considered to be large enough to handle the required quantities. Depleted oil and gas fields have been suggested as a promising storage place. Here wells are already drilled, and equipment for injection of CO_2 to the underground will in many cases be available. Oil wells are especially attractive because injection of CO_2 can lead to increased oil recovery, such that the cost of storage can be reduced.

2.1.1 Post combustion capture

In IPCC (2005) post combustion capture is defined as; 'Capture of CO_2 from flue gases produced by combustion of fossil fuels and biomass in air'. After the combustion process, the exhaust gas passes through equipment which separates out most of the CO_2. An advantage is that one can use

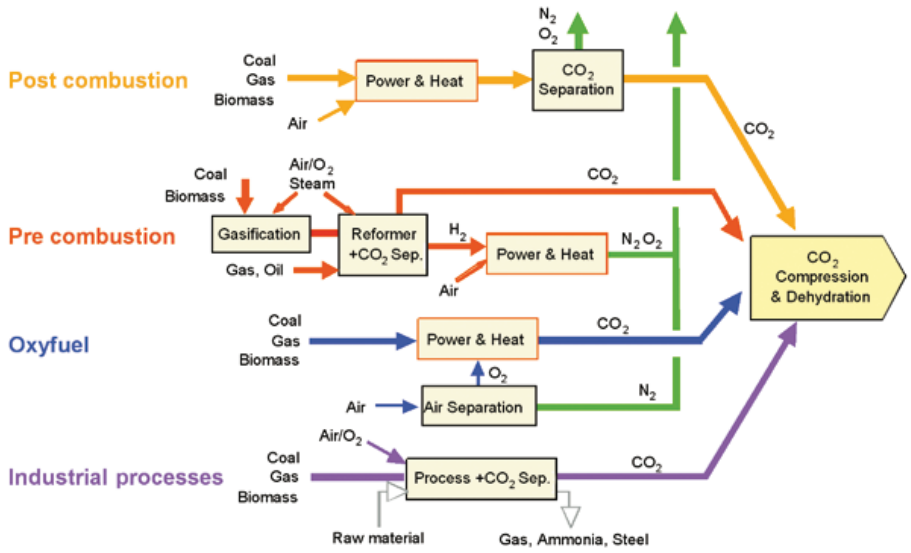

Figure 2.3: CO_2-capture systems (IPCC, 2005).

an existing power plant and just add a CO_2 separation unit. Technology for separation of CO_2 from exhaust gases is commercially available, and absorption processes based on chemical solvents, usually amines, are considered to be most promising. In practice one can capture between 80-95% of the CO_2 using this technology. The exact number is an economical trade off, as a high capture percentage leads to a more expensive separation unit and more energy usage. For large high efficiency gas turbines, a challenge is that the CO_2 concentration in the exhaust is low. Hence, the post combustion capture unit must treat large gas quantities which adds substantially to costs.

There are many planned CO_2 capture pilot plants, and the Carbon Dioxide Capture and Storage Projects Database (MIT, 2009) is a good starting point to get an overview. In Pleasant Praire (US) a post combustion

CO_2 capture pilot plant has been in operation since 2008. The power plant is a 5 MW coal plant, and results are available in Kozak et al. (2009). A pilot plant for CO_2 capture from pressurized exhaust gases has also been built close to Stockholm (Sweden). According to Bryngelsson and Westermark (2009) the pilot tests have been sucessful, and a CO_2 capture efficiency larger than 98% was obtained.

2.1.2 Pre combustion capture

In a pre combustion capture process, one aims at removing the carbon from the fuel before combustion. This is possible for both coal and natural gas powered plants. One way to achieve this is to use a pre-reformer to create a mixture of hydrogen and carbon monoxide (syngas) from the natural gas. Then the carbon monoxide can be converted to CO_2 by use of either steam or oxygen, and afterward removed for storage. The resulting hydrogen rich fuel can then be used in a power plant with very low emissions of CO_2.

GreenGen (2009) is building a 250 MW coal fired pilot plant, and operation is planned to start in 2009.

2.1.3 Oxy-fuel

As oxy-fuel combustion is an important topic in this thesis, it will be given a more detailed description than the previous concepts. Oxy-fuel refers to burning fossil fuels in either pure oxygen or a mixture of oxygen and a CO_2 rich recycled gas. The idea behind the oxy-fuel concept is that when the fuel burns in a mixture without nitrogen, the exhaust gas will consist mainly of CO_2 and steam as shown below

$$CH_4 + 2O_2 = 2H_2O + CO_2.$$

The steam can be removed in a condenser, and the resulting exhaust can be removed for storage. Burning fuel in pure oxygen results in a very high temperature (about 3500 °C). In a typical gas turbine, the temperature is limited to about 1300-1400°C. Therefore, part of the CO_2 rich flue gas is usually recycled to cool the combustion process. An advantage of the

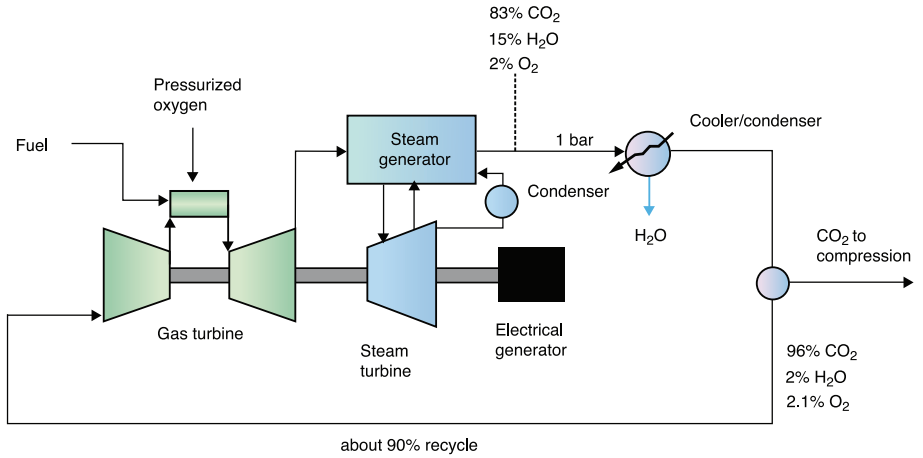

Figure 2.4: Principle of the oxy-fuel combined cycle gas turbine cycle (IPCC, 2005).

oxy-fuel concept is that almost 100% of the CO_2 is captured. Also, because only small amounts of nitrogen will enter the combustion chamber, the formation of NO_x will be smaller than for the other alternatives. The main drawback is that separation of oxygen is expensive, and will according to Bolland and Undrum (2003) reduce the efficiency of the power plant by 12%. However, 3-4% of the energy losses are recovered because the oxygen enters the combustion chamber at an elevated temperature and pressure. Hence, overall efficiency is reduced about 8%.

Figure 2.4 shows the principle of an oxy-fuel combined cycle gas turbine. A similar gas turbine cycle will be discussed in Chapter 3, where the focus is how power, temperatures and exhaust gas should be controlled.

Although the separation process (oxygen from air) is available technology, most of the required technology for building an oxy-fuel power plant is not commercially available. For a gas turbine, the change in working fluid

from air to CO_2 rich gas results in a number of changes in properties that are of importance for the design of the compressor, combustor and the hot gas path including the turbine. These changes have a significant impact on gas turbine components, requiring a completely new design of compressors, combustors and hot gas path (IPCC, 2005). Power plants that use fuel to produce steam are easier to realize. In Germany, a 30 MW coal pilot plant have been in operation since 2008, and results are published in (Strømberg et al., 2009). A 30 MW coal pilot plant is also under construction in Australia, with a planned start-up in 2010 (Cook, 2009). In southern France, a 30 MW pilot plant using heavy oil as feedstock, is built by Total. The plant is scheduled to start operation in 2009 (Aimard et al., 2008).

2.1.4 The cost of CO_2-capture

The capital cost of a power plant with CO_2 capture will be much higher than a conventional plant. In addition, more energy is required during operation. Figure 2.5 clearly shows the gains and losses by building CO_2 capture plants. CO_2 emissions are reduced significantly at the expense of increased energy use.

In Figure 2.6 the power generation efficiency is compared for different types of power plants with and without CO_2-capture. The figure is from IPCC (2005) and is based on design studies. The efficiencies are calculated with respect to the lower heating value (LHV) of the fuel used. In all the capture plants, between 85-90% of the CO_2 is captured, except for the oxy-fuel plants which have a capture percentage greater than 97%. The energy needed to compress the CO_2 to $110M$ Pa is included in the analysis. On top of this, there is the cost of transportation and storage of CO_2. It is clear that capture of CO_2 is expensive, and to make it commercially attractive, one must either increase the cost for CO_2 emissions, or improve CO_2 capture technology.

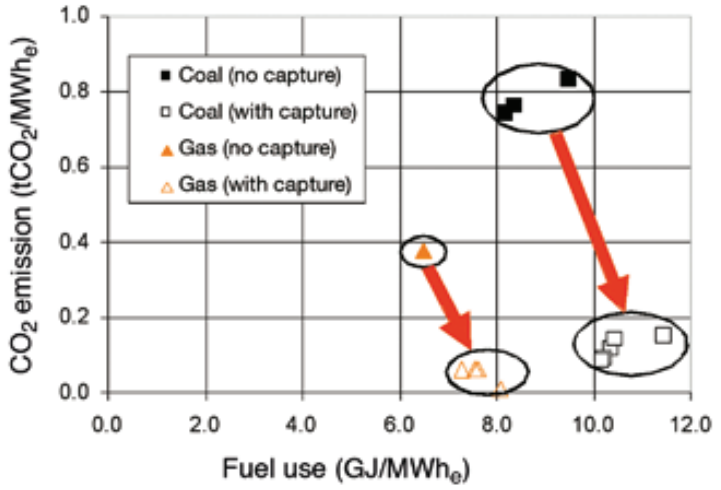

Figure 2.5: Fuel use for a reduction of CO_2 emissions using capture plants (IPCC, 2005).

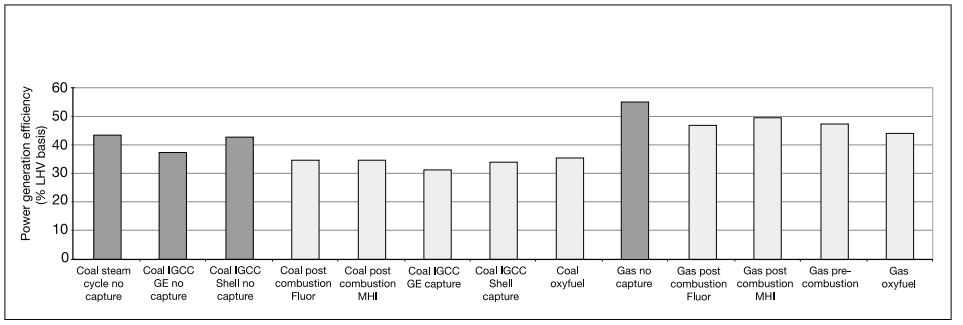

Figure 2.6: Thermal efficiency of power plants with and without CO_2-capture, IPCC (2005).

2.2 Combustion

Combustion is a central process in most peoples everyday life. For instance when you are driving a car, using a gas stove or creating a nice atmosphere by burning a candle. In addition, most of the electricity is produced from combustion of fossil fuels. It is an important process in industry, especially in metal production. Another use of combustion is to get rid of waste by incineration. It is clear that combustion is important in making our life easier, but there is a downside to combustion, pollution. Most combustibles contain hydrocarbons, leading to emissions of the greenhouse gas CO_2. Other pollutants, such as hydrocarbons and carbon monoxide are emitted as a consequence of bad or incomplete combustion (Ertesvåg, 2000). The combustibles can also contain other pollutants, for instance sulphur- and chlorine composition, and there are also emissions of nitrogen oxides, either as a result of reactions during the combustion, or as a pollution in the fuel.

In Turns (2000) combustion is defined as 'rapid oxidation generating heat, or both heat and light'. From this we see that combustion involves exothermic chemical reactions. Combustion can occur in either a flame or noflame mode. The flame mode is further categorized as either premixed flame or nonpremixed (diffusion) flame. In a premixed flame, the reactants are mixed at the molecular level, prior to the chemical reaction. This is the type of flame that is relevant when studying combustion in gas turbines. An example of a diffusion flame is a candle, where fuel and oxidizer is separated initially, and the reactions (and mixing) occur at the interface between fuel and oxidizer.

The combustion chamber is central when studying combustion. In experimental setups, the designs are usually quite simple. A sketch of the combustion chamber used in Ditaranto and Hals (2006) can be seen in Figure 2.7. The combustion chamber consists of a pre-mixing section, a burning section, and a section for the anchoring of the flame. Combustion chambers in for instance a gas turbine are more complex. Figure 2.8 shows a combustion chamber used in a GE (General Electrics) heavy duty gas turbine.

Combustion is a very broad topic, and the textbook (Turns, 2000) is a

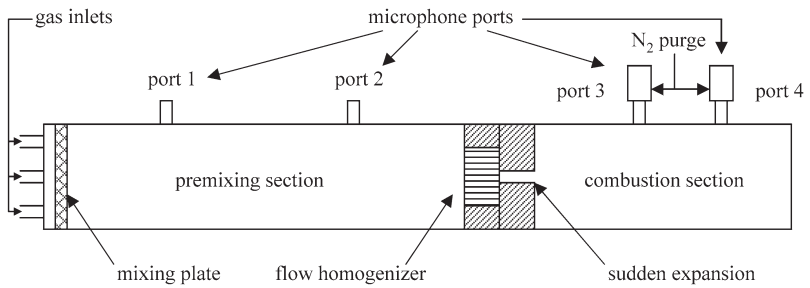

Figure 2.7: Sketch of the experimental setup used in Ditaranto and Hals (2006).

good starting point as an introduction to the field. In the remainder of this section we will concentrate on thermoacoustic instabilities and combustion modelling.

2.2.1 Thermoacoustic instabilities

Thermoacoustic instabilities can be a problem in continuous combustion systems. In this section we explain why thermoacoustic instabilities occur and the problems they can cause.

Thermoacoustic instabilities take the form of rather large pressure oscillations, typically oscillating with a frequency of several hundred Hz. Problems resulting from the instabilities include vibration and mechanical stress that may lead to structural damage and system failure. The oscillations may also cause problems for components downstream of the combustion chamber, for instance a turbine in a power plant.

The instabilities are caused by a dynamic coupling between flame dynamics and acoustics within the chamber. The velocity fluctuations associated with the acoustic waves within the combustion chamber alter the

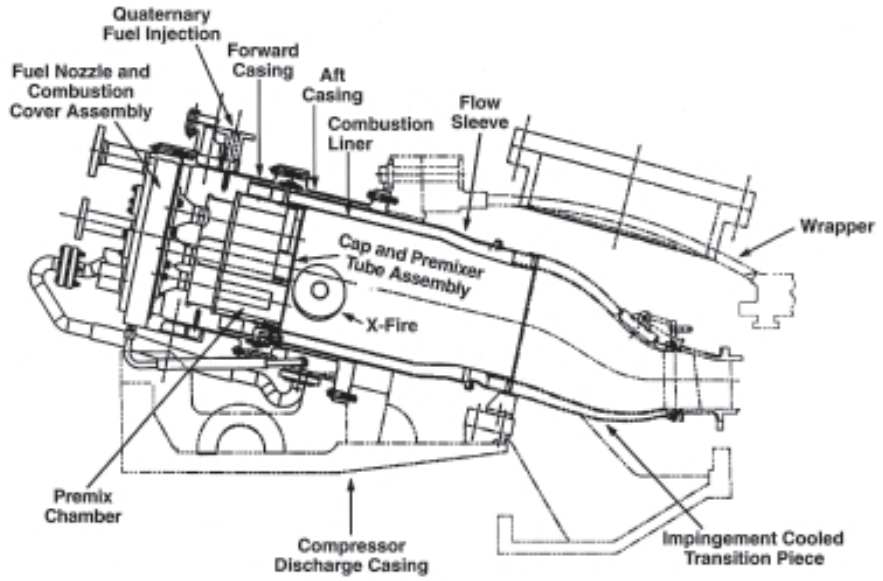

Figure 2.8: The DLN-2 combustion system for use in GE heavy duty gas turbines (Davis and Black, 2000).

heat release from the flame. At the same time the flame adds energy to the acoustics waves. Thus, they are coupled in a feedback loop (see Figure 2.9). The famous Rayleigh's criterion, dating back to 1878, states that when the heat-release rate from the combustion process is in phase with the pressure, the system is unstable, and when the heat-release rate is out of phase with the pressure, the system becomes stable (Rayleigh, 1878). In the unstable case, as long as the energy added by the flame exceeds acoustic losses at the outlet of the combustion chamber, the pressure oscillations will grow. At one point the acoustic losses equals the energy added by the flame, and the system continues to oscillate in a limit cycle.

Modern (conventional) premixed gas turbines have to operate at very

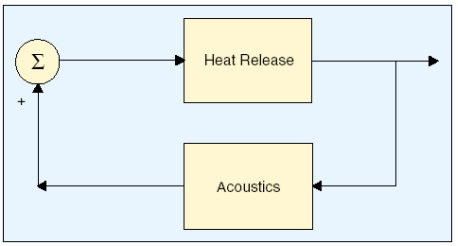

Figure 2.9: The heat-release and acoustics are coupled in a feedback loop, from Annaswamy and Ghoniem (2002).

lean conditions due stringent requirements on NO_x emissions. These operating conditions make the gas turbines prone to instabilities, and is an important reason for the attention thermoacoustic instabilities has received recently. This is also reflected in the numerous publications within the field in recent years. Reviews on thermoacoustic instabilities can be found in Annaswamy and Ghoniem (2002), Candel (2002), Dowling and Morgans (2005).

2.2.2 Combustion Modeling

Modelling of combustion systems is a very broad area. There is a large number of available models, and it is very important to choose a model which is suitable for the problem at hand. For instance, when studying how a flame interacts with a wall, another model is suitable than when studying how the composition of the gas varies across the flame surface. In both these cases however, the geometric scale is small and a detailed model is necessary.

In this section we will introduce the most commonly used models for studying pressure oscillations occurring from thermoacoustic instabilities. In general these are low order models, which focus on the coupling between heat-release and acoustics. To give the reader a basic understanding of combustion modelling, we will start by introducing the governing equations for reacting gas flows.

Governing equations for gas flow and kinetics

A combustion process can be described by the governing equations for a gas flow combined with kinetics. The governing equations for a gas flow include;

- Mass conservation (continuity)
- Mass conservation of the different species
- Conservation of moment
- Energy conservation

Together with chemical kinetics, they can form a model for the dynamics of a combustion process. The model presented herein is based on Turns (2000);

Mass conservation

$$\frac{dm}{dt} = \dot{m}_{in} - \dot{m}_{out}, \tag{2.1}$$

where $\dot{m}_{in}$ and $\dot{m}_{out}$ are mass flow rates in and out of a control volume.

Species conservation The general form of conservation of species A in a control volume, with inlet at x and outlet at $x + \Delta x$ (one dimensional case) is given by

$$\frac{dm_{A,cv}}{dt} = \left[\dot{m}_A'' A\right]_x - \left[\dot{m}_A'' A\right]_{x+\Delta x} + \dot{m}_A''' V, \tag{2.2}$$

where $\dot{m}_A''$ is the mass flux (mass flow pr area) and $\dot{m}_A''' V$ is the production or destruction of species A due to chemical reactions.

When species A and B are mixed in a control volume, Ficks law can be used for diffusion

$$\dot{m}_A'' = Y_A \left(\dot{m}_A'' + \dot{m}_B''\right) - \rho \mathcal{D}_{AB} \frac{dY_A}{dx}. \tag{2.3}$$

Y_A is the mass fraction of component A, ρ is the density of the mixture and $\mathcal{D}_{AB}$ is the diffusion coefficient between species A and B.

Combining (2.2) and (2.3) give

$$\frac{d(\rho Y_A)}{dt} = -\frac{\partial}{\partial x}\left[Y_A \dot{m}'' - \rho \mathcal{D}_{AB}\frac{dY_A}{dx}\right] + \dot{m}_A'''. \tag{2.4}$$

Momentum conservation A general one-dimensional form is given by

$$\Sigma F = \dot{m} v_{out} - \dot{m} v_{in}, \tag{2.5}$$

where F is force and v is velocity. Letting the forces be given by pressures and again assuming a one-dimensional geometry, we get the following differential equation

$$-\frac{dP}{dx} = \rho v_x \frac{dv_x}{dx}. \tag{2.6}$$

Energy conservation A rather general energy balance can be formulated as

$$\dot{Q} - \dot{W} = -\dot{m}\left[\Delta h + \frac{\Delta v^2}{2} + g\Delta z\right], \tag{2.7}$$

where Q is heat, W is work, h is enthalpy, g is the gravity constant and z is elevation. If potential energy is neglected, this can be formulated as

$$-\frac{d\dot{Q}_x''}{dx} = \dot{m}''\left(\frac{dh}{dx} + v_x\frac{dv_x}{dx}\right). \tag{2.8}$$

The heat flux $\dot{Q}_x''$ is given by Fourier's law

$$\dot{Q}_x'' = -k\frac{dT}{dx} + \Sigma \rho Y_i \left(v_{ix} - v_x\right) h_i, \tag{2.9}$$

where k is conductivity and T is temperature. Combining (2.8) and (2.9) (and some algebra) gives

$$\Sigma \dot{m}_i''\frac{dh_i}{dx} + \frac{d}{dx}\left(-k\frac{dT}{dx}\right) + \dot{m}'' v_x \frac{dv_x}{dx} = -\Sigma h_i \dot{m}_i'''. \tag{2.10}$$

Kinetics The simplest way to model the chemical kinetics is to use one global reaction, for instance

$$CH_4 + 2O_2 \rightarrow CO_2 + 2H_2O, \tag{2.11}$$

and then assume instantaneous and full combustion (all methane is burned and transformed to CO_2 and water instantaneously). However, when studying combustion, the reaction rates might be important as they introduce time delays. The reaction rates for (2.11) may for instance be modeled as

$$\frac{d[X_{CH_4}]}{dt} = -k_G(T)[X_{CH_4}]^n[X_{O_2}]^m$$

where $[X_i]$ is the molar concentration of species i, k_G is the global rate coefficient, n is the reaction order for the fuel and m is the reaction order of the oxidizer. These three coefficients are found from experiments using curve fitting and are usually available from tables.

In reality combustion is not complete since reactions can go both ways. An equilibrium coefficient may hence be used to determine how much of the mixture that reacts.

Multi step reaction mechanisms During one reaction usually only one atom-bond is broken in a reaction. Thus, to model a simple reaction such as

$$2H_2 + O_2 \rightarrow 2H_2O,$$

one needs several reactions. Some of the steps in the reaction above are

$$H_2 + O_2 \underset{k_{r1}}{\overset{k_{f1}}{\Leftrightarrow}} HO_2 + H,$$

$$H + O_2 \underset{k_{r2}}{\overset{k_{f2}}{\Leftrightarrow}} OH + O,$$

$$OH + H_2 \underset{k_{r3}}{\overset{k_{f3}}{\Leftrightarrow}} H_2O + H,$$

where k_{fi} is the forward rate coefficient and k_{ri} is the reverse reaction rate. The concentration of oxygen and hydrogen is then given by

$$\frac{d[O_2]}{dt} = k_{r1}[HO_2][H] + k_{r2}[OH][O] + \cdots$$
$$\frac{d[H]}{dt} = k_{f1}[H_2][O_2] + k_{r2}[OH][O] + k_{r3}[OH][H_2] + \cdots$$

which can be described using a nonlinear state space model

$$\frac{d[X_i]}{dt} = f_i([X_1](t), [X_2](t), \ldots, [X_n](t))$$

For a compact notation of this, see for instance p. 121 in Turns (2000).

As an example of complexity, GRI MECH 3.0 (Smith et al., 2009) maintain that for an accurate model of combustion of methane with oxygen, 325 such equations involving 53 species is necessary.

Model complexity

As the governing equations are PDE's (Partial Differential Equations), they need to be discretized by some method. The common way to do this is to divide the geometry of interest into small controll volumes (i.e make a CFD model). The size of such a control volume depends upon the problem at hand, but in the case of turbulent flow combined with a flame, they need to be small to capture the dynamics. Such a model can contain millions (or even billions) of states. On top of this, the time span can be very large, from large eddies in the flow, moving at m/s, to fast kinetics in the μs or even ns range. Even with the fast computers we have today, such models are hard (or impossible) to simulate. In Bell et al. (2007) they simulated a model of a laboratory scale turbulent slot flame (see Figure 2.10). They used about $100 \cdot 10^6$ control volumes, and a kinetic mechanism involving 20 species, which combined with the governing equations results in 24 states in each control volume, and thereby a total number of states close to $2.5 \cdot 10^9$.

One way to reduce the number of states is to use LES (Large Eddy Simulations). In a LES model, eddies with size below a threshold are not

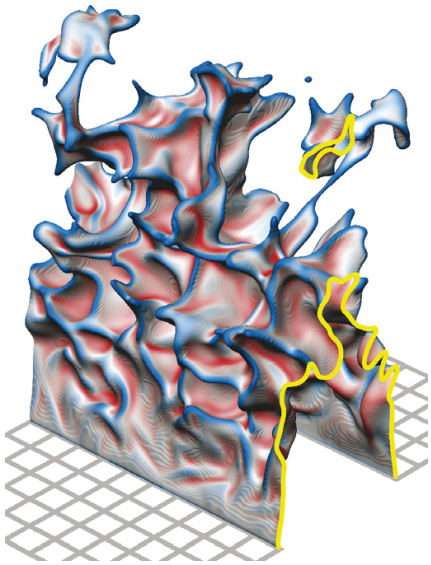

Figure 2.10: Instantaneous flame surface from a simulation of a laboratory scale slot flame, from Bell et al. (2007).

solved, thus reducing the number of control volumes. This is a promising technology, and makes it possible to simulate more advanced combustor geometries. For instance in Lartigue et al. (2004), LES was used to investigate thermoacoustic instabilities in a scaled gas turbine. However, they still needed $5 \cdot 10^5$ control volumes.

Low order models

Models based on solving the governing equations with kinetics usually results in a very high number of states. For control design and analysis, one usually prefers much simpler models, which contains the most important dynamics for the process. One possible approach to obtain such a model is

to use a model reduction technique (for instance Proper Orthogonal Decomposition (POD)) on a large and accurate model. It is however still an open question how to guarantee that controller designs based on such reduced models will stabilize the original system.

There exists analytical models that focus primarily on the dynamics related to acoustics and heat-release. This is a natural approach, as these effects are sufficient to explain the instability observed in combustors. Low order models based on this approach have been used successfully in model-based control design, both on experimental rigs and in simulation. A linear approach is most common. One then uses a one-dimensional form of the linear wave-equation to describe the acoustics, where the heat-release enters the equation as an energy source. To keep the number of states low, a Galerkin expansion is used instead of a spacial discretization. This implies that the low frequency part of the solution is kept, and thus throw away all high-frequency solutions. More on this method can be found in Section 5.3.2.

To model the heat release, two different approaches have been used; heat release rate from a thin wrinkled flame and heat release from a well-stirred reactor (WSR). If the flow is mildly turbulent, such that the chemical time-constants are small compared to the flow, the heat release rate from a thin wrinkled flame is used. While if the flow is highly turbulent, such that the chemical time-constants are dominating the dynamics, the well-stirred reactor should be preferred (Annaswamy and Ghoniem, 2002). More details of the WSR model can be found in Turns (2000), while the thin wrinkled flame model will be described in Section 5.3.1.

2.3 Control of thermoacoustic instabilities

In combustion devices it is necessary to reduce the amplitude of the unwanted pressure oscillations. To achieve this, the feedback interaction between flame dynamics and acoustics must be interrupted or broken. Traditionally passive control strategies have been employed to achieve this. A passive control strategy has little to do with what a control engineer

would perceive as control. When using a passive control strategy, one aims at reducing the susceptibility to acoustic excitation by modifying the design of the process or installing extra equipment. Examples of passive control strategies can be to modify the combustor geometry, install acoustic dampers or install vortex generators in the flow. One of the problems with passive control is that it is not very robust since it only has the desired effect in a limited range of operating conditions (Dowling and Morgans, 2005). In addition the redesign and use of extra equipment can be costly and time consuming.

An alternative to passive strategies is to use feedback control. In the combustion literature this is usually referred to as active control. By directly modulating the flow and/or composition of the reactants, one can reduce the pressure oscillations.

The first demonstration of active control of combustion instabilities took place on laboratory scale combustors in the early 1980's. They showed that it was possible to reduce the amplitude of the pressure oscillations by several orders of magnitude. A general control system for active control of combustion instabilities is shown in Figure 2.11. In this section we take a look at the different components of such a control system. First we present sensors and actuators which have been used to control combustion instabilities. Then we introduce the control algorithms which have been used to suppress thermoacoustic instabilities. The difference between conventional combustion and oxy-fuel combustion from a control point of view, is the topic of the last part of this section.

Because we are dealing with high frequency pressure oscillations, there will be strict requirements on the bandwidth of the control systems. This means that both actuators and measurements must be sufficiently fast. The bandwidth requirements also means that the computation time of the controller algorithm must be sufficiently low.

2.3.1 Sensors

Microphones and pressure transducers are the most commonly used sensors (Dowling and Morgans, 2005). As the acoustic waves propagate through

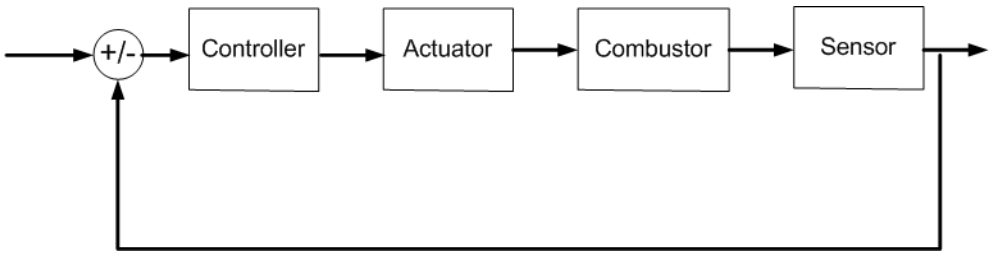

Figure 2.11: A general structure for active control of thermoacoustic instabilities.

the combustion system, these sensors have the advantage that they do not have to be placed in the high temperature zone close to the flame. An alternative to pressure measurements is to measure the heat release from the flame. These sensors are optical, and thus require optical access to the combustion chamber. By use of optical filters in front of photo multipliers, the light emitted from radicals (usually C_2, OH or CH) in the flame can be measured. This type of sensor was used in the first experimental demonstration of feedback control of combustion instabilities (Dines, 1983), where CH radicals were measured using optical fiber and photo multipliers. Soot formation can limit the optical access to the chamber and may cause problems for optical sensors. Also, if the location or size of the flame changes (for instance due to a change in the stability of the flame), optical sensors can have problems due to a limited optical access to the flame. A review of sensor technology for combustion systems can be found in Docquier and Candel (2002).

2.3.2 Actuators

The first successful demonstrations of active control of combustion instabilities used a loudspeaker to actuate the system. By mounting a loudspeaker at one end of the combustor, one could modulate the flow sufficiently to stabilize the system (see Figure 2.12). A loudspeaker is however not suffi-

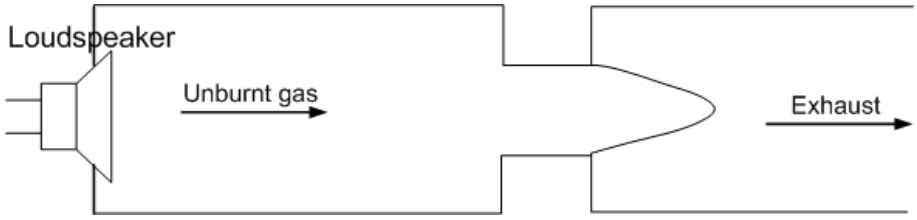

Figure 2.12: Active control by use of loudspeaker.

ciently robust for an industrial system, and the power requirements becomes prohibitive for large scales (Dowling and Morgans, 2005). Because of this, one tried to find actuators that could better handle the scale-up from small laboratory scale combustion rigs to industrial systems. The actuator that is now most commonly used is fuel-injection. By injecting a small amount of fuel close to the flame location (Figure 2.13), small perturbations in the mass flow and heat release is achieved. The first successful fuel modulation system was reported in Langhorne et al. (1990), where a car fuel injector was used to stabilize the system.

The design of fuel-injectors is an important challenge. The frequency of the unstable modes can be of several hundred Hz. Thus, the response of the injector needs to be very fast, preferably at least twice as fast as the unstable mode. It must also be able to modulate enough flow to give the control system sufficient control authority. Solenoid valves and magneto-restrictive valves are examples of valves that are available and have been used for control. They do, however, just barely satisfy the bandwidth and control authority requirements. An improvement in injector technology is not the prime focus of these thesis, but it is clearly important for the advancement of active control.

2.3.3 Control algorithms

In the early experiments (for instance Dines (1983) and Langhorne et al. (1990)) the so-called phase-shift controller was used. The idea here is to

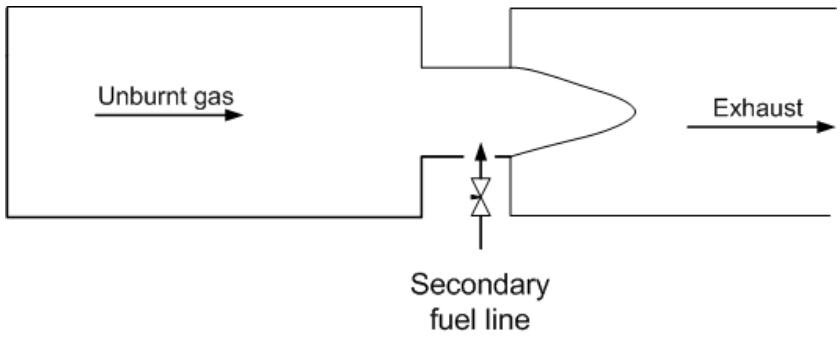

Figure 2.13: Active control by use of fuel-injection.

measure a signal, add an appropriate phase and feed it back to the actuator. Usually the appropriate phase was found empirically by trial and error, and the optimal phase delay changes with operational conditions. While it was shown that the controller was able to suppress the unstable mode, it was also found that it might introduce a new oscillation mode, which for high gains becomes unstable (Fleifil et al., 1998, Langhorne et al., 1990). Also in the presence of multiple acoustic modes, the control design proves to be very challenging (Annaswamy and Ghoniem, 2002). The controller offers no guarantee of stability, and a bad choice of control parameters may increase the amplitude of the unstable oscillations. According to Dowling and Morgans (2005), a dynamic controller which can introduce suitable gains at different frequencies is needed.

As a consequence of the problems found with the phase-shift controller, more advanced control strategies have been developed. They utilize knowledge about the system, either from system identification (i.e identifying empirical models) or by use of low order physics based models, as discussed in Section 2.2.2. One possibility is to find a controller by solving an optimization problem. A LQG-LTR controller was developed in Annaswamy et al. (2000), where the objective function minimizes the amplitude of the pressure oscillation and input usage. In the same paper H_∞-control was in-

vestigated. H_∞-control seems like a natural choice for combustion systems, as it allows the designer to specify the frequency ranges where good control is important. Other examples of H_∞-control can be found in Tierno and Doyle (1992) and Campos-Delgado et al. (2003).

When fuel injection is used for control, time-delays in the loop can become rather large due to transport of the injected gas to the burning zone. Thus it can be necessary with controllers that explicitly include time delays in the design. In Hathout et al. (2000) a controller based on the Smith predictor is used to stabilize a simulation model with large time delays, while a neural network was trained to predict the combustor output in Liu and Daley (1999), as a means to overcome the problem of time delay.

Numerous publications have used adaptive strategies. An adaptive controller is capable of self-correction, and should be able to stabilize a wider range of operating conditions. The first algorithm used was Least Mean Squares (LMS) in Billoud et al. (1992) and Kemal and Bowman (1996). However, according to Dowling and Morgans (2005) the LMS controllers are unlikely to be sufficiently robust for use in practical applications. They rely on assumptions such as the primary noise source being slowly varying and there are no theorems available to guarantee global stability. The Self Tuning Regulator (STR) is another popular approach which has been used in for instance Annaswamy et al. (1998), Krstic et al. (1999) and Evesque et al. (2003).

2.3.4 Control of oxy-fuel combustion

To the authors knowledge there are no publications on active control of oxy-fuel combustion. It seems natural, however, that the controller algorithms developed for conventional combustion are applicable for oxy-fuel. Figure 2.14 illustrates that oxy-fuel combustion has one extra degree of freedom compared to conventional combustion. This gives the opportunity to inject CO_2 instead of fuel (or air) that have been used for conventional combustion systems. Both fuel and air injection will change the equivalence ratio of the gas mixture. This is not so for CO_2 injection, which only changes the composition of the oxidizer. In this thesis we will investigate if active control

by use of CO_2 injection can perform better than fuel injection. Further, we will develop control algorithms that are robust to operational changes of the combustor and the time delay associated with the transport of injected gas from the injector to the burning zone. This will be discussed in Chapter 6 and 7.

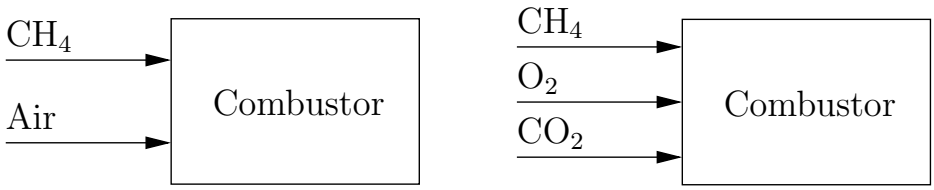

(a) Conventional combustion chamber (b) Oxy-fuel combustion chamber

Figure 2.14: Conceptual difference between a conventional combustion chamber and an oxy-fuel combustion chamber from a control point of view.

Chapter 3

Control design for a gas turbine cycle with CO_2 capture capabilities

This chapter is based on Snarheim et al. (2005), as published in Proceedings of 16th IFAC World Congress (2005), Prague, Czech Republic.

Abstract

The semi-closed oxy-fuel gas turbine cycle has been suggested in Ulizar and Pilidis (1997) as an alternative for power production with CO_2 capture capabilities. This article is concerned with two critical design decisions for a similar process. Optimizations are used on a simulation model to evaluate part load performance for four different control structures. Finally a model predictive controller is implemented for each of the structures, and closed loop simulations are used to assess the different control structures.

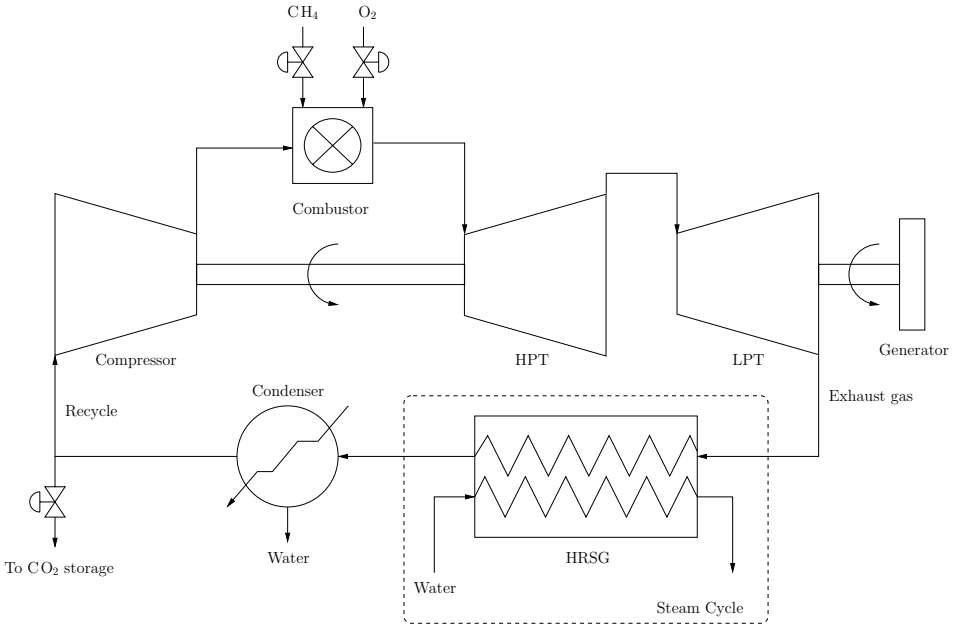

Figure 3.1: Process layout

3.1 Introduction

Fossil fuels are today a major source of power, and are likely to remain so in foreseeable future. At the same time, there is today an increasing concern about global warming and climate changes resulting from emission of CO_2 to the atmosphere. This gives a clear incentive to investigate fossil fuel-based power processes where the produced CO_2 is *captured*.

It is generally acknowledged (see e.g. Bolland and Undrum (2003)) that there are three main concepts for CO_2 capture from combustion of fossil fuels: a) Conventional power cycles where CO_2 is removed from the exhaust (post-combustion removal), b) Removal of carbon from fuel (pre-combustion removal), and c) Combustion with pure oxygen (instead of air), which leaves the exhaust consisting of CO_2 and water (easily condensed to obtain pure

CO_2). All these concepts have in common that they thermodynamically are less efficient compared to alternatives that emit (all) CO_2.

These processes are generally highly integrated, involving energy and mass recycle, and optimizing efficiency might lead to operational (control) challenges. Therefore it is important to look at the interplay between process design and control.

The process we study herein (described in more detail in Section 3.2), is based on concept c) above. The exhaust gas from a gas turbine with CO_2 as working fluid, is used as heating medium for a steam cycle (similarly to a conventional "combined cycle"), before water is removed and the CO_2 is recycled as working fluid in the gas turbine.

The purpose of this paper is to investigate two critical design decisions; that is use of compressor variable guide vanes, and constant vs. "floating" HRSG pressure, and their effect on controllability and part-load efficiency.

The literature on this specific process is scarce, at least as far as dynamics and control are concerned. Conventional (open) gas turbine processes has received considerably more attention, for instance Rowen (1983) and Ordys et al. (1994). Predictive control of conventional gas turbines is suggested in Vroemen et al. (1999) with experiments in Van Essen and De Lange (2001). The modeling in this work is based on Ulfsnes et al. (2003).

3.2 Process Description

A sketch of the process is shown in Figure 3.1. In the combustion chamber natural gas (here assumed to consist of methane (CH_4) only) burns in pure oxygen (O_2). Complete combustion is assumed and a perfect flow/ratio controller is assumed to provide oxygen at a ratio slightly above the stoichiometric ratio. Recycled gas, mainly consisting of CO_2, is compressed (in the compressor) and used as an inert in the combustion to limit temperatures in the combustion chamber and turbine inlet. Variable guide vanes (VGV) in the compressor can be used to reduce the mass flow through the compressor (and thus be used to control the high pressure turbine inlet temperature (TIT)). The gas leaving the combustor expands through two

turbines. The high pressure turbine (HPT) is used to drive the compressor, while the low pressure turbine (LPT) is connected to a generator. The temperature at the inlet of the HPT is very high, and therefore some of the compressed CO_2 from the compressor is used as a cooling medium for the HPT. This twin shaft set up gives the process more flexibility (than a single shaft turbine) because the compressor does not have to operate at a fixed speed (the study of a single shaft turbine is ongoing work). The exhaust gas leaves the LPT with a temperature well suited to deliver heat to a steam bottoming cycle. In the heat recovery steam generator (HRSG), as much heat as possible is removed from the exhaust gas to produce power in a steam turbine. After the HRSG the gas is further cooled in a condenser to remove water from the cycle. A controller is assumed to keep the temperature out of the condenser constant by manipulating the cooling water stream in the condenser. The exhaust gas, now mainly consisting of CO_2 is split into two streams, one stream is recycled to the compressor; the other stream is removed from the cycle for storage. The CO_2-valve controls the ratio between the streams. Some typical ("design") values for key variables are given in the table below:

Variable	Symbol	Typical value
LPT power output	$\dot{W}_{\mathrm{LPT}}$	92.9MW
Turbine inlet temperature	TIT	1600K
Compressor mass flow	$\dot{m}_{\mathrm{c}}$	227kg/s
Exhaust gas temperature	TET	982K
Mass flow CO_2 to storage	$\dot{m}_{CO_2}$	16.7kg/s
Fuel mass flow	$\dot{m}_{CH_4}$	5.8kg/s
O_2 mass flow	$\dot{m}_{O_2}$	23.6kg/s
Compressor inlet temp.	T_{in}	290K
Compressor pressure ratio	π_c	18.5

For space reasons we will not provide the complete modeling of the process. Instead the interested reader is referred to Imsland et al. (2004) or Ulfsnes et al. (2003) where the modeling is presented. Some few additions have been made; VGV have been implemented in the compressor (by parametrization of the compressor map along the VGV position), and we

now also use turbine cooling (some of the compressed CO_2 is mixed with the combustion exhaust before entering the HPT).

In a conventional combined cycle VGV are used to increase heat flow to the HRSG, when operating at part load. When VGV are used, the gas turbine becomes less effective, but as more heat is transferred to the HRSG, the combined cycle efficiency increases. This means that to be able to study use of VGV for this process, it is necessary to calculate the power production in the HRSG. As it was chosen to not create a detailed model of the cold side of the HRSG, the power production must be estimated. To do this the gas turbine simulation tool GTPRO was used. Using this program we simulated a conventional HRSG in an operating range similar to "our" process. From this data we used curve fitting to generate a function for the power output as a function of TET and exhaust gas mass flow rate.

The complete simulation model was implemented in gPROMS (gPROMS). Thermodynamic properties have been determined with Multiflash©, a physical property package.

3.3 Control structure

The control problem we consider, is that of load control: operate the process such that the overall power demand is met, and such that the power output responds fast enough to disturbances. As the process is open loop stable, the control objective is to operate the process as efficiently as possible, under varying disturbances. The major disturbances that affect the operation and are considered herein are load changes. This study does not include start-up and shutdown of the system.

We will first briefly explain the manipulated variables available, before we discuss the different control structures that are investigated.

Manipulated variables: The manipulated variables available are the fuel valve, O_2 valve, CO_2 storage valve, compressor variable guide vanes (VGV), and a number of variables affecting the operation of the HRSG and the condenser. As explained in Section 3.2, a perfect ratio controller has been assumed to manipulate the O_2 valve to obtain a constant ratio of

inflow of CH_4 and O_2. A well-tuned controller is also assumed to control the fuel valve, leaving the fuel flow reference value as a manipulated variable. As the cold side of the HRSG has not been modeled in any detail, the manipulated variables in the HRSG are not available. However, according to Kehlhofer et al. (1999) these variables are not normally used for load control in a conventional combined cycle. Thus, for the steam bottoming cycle, these manipulated variables should be used to operate the steam cycle as efficiently as possible for varying loads, removing as much heat as possible from the turbine exhaust.

The manipulated variables used for control are thus the opening of the CO_2 storage valve, the fuel flow reference value and the variable guide vanes.

Controlled variables: To make sure that the correct load is delivered to the grid, we need to control the overall combined cycle power output. But as the dynamics in the steam turbine in the HRSG are much slower than the gas turbine, faster response can be achieved by controlling the LPT power output. The setpoint for $\dot{W}_{\mathrm{LPT}}$ must be set such that the combined cycle power output becomes as desired.

The remaining degrees of freedom should be used to keep the power production as efficient as possible while respecting important process constraints. Among the many constraints in this process, the TIT and the pressure in the HRSG are the most important ones. Violation of these constraints can cause severe damage on the process equipment, but at the same time the process needs to be operated close to these constraints to keep the cycle efficiency high. In a conventional combined cycle gas turbine, VGV are used to keep TIT high to increase heat flow to the HRSG when operating at part load. The main difference between this process and a conventional gas turbine is that the exhaust gas is recycled to the process and the working medium is CO_2. It is therefore not given beforehand that use of VGV are beneficial for this process, and this is one of the issues we want to investigate.

As this process operates in a semi-closed cycle it is necessary to control the pressure in the HRSG. If a conventional HRSG is used, this pressure must be kept constant at about atmospheric pressure, due to wall thickness in the heat exchangers in the HRSG. However, if this pressure can be allowed

to vary, greater combined cycle efficiency can be achieved when the power plant is operating at part load. This is because if the pressure on the low pressure side of the compressor and turbines can be allowed to change, the pressure ratio in these components can remain almost constant, even though the mass flow is reduced.

Four different control structures were compared. In structure S1 and S2 the pressure in the HRSG is allowed to vary and the pressure setpoint depends on the desired power production (and is found by use of off-line optimizations). The pressure is still constrained between 0.8 bar and 1.2 bar. In control structure S3 and S4 the pressure is kept constant at 1 bar. In structure S1 and S3 VGV are used, which means that it is possible to keep the temperature at a setpoint (1600K) at part load. These control structures are summarized in the table below.

	Contr. var.	VGV	Pressure	TIT
S1	$\dot{W}$,p,TIT	yes	$p_d = p_d(\dot{W})$	T_d=1600K
S2	$\dot{W}$,p	no	$p_d = p_d(\dot{W})$	-
S3	$\dot{W}$,p,TIT	yes	$p_d = 1\,\text{bar}$	T_d=1600K
S4	$\dot{W}$,p,TIT	no	$p_d = 1\,\text{bar}$	-

To investigate the impact of using VGV and varying pressure in the HRSG, the optimization tool in gPROMS was used. At different part loads an optimization problem was solved to minimize the use of methane feed when operating at the desired load, subject to constraints. The constraints used were TIT< 1600K, the pressure constraint for the given control structure and that the solution had to be a steady state solution. The results from the optimizations are shown in Figure 3.2, where a relative value means the actual value divided by the value when the process is operating at its design point (i.e relative power means $\frac{\dot{W}}{\dot{W}_{\text{design}}}$). Efficiency is calculated as

$$\eta = \frac{\dot{W}_{out}}{\dot{m}_{CH_4} \cdot \text{LHV}},$$

where LHV is the lower heating value of CH_4 and $\dot{W}_{out}$ is the total power production from both the low pressure turbine and the steam bottoming

cycle. This means that losses in efficiency due to O_2-production and compression of CO_2 before storage are not considered.

For each of the control structures, Figure 3.2 shows the optimal steady state operating point for a given part load. As one can see the efficiency at part load is higher if one can vary the pressure in the HRSG. It can be seen that with control structure S1 and S2 the process can be operated at its optimal efficiency down to about 75% part load (the relative efficiency is larger than one in this region because there has not been put much effort on optimization of the design point). In fact these solutions are identical in this region because it is not optimal for structure S1 to use VGV. At 75% part load the 0.8 bar constraint becomes active. Then the pressure ratio in the compressor and turbines decreases, which results in a less efficient cycle. If the pressure constraint can be reduced, the range of optimal relative efficiency can be widened. The figure also shows that there is a small gain in efficiency when VGV are used. This gain is very dependent on the relation between TET and steam turbine power output in the HRSG. Due to the uncertainty related to the estimation of the power production in the HRSG, it is difficult to arrive at a reliable conclusion regarding whether use of VGV is beneficial or not. However, keeping TIT constant with use of VGV also has the benefit that large temperature gradients in the system can be avoided.

3.4 Control and closed loop simulations

The four control structures are implemented with linear MPC. We will first give a short introduction to the MPC used, and then present closed loop simulations.

3.4.1 Predictive control

Linear MPC refers to an online optimization where, at each sample instant, the control is determined by optimizing future behavior as predicted by a linear process model, subject to constraints on states (or controlled variables) and inputs, then applying the first part of the computed control on

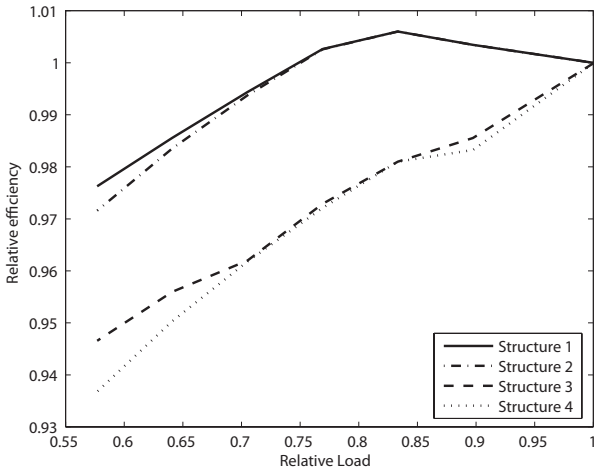

Figure 3.2: Optimal steady state combined cycle efficiency for the four different control structures when operating at part load.

the process (Maciejowski, 2002).

The main advantages of MPC is that it handles multivariable control problems, and that the controller can take actuator limitations and process constraints into account in a simple and structured manner. This makes predictive control well suited for this process.

The linear discrete-time process model used for prediction is on standard state-space form,

$$\begin{aligned} x_{k+1} &= Ax_k + Bu_k + Ed_k, \\ z_k &= C_z x_k + D_z u_k + F_z d_k, \\ y_k &= C_y x_k + D_y u_k + F_y d_k \end{aligned}$$

where z_k are the controlled outputs, and y_k are the measured outputs. We have used TET, rotational speed of the compressor, $\dot{W}_{\mathrm{LPT}}$, temperature and pressure at outlet of the HRSG, the position of VGV and the state of the condenser (the integral error of the PI controller controlling the outlet

temperature of the condenser) as measured variables (y). A standard linear Kalman filter is used to estimate the state (x_k) from the measured variables and the inputs (u_k). The d_k is a disturbance state used in the Kalman filter to compensate for model mismatch when operating far from the linearization point. The linear model is obtained using the `LINEARIZE`-function of gPROMS at the design operating point. We assume linear constraints on states (or controlled outputs), input and input rate,

$$Ex_k \leq b_z, \quad Fu_k \leq b_u, \quad G(u_k - u_{k-1}) \leq b_{\Delta u}.$$

We choose to minimize a quadratic objective function of the following form[1],

$$V(k) = \sum_{i=1}^{H_p} \|\hat{z}(k+i|k) - r(k+i)\|_Q^2 + \sum_{i=0}^{H_u} \|\hat{u}(k+i|k) - \hat{u}(k+i-1|k)\|_R^2$$

where $\hat{z}(k+i|k)$ and $\hat{u}(k+i|k)$ are predicted variables at time k (with $\hat{u}(k-1|k) = u(k-1)$), and $r(k)$ is a reference trajectory for the controlled variables.

The most important constraints that are imposed here, are the upper limit on TIT (1600K), the limits on pressure in HRSG and the constraints on valve operation (opening between 0 and 1, stroke time 15s). We used $H_p = H_u = 50$, with sample time 0.5s.

3.4.2 Closed loop simulations

To compare the dynamic properties of the control structures proposed in Section 3.3, closed loop simulations using the MPC in Section 3.4.1 were performed for each structure.

[1] The norm $\|\cdot\|_H$ is defined by $\|z\|_H = \sqrt{z^{\mathrm{T}} H z}$, $H > 0$.

The simulations are performed in gPROMS, while the controller calculations are done in Matlab. gPROMS communicates with Matlab via gPROMS' Foreign Process Interface. The QP-problem is solved using `quadprog` from the Optimization Toolbox in Matlab. At each sample instant, the measurements are transferred from gPROMS to Matlab, where an optimal control trajectory is computed, and the manipulated variables for the next sample interval are returned to gPROMS.

The closed loop simulations are shown in Figures 3.3-3.4. The first disturbance (at 20s) is a change in relative power from 1 to 0.9, and at three minutes there is a new load change from 0.9 to 0.7. Note that all the different control structures distribute the load between the steam cycle and LPT differently, and it is necessary to calculate the setpoint for the LPT load (which is the controlled variable) for each structure independently. The power control is very fast and load changes are done in a few seconds. Also note the large differences in TIT between the different structures. A combined cycle efficiency plot shows that after the second load change, the efficiencies are higher than what was found in Figure 3.2. The reason for this is the steady state offset in pressure (the constraints are violated by a small margin) which causes a more efficient cycle. As long as we cannot measure TIT, there will be steady state offsets when operating this far from the linearization point. Remedies for this might be to use a nonlinear model or to include constraints in the state estimator.

3.5 Discussion

Modeling: The developed model (see Imsland et al. (2004)) is mainly based on first principles and thermodynamics. However, as no such process exists today, there is considerable uncertainty related to several dimensions and characteristics. As we see it, the main uncertainty factor related to the dynamics is the modeling of the HRSG/condenser. Other issues that will be looked upon are a more realistic compressor map, and using a single shaft gas turbine. Introducing isentropic efficiency maps for the compressor and the turbines will also increase model confidence, but we believe that

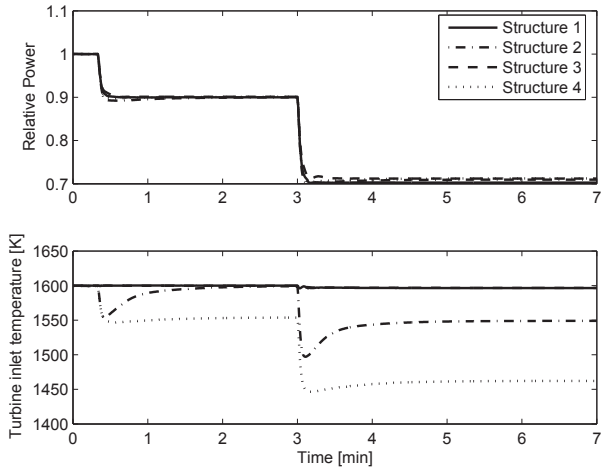

Figure 3.3: Relative Combined cycle power and TIT for the four different control structures during load changes.

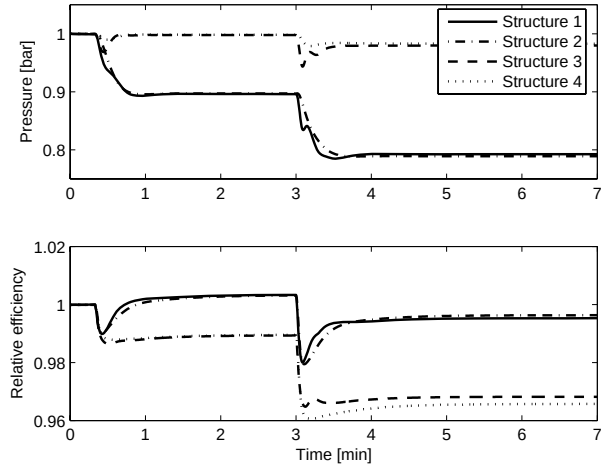

Figure 3.4: Pressure in HRSG and Combined cycle efficiency for the four different control structures when operating at part load.

this will not have a significant influence on the dynamic properties of the process.

VGV: From the results presented it is difficult to conclude whether VGV should be used or not. The use of VGV is very dependent on the relation between TET and the steam turbine power output. In Kehlhofer et al. (1999) there is a plot relating steam turbine output to the gas turbine exhaust temperature. In this plot the relations between the steam turbine power and TET is much steeper than what we found using GTPRO. If we had chosen to use this relation instead, the benefits of using VGV would have been much larger.

HRSG pressure: In the results presented, better part load performance was achieved when the pressure in the HRSG was allowed to go below atmospheric pressure. However, if underpressure is undesirable, it should be possible to design the process such that the HRSG design must deal with over pressure instead. The process can be designed to have a higher pressure in the HRSG when operating at the design point. Then when the power plant operates at part load, the pressure can be allowed to decrease till atmospheric pressure is reached. The cost of this is that the oxygen and natural gas must be compressed to a higher pressure before entering the combustion chamber. At the same time less energy is needed to compress CO_2 for storage, because the exhaust will be at a higher pressure.

3.6 Conclusion

The results show that if the pressure in the HRSG can be allowed to vary, a large gain in combined cycle efficiency can be achieved when operating at part load. But to allow for this kind of control, wall thickness in the heat exchangers must be increased, which will increase the development costs for the plant. When deciding whether to keep the low pressure part of the power plant constant at atmospheric pressure or not, it is necessary to consider how the power plant will be operated. Many gas turbines are used to manage peaks in the power demand, and operate at part load for a considerable amount of their lifetime. In such cases the extra costs should

at least be considered.

For the two control structures that used VGV to keep a constant TIT, there was not a significant gain in efficiency. Thus, to be able to draw more firm conclusions, it is necessary with a more accurate model of the HRSG.

The closed loop simulations showed that all the different control structures are feasible, and confirm the results found from the off-line optimizations. The control structures that use VGV have the benefit that large temperature changes in the cycle can be avoided.

Chapter 4

Impact of microjet actuation on stability of a backward-facing step combustor

This chapter is based on Altay et al. (2007), as published in Proceedings of 45th AIAA Aerospace Sciences Meeting and Exhibit (2007), Reno, Nevada.

Abstract

In this paper, we investigate the effect of using steady air injection in the cross-stream direction near the step to stabilize combustion in a backward-facing step combustor. Air is injected from a 2 mm wide slot extending across the entire span of the combustor, or from twelve 0.5 mm diameter evenly spaced microjets. The microjet flow is choked, while the slot flow is not and may couple with the pressure oscillations in the combustor. The combustor dynamics are examined when the fuel bar is located 35 cm or 95 cm upstream of the step, without or with hydrogen addition to the primary

fuel, in this case propane. The combustor dynamics showed significant sensitivity to the fuel bar location. When the fuel bar was located closer to the step, both the microjets and the slot were able to suppress the instability. However, to produce equivalent reductions in the sound pressure level, the slot requires 3 times as much air flow as the microjets. The effect of hydrogen addition is not significant in this case. When the fuel bar was located further upstream of the step, the combustor was more unstable, the microjets were less effective, and the hydrogen enrichment had stronger impact on the combustion dynamics.

4.1 Introduction

Continuous combustion systems common in propulsion and power generation applications are susceptible to thermoacoustic instability, which occurs under lean burn conditions, where most emissions and efficiency benefits are achieved, or at high power density where the equivalence ratio is close to stoichiometry. Under these conditions, acoustic resonances occur due to feedback interactions between acoustics and heat-release fluctuations. Several mechanisms appear to be present in a combustor that initiate and promote such interactions, including flame-acoustic wave interactions, flame-vortex interactions, equivalence-ratio fluctuations, flame-wall interactions, and the effects of unsteady stretch (Culick, 1996, Ducruix et al., 2003, Lieuwen, 2003, Zinn, 1986). In general, heat release fluctuations arise due to the modification of the local burning rate; the flame's surface area; or both, in response to these mechanisms.

In order to eliminate thermoacoustic instabilities, several active control strategies have been developed, primarily focusing on the actuation of the primary fuel (Langhorne et al., 1990, Annaswamy et al., 2000, Murugappan et al., 2003) and injection of secondary fuel close to the flame zone (Paschereit et al., 2006). While active control is effective, actuators required for its implementation are not readily available and can be cumbersome. Alternatively, our preliminary work (Ghoniem et al., 2005b) and experiments in Uhm and Acharya (2006) on passive control/suppression showed that air

injection from a secondary line is an effective and simple control approach. The objective of this work is to examine thermoacoustic instability suppression by injecting air perpendicular to the step using two different injector geometries in a backward facing step dump combustor: i) a slot with dimensions 2 mm x 160 mm extending across the entire span of the combustor just upstream of the step, ii) a row of twelve 0.5 mm diameter microjets just upstream of the step. In this paper we focus on steady injection. Experiments with actuated injection are currently being performed. We also enrich the primary fuel, or propane, with small amount of hydrogen, that is 24% / 1.1% hydrogen by volume/mass, respectively, and observe the effect of hydrogen enrichment on combustion dynamics and stability.

The experiments are performed for two different locations of the fuel bar, 35 cm or 95 cm upstream of the step. The impact of changing the fuel bar location on combustion dynamics, instability and response to air injection are examined. The fuel bar location affects combustion dynamics through its impact on air-fuel premixing, amplitude of equivalence ratio oscillations, and on the convective time scale (Lieuwen et al., 2001).

4.2 Experimental setup

Experimental tests are conducted in a backward-facing step combustor, in which a sudden expansion is used to anchor the flame, as shown in Figure 4.1. The combustor consists of a stainless steel duct with a rectangular cross section 40 mm high and 160 mm wide. The air inlet is choked. A distance 0.5 m downstream from the choke plate, a 0.2 m long ramp contracts the channel height from 40 mm to 20 mm, followed by a 0.2 m long constant-area section that ends with a sudden expansion back to 40 mm. The step height is 20 mm. The overall length of the combustor is 5.0 m. A circular exhaust pipe comprises the last 3.0 m of the tunnel. The test section is equipped with quartz viewing windows. An air compressor supplies air up to 110 g/s at 883 kPa. A pair of Sierra C100M mass flow controllers allow an arbitrary propane/hydrogen mixture at a maximum flow rates of 2.36 g/s for propane and 0.30 g/s for hydrogen. Fuel is injected through

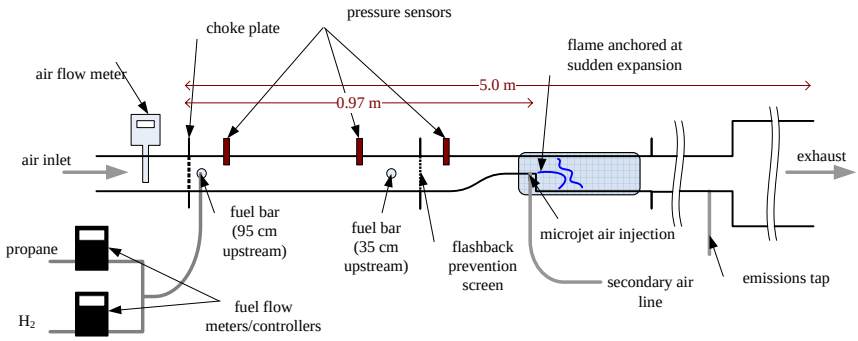

Figure 4.1: Schematic of the MIT backward-facing step combustor.

several spanwise holes in a manifold located 35 cm or 95 cm upstream of the step. Images of the flame are captured using a Phantom v7.1 high-speed camera and used to examine the combustion dynamics and estimate spatial and temporal variations in the heat release rate. Pressure measurements are obtained using Kistler pressure sensors designed for small combustion engines and laboratory investigations. All data are acquired using a National Instruments PCIe-6259 data acquisition board and the Matlab Data Acquisition Toolbox. A custom Matlab code is used to store the data and control the experiment.

4.3 Results

In this section we present the experimental results showing the effect of air injection from the slot and the microjets when the fuel bar is placed either 35 cm or 95 cm upstream of the step. The mean pressure and the inlet temperature are at atmospheric conditions.

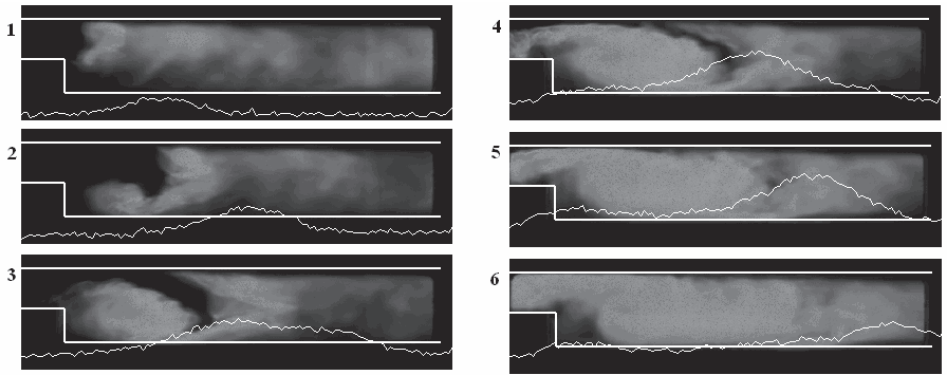

Figure 4.2: Sequential flame images in a typical unstable cycle. The white lines show the CH* chemiluminescence.

4.3.1 Fuel bar 35 cm upstream of the step

First we placed the fuel bar 35 cm upstream of the step. In this configuration the combustor is almost always unstable, independent of the Reynolds number and the equivalence ratio, ϕ. The lean flammability limit is at $\phi \sim 0.50$. The instability involves the unsteady interaction between the wake vortex and the flame, as shown in Figure 4.2.

The figure shows flame images and the CH* chemiluminescence, obtained without air injection while using propane as the fuel, in a typical instability cycle. The CH* chemiluminescence is used as an indicator of the heat release rate. The Reynolds number and the equivalence ratio were fixed at 8500 and 0.55, respectively, which correspond to an air mass flow rate of 23.1 g/s. The images suggest that the cyclical formation of the wake vortex and its interaction with the flame controls the heat release rate dynamics. The heat release rate begins to rise as the flame starts its convolution around the newly formed vortex and continues to rise as the vortex grows. As the vortex reaches its maximum size, the flame touches the upper wall and its leading edge folds, trapping a large pocket of reactants. Soon after, the pocket is consumed and maximum heat release is reached. The periodic

heat release supported by the flame-vortex interactions couples positively with the acoustic pressure field, causing combustion instability. Next, we performed experiments to investigate the effect of air injection perpendicular to the primary flow direction from a location 12 mm upstream of the step. We used two different injector geometries: i) a slot with dimensions of 2 mm by 160 mm, or ii) twelve 0.5 mm diameter choked microjets drilled along the span of the combustor. We compare the effectiveness of the slot and the microjets in suppressing the pressure oscillations using propane and propane/hydrogen mixture as fuels. As before, the Reynolds number and the equivalence ratio without air injection are fixed at 8500 and 0.55, respectively. The volume and mass percentage of hydrogen to total fuel for the cases using propane/hydrogen mixture was 24% and 1.1%, respectively. Figure 4.3 shows the overall sound pressure level (OASPL) as a function of the secondary air-flow to the primary air-flow ratio, μ, with different fuel compositions, using the slot and the microjets to inject the secondary air.

We observe that under the conditions which result in the lowest OASPL, the combustor is stabilized at $\mu = 0.13$ in the case of the slot, compared to $\mu = 0.04$ in the case of the microjets. Furthermore, the OASPL is 2 dB lower when the stabilization is achieved using the microjets. Using the slot without hydrogen enrichment, when the secondary air flow rate is low, $\mu < 0.1$, the combustor becomes extremely unstable, and the flame blows out within the range $0.03 < \mu < 0.1$. In a previous study, we demonstrated that the reactive coupling between the secondary-air line and the pressure oscillations is the reason for the destabilization and blow out (Ghoniem et al., 2005a). Hydrogen enrichment does not prevent the destabilization and shifts the blow out region to $0.045 < \mu < 0.1$. In the case of microjets, the air flow is choked, and destabilization is not observed (which demonstrates the validity of the reactive mechanism). Furthermore, with microjets, the flame blows out when $\mu > 0.1$, independent of the fuel composition. This might be caused by the extensive cooling of the flame at high microjet flow rates. This effect will be explored further in the future by heating the injected air. In Figure 4.4, we compare the stable combustor operation with air injection using the slot and the microjets, without hydrogen. Note that the secondary air flow rate used to achieve stable com-

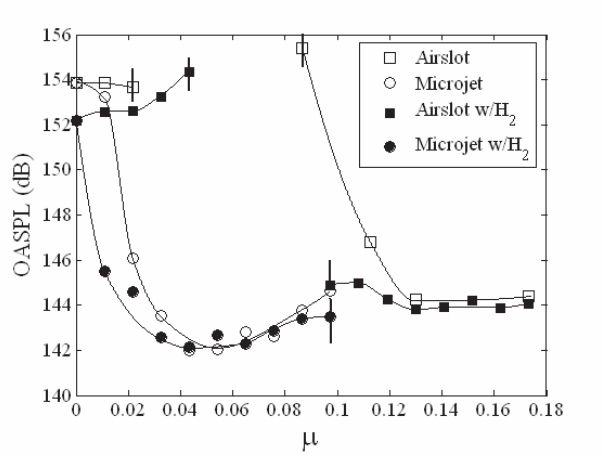

Figure 4.3: Overall sound pressure level upon the secondary air-flow to primary air-flow ratio using slot or microjets to inject the secondary air, without and with hydrogen addition to propane. The bars show the blowout limits. The fuel bar is located 35 cm upstream of the step.

bustion is 3 g/s, or $\mu = 0.13$, with the slot, and 0.75 g/s, or $\mu = 0.03$ with the microjets. The overall equivalence ratio becomes 0.49 and 0.53 with the slot and microjets, respectively. The flame is anchored upstream of the window when microjets are used. With the slot, the flame hardly moves upstream of the slot location. Examining movies of the flame, we observe that there are more dynamics associated with the vortex shedding in the case of the slot compared to the case of the microjets, which is also verified from the higher OASPL value in the case of the slot.

Figure 4.5 shows the sound pressure level spectra without air injection, and using the slot or microjets to inject 3 g/s and 0.75 g/s air, respectively. Note that higher harmonics are also excited when the combustor is unstable. Using the slot and the microjets, the peaks decrease considerably. Next, we demonstrate the results after moving the fuel bar 95 cm upstream of the step

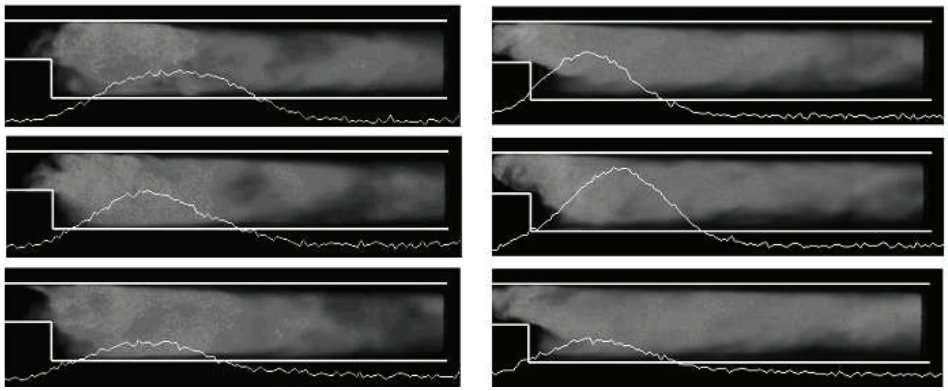

Figure 4.4: Sequential flame images of propane flames stabilized using air injected from a) slot and b) microjets. The white lines show the CH* chemiluminescence. The fuel bar is located 35 cm upstream of the step.

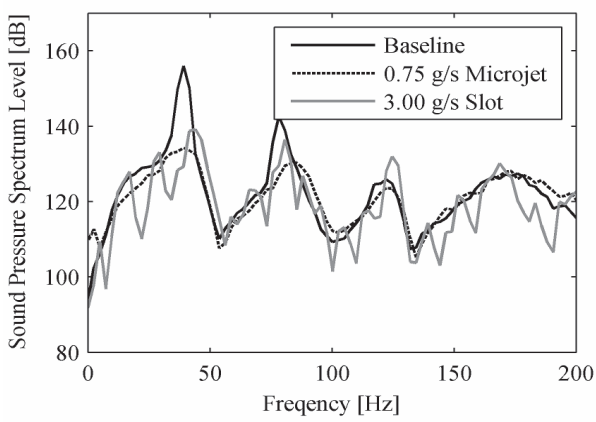

Figure 4.5: Sound pressure spectrum level without air injection, using microjets or the slot to inject 0.75 g/s ($\mu = 0.03$) and 3 g/s air ($\mu = 0.13$) , respectively. The fuel bar is located 35 cm upstream of the step.

4.3.2 Fuel bar 95 cm upstream of the step

In a second series of experiments, we moved the fuel bar 95 cm upstream of the step. In this case, the air and fuel have more time for mixing before burning. Moreover, equivalence ratio oscillations are expected to be reduced significantly as a result of two factors: i) the amplitude of equivalence ratio oscillations established at the fuel bar are smaller since the fuel bar is located near the choke plate where velocity oscillations are small and ii) the convective time scale, $\tau = L/U$, is much longer, and there is more time for the oscillations to be damped out by turbulent mixing before reaching the combustion zone. Measurements of equivalence ratio oscillations at the burning zone will be performed in future experiments to confirm the above statements. With this fuel bar configuration, the combustor exhibits three distinct dynamics regimes depending on the Reynolds number, the equivalence ratio and the history. These are shown in Figure 4.6.

When we operate the combustor very close to the lean flammability limit, that is $\phi = 0.63$ in this case, the flame is stable and the overall sound pressure level is 136 dB. In the stable mode, smaller vortices are shed from the step at a higher frequency which does not correspond to the acoustic mode of the combustor, and thus there is no coupling between heat release rate and pressure. As the equivalence ratio rises beyond a certain threshold, the combustor transitions to a quasi-stable operating condition with a sound pressure level close to 145 dB. Under quasi-stable operating conditions, the flame remains anchored at the step, while experiencing oscillation downstream. Increasing the equivalence ratio reduces the OASPL while the dynamics remain in the quasi-stable regime. When the equivalence ratio rises above $\phi \sim 0.77$, the combustor transitions into a strongly unstable regime with a sound pressure level close to 162 dB. In the unstable regime, the flame periodically flashes back upstream of the step, while undergoing strong interaction with the large wake vortex. These dynamics are illustrated above in Figure 4.2. Note that for this location of the fuel bar, the sound pressure level of the unstable mode is around 10 dB higher than in the case when the fuel bar was located 35 cm upstream of the step.

When we operate the combustor initially in the unstable region and de-

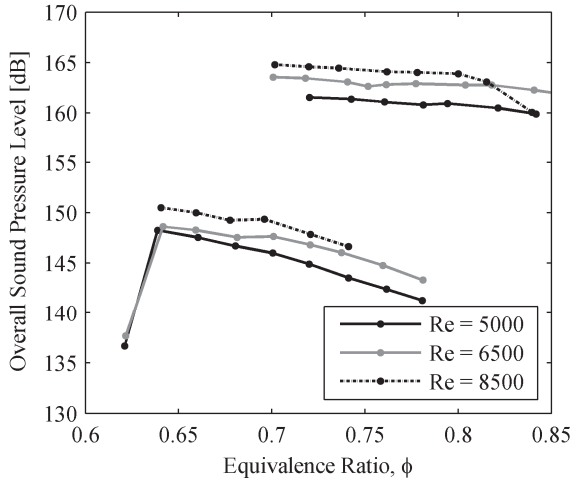

Figure 4.6: Overall sound pressure level as a function of equivalence ratio for three different Reynolds numbers. The fuel bar is located 95 cm upstream of the step.

crease the equivalence ratio, the dynamics remain in the unstable region until $\phi \sim 0.70$. Reducing the equivalence ratio below this value shifts the dynamics to the quasi-stable regime. As we reduce the equivalence ratio further to reach values very close to the lean flammability limit, the combustor operates in the stable mode. The dependence of the combustor dynamics on the history, i.e. the presence of hysteresis, is attributed to the highly non-linear nature of the system.

As we increase the Reynolds number, the pressure level increases and it becomes difficult to reach a stable operating condition before the lean blow-out limit.

Next, we performed experiments to investigate the impact of using either the slot or the microjets to inject air near the step, without and with hydrogen enrichment, to suppress the instability. The Reynolds number and the equivalence ratio without air injection were fixed at 8500 and 0.70,

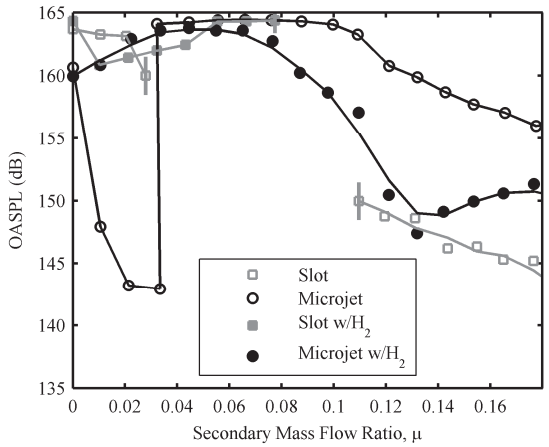

Figure 4.7: Overall sound pressure level upon the secondary air-flow to primary air-flow ratio using slot (gray) or microjets (black) to inject the secondary air, without (open markers) and with (closed markers) hydrogen addition. The bars show the blowout limits. The fuel bar is located 95 cm upstream of the step.

respectively. When hydrogen is added to propane, the volume and mass percentages of hydrogen to total fuel was again 24% and 1.1%, respectively. Figure 4.7 shows the OASPL as a function of the secondary air-flow to the primary air-flow ratio, μ, with different fuel compositions, using the slot or the microjets to inject the secondary air. Figure 4.7 shows that when air is injected from the slot and without hydrogen enrichment, the combustor becomes more unstable in the range, $0.03 < \mu < 0.11$, leading to blowout. As $\mu > 0.11$, OASPL decreases monotonically. At $\mu = 0.18$, the maximum amount of air we can inject, there is approximately 20 dB reduction in the OASPL compared to the case without air injection. Adding hydrogen to the primary fuel shifts the blowout to a higher secondary air mass flow rate, $\mu = 0.08$. We could not stabilize the combustion with hydrogen enrichment for $\mu > 0.08$.

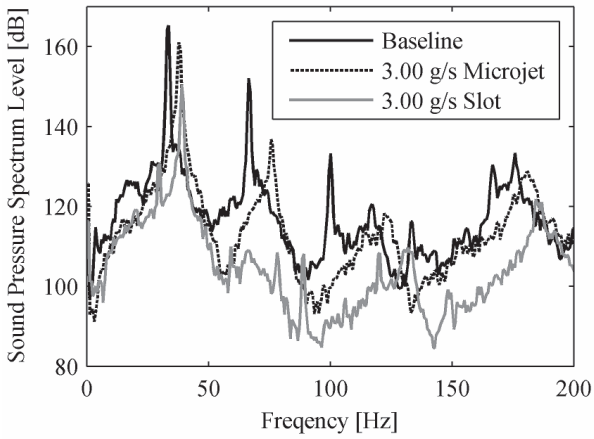

Figure 4.8: Sound pressure spectrum level without air injection, using slot injection at 3.0 g/s or microjet injection at 3.0 g/s air ($\mu = 0.13$).

When the microjets are used without hydrogen enrichment, the flame is stabilized for secondary air mass flow rates corresponding to $\mu = 0.03$, similar to the previous case. The OASPL was reduced by 17 dB compared to the case without air injection. However, as the secondary air flow rate is increased further, the OASPL suddenly jumps to much higher values. When hydrogen is added to the primary fuel, the OASPL initially increases then decreases as μ increases, reaching a minimum at $\mu = 0.13$, leading a 10 dB reduction in the sound pressure level. In Figure 4.8, we plot the sound pressure level spectra without air injection, using the slot or the microjets to inject 3.0 g/s air. When the microjets are used, the reduction in the sound pressure in the primary mode is smaller, and the second peak is not suppressed. Furthermore, there is around 10 Hz frequency shift when either the slot or the microjets are used.

4.4 Conclusions

In this paper we compared the effectiveness at suppressing thermoacoustic instability of steady cross-stream air injection from a slot or microjets near the step of a backward-facing step combustor. We also used hydrogen enrichment of the primary fuel and investigated its impact on combustion dynamics. We placed the fuel bar at two different locations to examine the robustness of these solutions. When we moved the fuel bar, the combustor dynamics showed significant differences. The lean blowout limit increased from $\phi = 0.5$ to $\phi = 0.63$ when the fuel bar was moved from 35 cm to 95 cm upstream of the step. The sound pressure level during unstable combustor operation was 10 dB higher when the fuel bar was located further from the step. We also observed that the impact of air injection from the slot or the microjets, and that of hydrogen enrichment are very different in the two cases. Although hydrogen addition does not have much impact on suppressing the instability when the fuel bar is located 35 cm upstream of the step, when the fuel bar is located 95 cm upstream of the step, it helps reduce the OASPL when used in conjunction with the microjets. These differences might be attributed to the change in the degree of premixing and the contribution of the equivalence ratio oscillations to combustion instability. Both will be explored in a further study. Results show that air injection could be used as a simple way to suppress combustion instability. To be effective, air should be injected at or near the flame anchoring zone, at flow rates determined by the operating conditions and the design of the air injector. In this study, choked microjets were more effective when the fuel bar was located close to the flame anchoring zone. On the other hand, when the fuel bar was located further upstream the slot was more effective. The controlling mechanisms in both cases will be explored in future studies. In future experiments, we also plan to explore the potential of modulating the flow through the slot or the microjets to gain further suppression in the overall sound pressure level, using less secondary air flow.

Chapter 5

Modelling of oxy-fuel combustion

This chapter is based on Snarheim et al. (2007), as published in Proceedings of European Control Conference (2007), Kos, Greece.

Abstract

Semi-closed gas turbine cycles based on oxy-fuel combustion have been proposed as an alternative to conventional gas turbine cycles for achieving CO_2-capture for CO_2 sequestration purposes. While combustion instabilities are a problem in modern conventional gas turbines in general, recent experimental results indicate that such instabilites also occur in oxy-fuel combustion. For conventional combustion processes, model based controllers have been successful at suppressing thermoacoustic instabilities. As a first step towards achieving the same for oxy-fuel combustion, we develop a control relevant model of oxy-fuel combustion. In oxy-fuel combustion CO_2 is used as working medium instead of air. From a control point of view, this gives an extra degree of freedom (compared to conventional combustion control). Analysis on the developed model show that secondary injection of CO_2 close to the flame is probably a better manipulated variable than fuel-injection,

which has been a popular choice for control in conventional combustion processes.

5.1 Introduction

Gas turbines are widely used for power production from gaseous fossil fuels. Although gas turbine engines are relatively clean burning, there is inevitably a production of CO_2 from combustion of fossil fuels. Thus, with today's increasing concern about global warming and climate change, there is an incentive to investigate gas turbine processes with CO_2 capture.

One attractive concept for this is the semi-closed gas turbine cycles using CO_2 as working medium. This process has been studied in e.g Bolland and Saether (1998), Ulizar and Pilidis (1997), Ulfsnes et al. (2003). The concept is based on combustion of natural gas with O_2 in an (inert) CO_2 atmosphere. Hence, the gas leaving the combustion chamber contains (almost) pure CO_2 and water. The water can be removed using a condenser, and we are left with (almost) pure CO_2, of which most is recycled for use as working medium, while to avoid accumulation, some must be removed from the cycle. The removed CO_2 must be compressed for long term safe storage, to have the desired positive effect on the global warming (carbon sequestraion).

While overall process dynamics has been studied in Snarheim et al. (2005), Imsland et al. (2005), in this paper, we concentrate on the dynamics of the combustion chamber. It is known that conventional gas turbine combustion chambers might exhibit detrimental instabilities under some operating conditions (Annaswamy and Ghoniem, 2002). Recent experimental work (Ditaranto and Hals, 2006) indicates that similar instabilities also occur in oxy-fuel combustion, possibly even more severe than in the conventional case.

This gives a clear motivation for studying if it is possible to use active feedback control for alleviating these instabilities for oxyfuel combustion, as has been successfully done for conventional combustion (Annaswamy and Ghoniem, 2002). This paper provides a first step in that direction: We will

first develop a new linear low-order model, inspired by similar models for conventional combustion, for studying the dynamics that are at the root of the observed instabilities. Due to the fact that the number of control degrees of freedom is higher for oxyfuel combustion than for conventional combustion, we thereafter use the developed model to study which of the degrees of freedom is more suitable for active feedback stabilization, and to give indications towards requirements for actuation devices.

The paper is briefly outlined as follows: In Section 5.2 we give some background on combustion instabilities in general, then we proceed to discuss the special case oxy-fuel combustion. The modelling of the process is presented in Section 5.3, while Section 5.4 looks at requirements for the input part of a control system to stabilize the plant. We end the paper with some concluding remarks.

5.2 Thermodynamic instabilities in oxy-fuel combustion

Thermodynamic instabilites have been recognized as a problem in combustion processes for a long time. These instabilities take the form of large pressure oscillations in the combustion chamber. The fact that the coupling between heat release oscillations and acoustic pressure can be a driving mechanism for thermodynamic instabilities was identified as early as 1878 (Rayleigh, 1878). The heat release and acoustics are coupled in a feedback loop, and depending on the phase difference between the signals, the heat release either remove from or add energy to the pressure oscillations, the latter case making the system unstable. Obvious implications of these instabilities are vibrations and mechanical stress that may lead to structural damage and system failure. Alleviating the oscillations might allow for better energy utilization and less pollutant emissions.

Modern (conventional) premixed gas turbines have to operate at very lean conditions due stringent requirements on NO_x emissions. These operating conditions make the gas turbines prone to instabilities, and is an important reason for the attention active control of thermoacoustic instabili-

ties has received recently. This is also reflected in the numerous publications within the field in recent years. Reviews on thermoacoustic instabilities and active control can be found in Annaswamy and Ghoniem (2002), Candel (2002), Dowling and Morgans (2005).

However, when it comes to oxy-fuel, the literature on instabilities is scarce. Experimental results on a laboratory scale combustor are published in Ditaranto and Hals (2006). They show that up to a certain threshold in oxidizer composition (the ratio between oxygen and carbon dioxide in the oxy-fuel mixture), the instability patterns are similar to what is found when burning fuel with air. Above this threshold, however, the instabilities tend to grow even stronger. Figure 5.1 shows sound pressure level plots from the experiments in Ditaranto and Hals (2006). The main oscillation frequencies are easy to identify by the peaks. Due to the geometry of the combustion chamber, there exists several acoustic modes that can be triggered. Which one depends on the operating conditions. This gives a clear incentive to investigate active control strategies for this type of combustion. Moreover, it also indicates that a good controller must be able to reduce pressure oscillations over a broad frequency range, possibly broader than for conventional combustion instabilities.

In oxy-fuel combustion it is possible to change the composition of the oxidizer (the ratio between O_2 and CO_2). Compared to conventional combustion in air, this is the equivalent of changing the ratio between nitrogen and oxygen, which generally is hard and expensive. The difference between plot b) and c) in Figure 5.1 indicates that the oxidizer composition is very important. The difference is only 1% in oxidizer ratio. From a control point of view, this means that for oxy-fuel there exists a new degree of freedom that can be used to stabilize the system. One focus of this paper is to model the effect of perturbations in oxidizer composition, and investigate the use of this variable for control. The extra degree of freedom is illustrated in Figure 5.2.

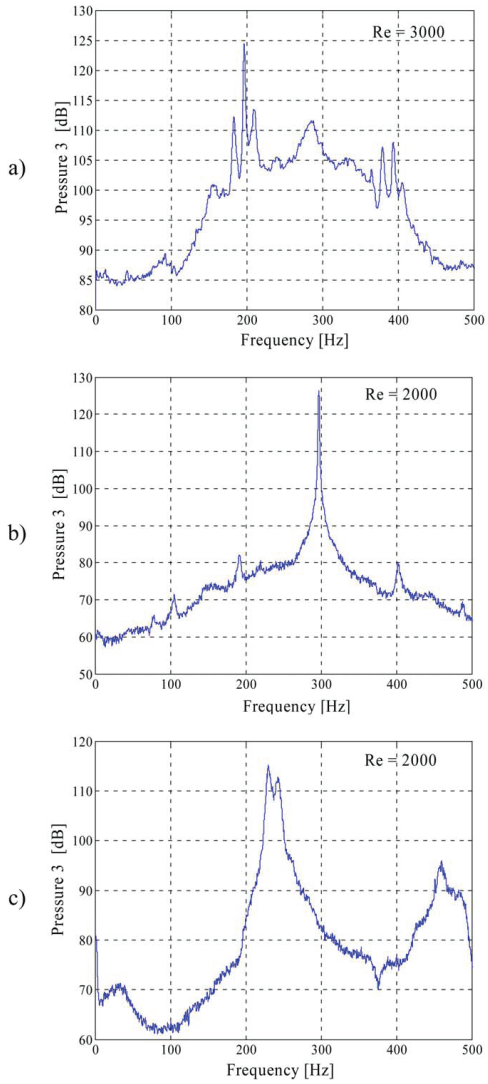

Figure 5.1: Experimental results from oxy-fuel combustor. The triggered frequency and instability peak depend on operating conditions: a) $\lambda_{O_2} = 0.42$, $\phi = 0.9$, Re $= 3000$; b) $\lambda_{O_2} = 0.41$, $\phi = 0.9$, Re $= 2000$; c) $\lambda_{O_2} = 0.42$, Re $= 2000$, $\phi = 0.9$. λ_{O_2} and ϕ are defined in (5.1) and (5.2). (from Ditaranto and Hals (2006)).

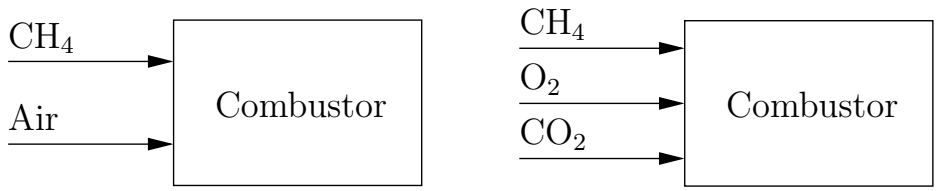

(a) Conventional combustion chamber (b) Oxy-fuel combustion chamber

Figure 5.2: Conceptual difference between a conventional combustion chamber and an oxy-fuel combustion chamber from a control point of view.

5.3 Modelling

In combustion processes there are several components that contribute to the overall dynamics. These include acoustics, fluid dynamics, transport processes, chemical kinetics, flame kinematics, heat transfer, feedline dynamics of the reactants, and atomization and vaporization dynamics. These phenomena are coupled, hence, developing a detailed model of such a complex system is an extremely challenging task (Annaswamy and Ghoniem, 2002). Moreover, such models are not well suited for controller design. For active control of conventional combustion, model-based controllers have proven to supress thermoacoustic instabilites better than empirical controllers. We expect the same to be true for oxy-fuel combustion. Thus, there is a need for low order models of oxy-fuel combustion. A common approach to capture the most important dynamics is to model acoustics, heat release and the coupling between them. A linear form of the wave equation is used for the acoustics. For the heat release dynamics we will use a thin wrinkled flame model developed by Fleifil et al. (1996). This model was extended for perturbations in the equivalence ratio by Hathout et al. (2000), and we will in the following extend it to include perturbations in oxidizer ratio. An early version of the model herein can be found in Nilsen (2006).

The combustion chamber that we model has a rectangular shape with length L and width D. As in Annaswamy et al. (1997) the burner consists of a perforated plate with n_f holes, each with a radius R. In each of these

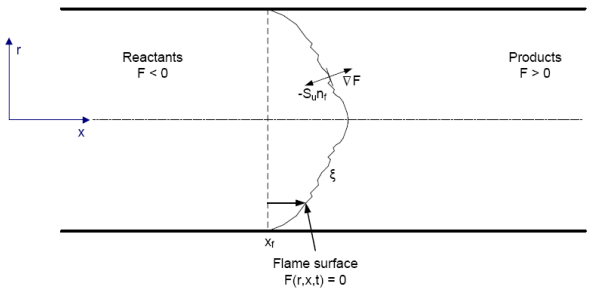

Figure 5.3: The flame front in the combustion chamber.

holes there is a flame at location x_f. Figure 5.3 shows a sketch of one such flame.

One important difference between oxy-fuel combustion and conventional combustion is the possibility of changing the oxidizer composition. To describe the composition we define the oxidizer ratio as

$$\lambda_{O_2} = \frac{n_{O_2}}{n_{O_2} + n_{CO_2}}, \tag{5.1}$$

where n_x refers to the number of moles of component x. Together with the equivalence ratio

$$\phi = \frac{(n_{\text{fuel}}/n_{O_2})_{\text{actual}}}{(n_{\text{fuel}}/n_{O_2})_{\text{stoichiometric}}}, \tag{5.2}$$

and the total mass flow ($\dot{m}_{\text{tot}}$) this gives complete information of the mass flows of the different components.

5.3.1 Heat release

The starting point for the modelling is the flame surface equation from (Fleifil et al., 1996) with modifications to take λ_{O_2} into account

$$\frac{\partial \xi}{\partial t} = u - v\frac{\partial \xi}{\partial r} - S_u\left(\phi, \lambda_{O_2}\right)\sqrt{1 + \left(\frac{\partial \xi}{\partial r}\right)^2}. \tag{5.3}$$

$\xi(r,t)$ is a single-valued function describing the axial displacement of the flamesurface, u is the axial velocity, v is the radial velocity and S_u is the laminar burning velocity. This is illustrated in Figure 5.3. The area of the flame can be found by computing a surface integral of the variable ξ, and the heat release from the flame is assumed to be proportional to the flame area (A_f),

$$Q = \rho_u\left(\phi, \lambda_{O_2}\right) S_u\left(\phi, \lambda_{O_2}\right) \Delta h_r\left(\phi, \lambda_{O_2}\right) A_f, \tag{5.4}$$
$$A_f = 2\pi \int_0^R r\sqrt{1+\left(\frac{\partial \xi}{\partial r}\right)^2}\, dr.$$

Here, ρ_u is the density of the unburnt mixture, Δh_r is the heat of reaction per unit mass of the mixture and R is the radius of the burner. So far the main difference from conventional combustion is that λ_{O_2} enters the equations through ρ_u, Δh_r and λ_{O_2}. We now proceed to extend the model in a similar way as in (Hathout et al., 2000), with necessary modifications for λ_{O_2}.

We assume very small radial velocity and v is thus neglected. Also, ρ_u will not change much with perturbations in ϕ and λ_{O_2} and will hence be assumed constant. We denote mean values as $\bar{\cdot}$ and deviation value as $(\cdot)'$, and linearize (5.3) around $\bar{u}$, $\bar{\phi}$, $\bar{\lambda}_{O_2}$ and $\bar{\xi}$, to get

$$\frac{\partial \xi'}{\partial t} = u' + \bar{S}_u \frac{\partial \xi'}{\partial r} + \frac{\partial \bar{\xi}}{\partial r}\left(\frac{\partial \bar{S}_u}{\partial \phi}\phi' + \frac{\partial \bar{S}_u}{\partial \lambda_{O_2}}\lambda'_{O_2}\right). \tag{5.5}$$

Note here that for brevity we use the notation $\frac{\partial \bar{S}_u}{\partial \phi}$ for $\left.\frac{\partial S_u}{\partial \phi}\right|_{\phi=\bar{\phi},\lambda_{O_2}=\bar{\lambda}_{O_2}}$. Similar notation is used throughout the article. The boundary and initial conditions for ξ' is

$$\xi'(R,t) = 0, \qquad \xi'(r,0) = 0.$$

Similarily, linearization of (5.4) gives

$$Q' = \bar{\kappa}\int_0^R \xi'(r,t)\, dr + d_1\phi' + d_2\lambda'_{O_2}, \tag{5.6}$$

where

$$\bar{\kappa} = 2\pi\rho_u \bar{S}_u \Delta\bar{h}_r,$$

and

$$d_1 = 2\pi\rho_u \left(\bar{S}_u \frac{\partial \Delta\bar{h}_r}{\partial \phi} + \Delta\bar{h}_r \frac{\partial \bar{S}_u}{\partial \phi} \right) \left(\int_0^R \bar{\xi}\,(r)\, dr \right),$$
$$d_2 = 2\pi\rho_u \left(\bar{S}_u \frac{\partial \Delta\bar{h}_r}{\partial \lambda_{O_2}} + \Delta\bar{h}_r \frac{\partial \bar{S}_u}{\partial \lambda_{O_2}} \right) \left(\int_0^R \bar{\xi}\,(r)\, dr \right).$$

Differentiating (5.6) and inserting (5.5) give

$$\dot{Q}' = \bar{\kappa} \int_0^R u' + \bar{S}_u \frac{\partial \xi'}{\partial r} + \frac{\partial \bar{\xi}}{\partial r} \left(\frac{\partial \bar{S}_u}{\partial \phi} \phi' + \frac{\partial \bar{S}_u}{\partial \lambda_{O_2}} \lambda'_{O_2} \right) dr + d_1 \dot{\phi}' + d_2 \dot{\lambda}'_{O_2}, \quad (5.7)$$

which is integrated over r as

$$\dot{Q}' = \bar{\kappa} \left(Ru' - \bar{S}_u \xi'\,(0,t) + d_5 \phi' + d_6 \lambda'_{O_2} \right) + d_1 \dot{\phi}' + d_2 \dot{\lambda}_{O_2}, \quad (5.8)$$

where

$$d_5 = -\xi(0) \frac{\partial \bar{S}_u}{\partial \phi}, \qquad d_6 = -\xi(0) \frac{\partial \bar{S}_u}{\partial \lambda_{O_2}}.$$

To proceed we need an expression for $\xi'\,(0,t)$. This is found by taking the Laplace transform of (5.5) and solving the resulting differential equation in r

$$\xi'\,(r,s) = \left(\frac{u'}{s} + \frac{\partial \bar{\xi}}{\partial r} \left(\frac{\partial \bar{S}_u}{\partial \phi} \frac{\phi'}{s} + \frac{\partial \bar{S}_u}{\partial \lambda_{O_2}} \frac{\lambda'_{O_2}}{s} \right) \right) \left(1 - e^{-(R-r)\frac{s}{\bar{S}_u}} \right). \quad (5.9)$$

Taking the inverse Laplace transform gives

$$\xi'(r,t) = \int_{t-\tau_r}^t u'\,(\tau)\, d\tau + \frac{\partial \bar{\xi}}{\partial r} \frac{\partial \bar{S}_u}{\partial \phi} \int_{t-\tau_r}^t \phi'\,(\tau)\, d\tau + \frac{\partial \bar{\xi}}{\partial r} \frac{\partial \bar{S}_u}{\partial \lambda_{O_2}} \int_{t-\tau_r}^t \lambda_{O_2}\,(\tau)\, d\tau, \quad (5.10)$$

where $\tau_r = \frac{R-r}{\bar{S}_u}$.

As in (Annaswamy et al., 1997) we approximate

$$\int_{t-\tau_r}^{t} u'(\tau)\, d\tau \approx \frac{R-r}{\bar{S}_u} u', \tag{5.11}$$

and in a similar way

$$\begin{aligned} \int_{t-\tau_r}^{t} \phi'(\tau)\, d\tau &\approx \frac{R-r}{\bar{S}_u} \phi', \\ \int_{t-\tau_r}^{t} \lambda'_{O_2}(\tau)\, d\tau &\approx \frac{R-r}{\bar{S}_u} \lambda'_{O_2}. \end{aligned} \tag{5.12}$$

Using these approximations in (5.10), then inserting in (5.6) and solving the resulting integral gives

$$Q' = \frac{\kappa R}{2} \frac{R}{\bar{S}_u} u' + \left(d_1 + \frac{\kappa R}{2\bar{S}_u} d_5 \right) \phi' + \left(d_2 + \frac{\bar{\kappa} R}{2\bar{S}_u} d_6 \right) \lambda'_{O_2}. \tag{5.13}$$

If we now evaluate $\xi'(0,t)$ using the approximations in (5.11) and (5.12) we obtain

$$\xi'(0,t) = \frac{R}{\bar{S}_u} u' + d_3 \frac{R}{\bar{S}_u} \phi' + d_4 \frac{R}{\bar{S}_u} \lambda'_{O_2}, \tag{5.14}$$

where

$$d_3 = \frac{\partial \bar{\xi}}{\partial r}|_{r=0} \frac{\partial S_u}{\partial \phi}|_{\bar{\phi}\bar{\lambda}_{O_2}}, \qquad d_4 = \frac{\partial \bar{\xi}}{\partial r}|_{r=0} \frac{\partial S_u}{\partial \lambda_{O_2}}|_{\bar{\phi}\bar{\lambda}_{O_2}}.$$

We then get an expression for u' from (5.13) and insert it in (5.14) resulting in

$$\begin{aligned} \xi'(0,t) = \frac{2Q'}{\kappa R} &- \frac{2}{\kappa R} \left(d_1 + \frac{\kappa R}{2\bar{S}_u} d_5 - \frac{\kappa R^2}{2\bar{S}_u} d_3 \right) \phi' \\ &- \frac{2}{\kappa R} \left(d_2 + \frac{\kappa R}{2\bar{S}_u} d_6 - \frac{\kappa R^2}{2\bar{S}_u} d_4 \right) \lambda'_{O_2}. \end{aligned} \tag{5.15}$$

Now this equation can be inserted into (5.8) to arrive at

$$\dot{Q}' + \frac{2\bar{S}_u}{R}Q' = \kappa R u' - \left(\frac{2\bar{S}_u}{R}d_1 - \frac{\kappa R}{\bar{S}_u}d_3\right)\phi' - \left(\frac{2\bar{S}_u}{R}d_2 - \frac{\kappa R}{\bar{S}_u}d_4\right)\lambda'_{O_2} + d_1\dot{\phi}' + d_2\dot{\lambda}_{O_2}. \quad (5.16)$$

5.3.2 Acoustics

We consider a tube with length L and use a one-dimensional wave equation to describe the pressure fluctuations $p' = p - \bar{p}$.

$$\frac{\partial^2 p'}{\partial t^2} - \bar{c}^2\frac{\partial^2 p'}{\partial x^2} = (\gamma - 1)\frac{\partial q'}{\partial t}(x,t).$$

p is pressure, q is the heat release per unit area $\left(q = \frac{Q}{\pi(D/2)^2}n_f\right)$, c is the speed of sound and γ is the specific heat ratio. The pressure oscillations are coupled to velocity perturbations by

$$\frac{\partial p'}{\partial t} + \gamma\bar{p}\frac{\partial u'}{\partial x} = (\gamma - 1)\, q'. \quad (5.17)$$

The combustion chamber is closed at the inlet and open at the outlet, resulting in the following boundary conditions

$$p'(L,t) = 0,$$
$$u'(0,t) = 0.$$

The wave equation is discretized using the Galerkin expansion

$$p'(x,t) = \bar{p}\sum_{i=1}^{n}\psi_i(x)\eta_i(t),$$

where $\psi_i(x)$ and $\eta_i(t)$ are modal shape and amplitude, $\psi_i(x) = \cos(k_i x)$. Using this expansion within the wave-equation and integrating over the combustor length (L) gives as in (Annaswamy et al., 1997)

$$\ddot{\eta}_i + \omega_i^2 \eta_\iota = \tilde{b}_i \dot{q}'_f,$$

where $\tilde{b}_i = \gamma a_0 \psi(x_f)/E$, $E = \int_0^L \psi_i^2(x)\,dx$, $a_0 = \frac{\gamma-1}{\gamma\bar{p}}$ and $\omega_i = k_i\bar{c}$. As in (Hathout et al., 2000) we also add a damping term ζ to account for heat and friction losses within the combustor

$$\ddot{\eta}_i + 2\zeta\omega_i\dot{\eta}_i + \omega_i^2\eta_i = \tilde{b}_i\dot{q}'_f, \tag{5.18}$$

In a similar way the Galerkin expansion is used on equation (5.17). Integration over the combustor length L then gives

$$u' = \sum_{i=1}^{n} \tilde{c}_i\dot{\eta}_i + \theta a_0 q' + u_c,$$

where $\tilde{c}_i = \frac{1}{\gamma k_i^2}\frac{d\psi_i}{dx}(x_f)$, $a_0 = (\gamma-1)/\gamma\bar{p}$ and θ represents the effect of the velocity ahead and behind the flame on q' and u_c is the velocity added by potential secondary injectors. We assume perfect mixing of the components in the unburnt mixture, and thus the pressure oscillations have no effect on the equivalance ratio (ϕ) and the oxidizer ratio (λ_{O_2}). Inserting the velocity relation into (5.16) gives

$$\dot{Q}' + \left(\frac{2\bar{S}_u}{R} - \kappa R\theta a_0 \frac{n_f}{A_c}\right) Q' = \kappa R \sum_{i=1}^{n} \tilde{c}_i\dot{\eta}_i + \kappa R u_c - \left(\frac{2\bar{S}_u}{R}d_1 - \frac{\kappa R}{\bar{S}_u}d_3\right)\phi' - \left(\frac{2\bar{S}_u}{R}d_2 - \frac{\kappa R}{\bar{S}_u}d_4\right)\lambda'_{O_2} + d_1\dot{\phi}' + d_2\dot{\lambda}_{O_2}. \tag{5.19}$$

As the flame is nearly conical, the slope at the tip will be close to zero. As d_3 and d_4 are proportional to the derivative of the mean flameshape at $r = 0$, they are close to zero and can be neglected. The resulting heat relase model then becomes

$$\dot{Q}' + \left(\frac{2\bar{S}_u}{R} - \kappa R\theta a_0 \frac{n_f}{A_c}\right) Q' = \kappa R \sum_{i=1}^{n} \tilde{c}_i\dot{\eta}_i + \kappa R u_c - \frac{2\bar{S}_u}{R}d_1\phi' - \frac{2\bar{S}_u}{R}d_2\lambda'_{O_2} + d_1\dot{\phi}' + d_2\dot{\lambda}_{O_2}. \tag{5.20}$$

5.3.3 Actuators

In this paper we study the use of secondary injectors to control the system. We choose to not model the dynamics of the actuators. This in spite of the fact that the dynamics of the actuators are important because their bandwidth will typically be close to the unstable frequencies they are used to stabilize. However, the actuator dynamics will have similar influence on all the inputs, and will not be important in the choice of manipulated variables for the system. The actuator dynamics will also be dependent on the specific valve chosen to actuate the system. Instead we use the model to analyse which requirements there will be on the actuators to be able to stabilize the system (see Section 5.4).

However, we do need linear relations between ϕ', λ'_{O_2} and the different mass flows (w). Starting with the definition of λ_{O_2} and ϕ ((5.1) and (5.2)), linearization around the operation point gives

$$\begin{aligned} \phi' &= \frac{1}{\bar{w}_{O_2}\alpha_0} w'_{CH_4} - \frac{\bar{\phi}}{\bar{w}_{O_2}} w'_{O_2}, \\ \lambda'_{O_2} &= \frac{1-\bar{\lambda}_{O_2}}{\alpha_1 \mathrm{MW}_{O_2}} w'_{O_2} - \frac{\bar{\lambda}_{O_2}}{\alpha_1 \mathrm{MW}_{CO_2}} w'_{CO_2}. \end{aligned} \tag{5.21}$$

where $\alpha_0 = \left(\frac{w_{CH_4}}{w_{O_2}}\right)_{\text{stoichiometric}}$, $\alpha_1 = \frac{\bar{w}_{O_2}}{\mathrm{MW}_{O_2}} + \frac{\bar{w}_{CO_2}}{\mathrm{MW}_{CO_2}}$ and MW_x is the molecular weight of compononent x. Then remembering that we have n_f holes with radius R, we get the following equation for u_c

$$u_c = \frac{\left(w'_{CH_4} + w'_{O_2} + w'_{CO_2}\right)}{\rho_u n_f \pi R^2}.$$

There will also be a transport delay (τ_c) assosciated with convection from the injector to the burning zone, $\tau_c = L_c/\bar{u}$, where L_c is the distance from the injector to the burning zone.

5.3.4 Heat of reaction and flame speed

The heat of reaction is the maximum heat release per kg fuel that can occur within the combustor. We calculate it using the lower heating value (LHV)

for methane, $\Delta h_r = \mathrm{LHV}_{CH_4} m_{CH_4}/m_{\mathrm{tot}}$. We can express Δh_r as a function of ϕ and λ_{O_2},

$$\Delta h_r = \mathrm{LHV}_{CH_4} \frac{\phi\lambda_{O_2}\mathrm{MW}_{CH_4}}{2\lambda_{O_2}\mathrm{MW}_{O_2} + 2\mathrm{MW}_{CO_2}(1-\lambda_{O_2}) + \phi\lambda_{O_2}\mathrm{MW}_{CH_4}}.$$

We can now calculate the partial derivates of Δh_r that enter the model equations

$$\frac{\partial \Delta h_r}{\partial \phi} = \mathrm{LHV}_{CH_4} \frac{2\lambda_{O_2}\mathrm{MW}_{CH_4}\left(\mathrm{MW}_{CO_2}(1-\lambda_{O_2}) + \lambda_{O_2}\mathrm{MW}_{O_2}\right)}{\left(2\lambda_{O_2}\mathrm{MW}_{O_2} + 2\mathrm{MW}_{CO_2}(1-\lambda_{O_2}) + \phi\lambda_{O_2}\mathrm{MW}_{CH_4}\right)^2},$$

$$\frac{\partial \Delta h_r}{\partial \lambda_{O_2}} = \mathrm{LHV}_{CH_4} \frac{2\phi\mathrm{MW}_{CH_4}\mathrm{MW}_{CO_2}}{\left(2\lambda_{O_2}\mathrm{MW}_{O_2} + 2\mathrm{MW}_{CO_2}(1-\lambda_{O_2}) + \phi\lambda_{O_2}\mathrm{MW}_{CH_4}\right)^2}.$$

As these equations only enter the model as constants, it is not necessary to linearize them.

It seems difficult to derive analytical expressions for S_u that use thermodynamic property tables. We chose instead to perform equilibrium calculations using a methane mechanism (GRI 3.0) to generate a lookup table for S_u. Curvefitting of this data was then used as a model. Figure 5.4 shows this relation, where the $\phi = 1$ line has been published in Ditaranto and Hals (2006). Note that S_u varies significantly more with λ_{O_2} than with ϕ. In a conventional combustion process, where λ_{O_2} is 21%, and ϕ may change, S_u is close to constant. On the other hand, for oxy-fuel combustion S_u can vary a lot, and we expect this to have an impact on the controllability of the process.

Based on the curvefits we obtain the following equations for the partial derivatives of S_u.

$$\frac{\partial S_u}{\partial \phi} = 1.7923\lambda_{O_2}^2 - 0.3780\phi\lambda_{O_2} + 0.43\lambda_{O_2} - 0.1930,$$

$$\frac{\partial S_u}{\partial \lambda_{O_2}} = 3.5846\phi\lambda_{O_2} - 0.1890\phi^2 + 0.43\phi + 2.837\lambda_{O_2}.$$

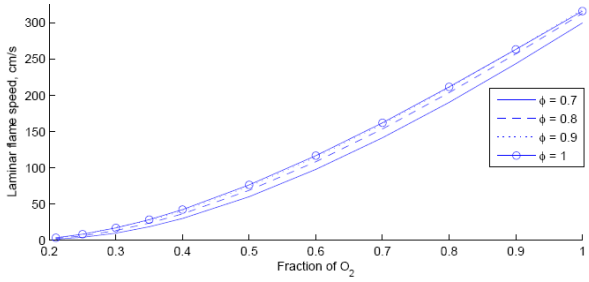

Figure 5.4: The laminar flames speed (S_u) as a function of equivalence ratio and oxidizer ratio.

5.3.5 Implementation and model validity

The complete model was implemented in Simulink using two modes for the acoustics. We kept the inputs on velocity form (du/dt), resulting in the following input vector $u = \begin{bmatrix} \dot{u}'_c & \dot{\phi} & \dot{\lambda}_{O_2} & \dot{w}_{CH_4} & \dot{w}_{O_2} & \dot{w}_{CO_2} \end{bmatrix}$, and used a similar geometry as in Annaswamy et al. (1997). The length of the combustion chamber $L = 0.49\,\mathrm{m}$, the width is $D = 0.04\,\mathrm{m}$ and the flame is located at $x_f = 0.24\,\mathrm{m}$. The chamber consists of $n_f = 80$ burners, each with a radius $R = 0.75\,\mathrm{mm}$. The cost of oxygen implies operation at close to stoichiometric conditions (Ditaranto and Hals, 2006). Thus we choose to operate the system near $\phi = 1$ and $\lambda_{O_2} = 0.35$. Based on this we can calculate $\bar{c} = 310.6$, $\rho_u = 1.47\,\mathrm{kg}/\mathrm{m}^3$ and $\Delta\bar{h}_r = 3.315\mathrm{MJ}/\mathrm{kg}$. We use $\bar{p} = 10^5\,\mathrm{Pa}$, $\gamma = 1.4$, , $\theta = 0.5$ and $\zeta = 0.01$.

As the literature on dynamics in oxy-fuel combustion is scarce, it is difficult to find data for validation of the model. Due to the need to keep the model simple (low order) and because we use a linear model, there are certain effects that the model cannot capture. Figure 5.5 shows the response of the uncontrolled system to a disturbance in the oxidizer ratio λ_{O_2}. The system is clearly unstable. In real combustion processes, the pressure os-

cillations will enter a limit cycle, an effect that this model cannot capture. If we look back at Figure 5.1, we cannot do similar sound pressure level calculations based on the model output. To calculate the sound pressure level only makes sense when the pressure oscillations are limited by a limit cycle. We can, however, use Fourier transforms to calculate the frequency of the oscillations. In Figure 5.5 the system oscillates with a frequency equal to $\omega_2 \approx 3000\,\mathrm{rad}\,/\,\mathrm{s}$, indicating that it is the second mode of the combustor that is unstable. Also note that there is a low frequency oscillation that brings the system back to zero, before the high frequency oscillations grows large. This is because the first acoustic mode is stable. If we look back at the experimental results (Figure 5.1), the unstable frequency differs for the different operating points. This is due to the geometry in the burner, where there exist modes based on the whole combustor length, and on the length of the premixing chamber and burning chamber only. A more advanced model for acoustics will be able to represent this. The growth rate of the instability is dependent on the damping ζ in (5.18). For $\zeta > 0.039$ the model becomes stable.

5.3.6 Scaling

To be able to compare the different manipulated variables available in the system, scaling is necessary. With scaling the process gains from the different manipulators will be comparable. We choose to scale the system by the manipulators influence on ϕ and λ_{O_2}. This ensures that the system is operated close to the operating point it was designed for. The following bounds are used on ϕ and λ_{O_2}

$$\left|\phi'\right|_{\max} = 0.05, \qquad \left|\lambda'_{O_2}\right|_{\max} = 0.05.$$

We then use the relations between each of the mass flows and ϕ, λ_{O_2} (5.21) to scale each of the mass flows so that they independently cannot

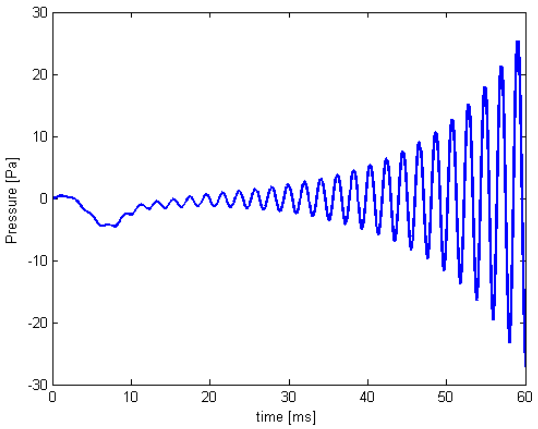

Figure 5.5: Response of uncontrolled system to a disturbance in λ_{O_2}.

violate the bounds on ϕ and λ_{O_2}. This gives

$$\begin{aligned}
\left|w'_{CH_4}\right|_{\max} &= \bar{w}_{O_2}\alpha_0 \left|\phi'\right|_{\max}, \\
\left|w'_{CO_2}\right|_{\max} &= \left(\frac{\bar{\lambda}_{O_2}}{\alpha_1 M_{CO_2}}\right)^{-1} \left|\lambda'_{O_2}\right|_{\max}, \\
\left|w'_{O_2}\right|_{\max} &= \max\left\{\left(\frac{\bar{\phi}}{\bar{w}_{O_2}}\right)^{-1} \left|\phi'\right|_{\max}, \left(\frac{1-\bar{\lambda}_{O_2}}{\alpha_1 M_{O_2}}\right)^{-1} \left|\lambda'_{O_2}\right|_{\max}\right\}.
\end{aligned}$$

The bound on u_c is then dependent on the largest mass flow. Looking at the numerical values for the scaling reveals that this is w'_{CO_2}, resulting in $|u_c|_{\max} = \frac{\left|w'_{CO_2}\right|_{\max}}{\rho_u n_f \pi R^2}$. We then collect all the scaling factors in a scaling vector D_u. If we denote the original system by $\hat{G}$, the scaled system is $G = \hat{G}D_u$. Note here that the actual manipulated variables are the derivatives on the variables we used for the scaling process. Differentiating the variables should have the same effect on all inputs, thus the relation between the

variables will remain the same. However this means that the scaling does not have the effect that all inputs are limited to be between -1 and 1.

5.4 Model analysis

In this section we will study the input part of the system. The variable we wish to control is the pressure (p'), which is relatively easy to measure. Other alternatives, for instance Q', are also possible. However, stabilization of p' will lead to stabilization of Q'. Based on the derived model, we will look at bandwidth requirements for the injectors, and how close to the flame we have to place the injectors to achieve good control. There are three different mass streams that can be used to manipulate the system. As mentioned earlier it is special for oxy-fuel that the composition of the oxidizer can be changed. We will use the developed model to investigate how the CO_2 stream compares to the other mass flows. It is also possible to use a combination of inputs to control the process. Because ϕ, λ, and u_c enters the model equations directly and are examples of such combinations, we will include these in the analysis. We choose to use the derivatives of the streams as inputs. The resulting model we use for analysis have 6 different inputs , $u = \begin{bmatrix} \dot{u}_c' & \dot{\phi} & \dot{\lambda}_{O_2} & \dot{w}_{CH_4} & \dot{w}_{O_2} & \dot{w}_{CO_2} \end{bmatrix}$.

5.4.1 Poles and zeros

The location of the poles and zeros of a plant G provides information about how easy it is to control G. The developed model has a pair of conjugate RHP-poles (right half plane) located at $p = 0.1129 \pm 3.0205i$. To stabilize a plant with RHP-poles, we need to react sufficently fast, and we must require that the closed loop bandwidth is larger than $\omega_c > 0.67\left(x + \sqrt{4x^2 + 3y^2}\right)$ for a pair of complex RHP-poles $p = x \pm jy$ (Skogestad and Postlethwaite, 2005). Thus we get a lower bound on $\omega_c = 3564\,\mathrm{rad/s}$. However, all the inputs except $\dot{u}_c'$ have zeros located close to $z = 750\,\mathrm{rad/s}$. RHP-zeros will always imply an inverse response in the time domain, and thus limit the achievable bandwidth. Using a low-frequency performance weight,

(Skogestad and Postlethwaite, 2005) gives $\omega_c < z/2 = 375\,\mathrm{rad/s}$ as an upper bound on the achievable bandwidth. It is of course impossible to satisfy both of these bounds, which means that this plant is difficult to control. All the inputs also have a set of zeros located at the imaginary axis, which again implies control problems at steady state (a RHP-zero z will give a very small gain at frequencies close to z).

Thus, one might consider tight control at frequencies sufficently higher than z. In this case the zero will give a lower bound on the bandwidth. By using a performance weight for tight control at high frequencies, Skogestad and Postlethwaite (2005) gives $\omega_c > 2z = 1500\,\mathrm{rad/s}$ as a lower bound on the bandwidth. As the focus in this application is to reduce high frequency oscillations, it makes sense to use this performance limitation. Thus it is the RHP-poles that determine the limit on lower bandwidth. Conversion to Hz gives 570 Hz as the bandwidth limitation. This is a very high bandwidth and might be problematic. In general solenoid valves have been popular for active control of combustion. For instance, the MOOG D633 DDV valve have been used in several experiments, and Bernier et al. (2003) showed that this valve had a flat frequency response up to 380 Hz. An alternative is to use magnetostrictive valves, for instance Sattinger et al. (2000) used a valve from Etrama Products Inc. with a bandwidth of 1000 Hz. Thus there should exist valves that are fast enough. Another problem is of course that the high bandwidth limits the complexity of the controller to be used.

5.4.2 Time delay

Depending on the location of the injectors, there will be a time delay associated with the transport of input changes to the flame zone, $\tau_c = L_c/\bar{u}$, where L_c is the distance from the injector to the burning zone. The time delay will impose a serious limitation on the achievable bandwidth, because every control action will be delayed by τ_c. An upper bound for the achievable bandwidth in a plant with a time delay θ is derived in Skogestad and Postlethwaite (2005) as $\omega_c < 1/\theta$. Figure 5.6 shows the minimum bandwidth requirement as a function of distance between injector and flameholder. As the poles already give a necessary bandwidth of about

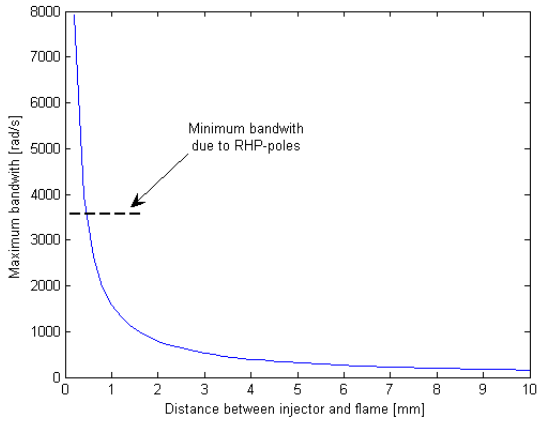

Figure 5.6: The bandwidth limitation imposed by a time delay due to the distance between injector and flame.

3500 rad / s, there is not much freedom in choosing the injector location. To satisfy the bound imposed by the RHP-poles, we need $L_c < 0.5$ mm. This is a very difficult requirement to handle, and in practice one will probably have to violate it. A time delay is a phenomena that might lead to oscillations if the design bandwidth of the controller is too high (too large gain). However, since setpoint control is not an objective and there is considerable measurement noise, these oscillations might not be too serious in closed loop operations. An example of control of a conventional combustion process with large time delay can be found in Hathout et al. (2000).

A problem that might occure when L_c is small, is poor mixing. When using fuel injectors, this have resulted in generation of hot spots on the flame surface, due to pockets of pure fuel entering the flamezone. In additon to hot spots, secondary diffusion flames due to poor mixing were reported in Hathout et al. (2002). If one use CO_2 injectors for control, the opposite might occur. Pockets of CO_2 might cause the flame temperature to be reduced. However, this is probably not as problematic as the hot spots.

Anyway, the injector placement will always be a trade-off between good mixing and problems related to time delay.

5.4.3 Manipulated variables

With the system scaled as in Section 5.3.6, we can compare the different manipulated variables control authority by investigating their process gain. According to Skogestad and Postlethwaite (2005) we should choose manipulators with a high gain at frequencies where control is needed. For a system with a single output, comparing the gains give the same results as relative gain array (RGA) analysis. Figure 5.7 shows a Bode plot for the for the transfer function between mass flows, $\dot{w}_{CH_4}$, $\dot{w}_{O_2}$ and $\dot{w}_{CO_2}$, and the pressure p'. We recognize the RHP-poles and zeros from the sharp peaks in the Bode plots.

The Bode plot shows that the gain is largest for $\dot{w}_{CO_2}$. This indicates that $\dot{w}_{CO_2}$ should be prefered as a manipulated variable over $\dot{w}_{CH_4}$, which is the common manipulated variable in active control of conventional combustion processes. It might seem surprising that $\dot{w}_{O_2}$ has the lowest gain. This is the only variable that can influence both ϕ and λ_{O_2}. However, if we look at (5.21) we see that it enters ϕ and λ_{O_2} with opposite signs. As these variables enter (5.20) with the same sign, increasing ϕ and λ_{O_2} tend to cancel each other. Why the gain is larger for $\dot{w}_{CO_2}$ can also be understood from the model equations. If we look back at Figure 5.4 we see that S_u has a much stronger dependance on λ_{O_2} than ϕ. A consequence is that d_2 is larger than d_1, and when we look at equation (5.20) we see that these are the constants that decide the gains of the system.

It is also possible to use several injectors simultanously to control the system. This will result in a more complex control structure and plant. However, if the gain from such an input is much higher than for the mass flows, one might consider to use such an input. Examples of such combinations are $\dot{\phi}$, $\dot{\lambda}_{O_2}$, and $\dot{u}_c$. Figure 5.8 shows the Bode plots for these variables. The only variable that has a gain comparable to $\dot{w}_{CO_2}$ is $\dot{\lambda}_{O_2}$. However, as there is not much to be gained, we prefer $\dot{w}_{CO_2}$ as the controlled variable for the system. It is somewhat surprising that using several

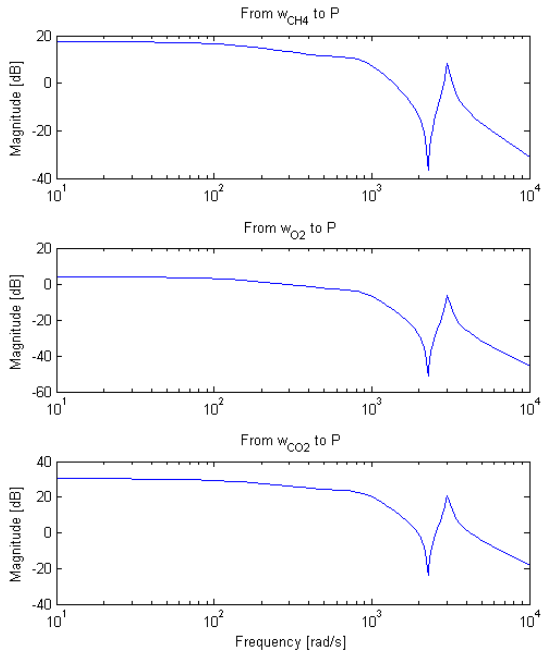

Figure 5.7: Bode plots for transfer function between $\dot{w}_{CH_4}$, $\dot{w}_{O_2}$, $\dot{w}_{CO_2}$ and p'

injectors do not give better control authority. However, other combinations of injectors might perform better than the ones analyzed.

There exists other advantages with using $\dot{w}_{CO_2}$ as the input, which is not revealed by the model. First, oxy-fuel will be used in processes where CO_2 is captured, thus the usage of CO_2 is free. Because we operate at near stoichiometric conditions, the usage of either $\dot{w}_{O_2}$ or $\dot{w}_{CH_4}$ will result in either incomplete combustion, or combustion with excess of oxygen. As both fuel and oxygen cost money, they are less desirable as inputs. Also, use of CO_2 does not influence the total amount heat produced in the combustion, and will therefore not cause significant fluctuations in power production in

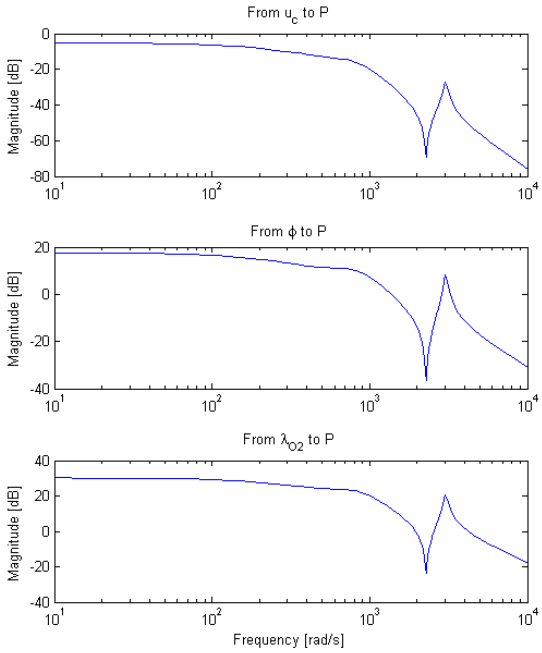

Figure 5.8: Bode plots for transfer function between $\dot{u}_c$,$\dot{\phi}$, $\dot{\lambda}_{O_2}$ and p'

for instance a gas turbine.

5.5 Conclusions

We have presented a linear low order model suitable for active control of oxy-fuel combustion. Analysis on this model shows that a secondary injector modulating a CO_2 stream can perform better than fuel injection, which has been a popular choice for active control of conventional combustion processes. The analysis also shows that oxy-fuel combustion is difficult to control, especially due to high bandwidth requirements and transport delays. A natural continuation of this work will be to use the derived model

to design a model based controller. Also, the model should be validated with experimental data, and ultimately pilot experiments should be performed.

Chapter 6

Active control of oxy-fuel combustion using preflame CO_2-injection

This chapter is based on Snarheim et al. (2009b), as accepted for European Control Conference (2009), Budapest, Hungary.

Abstract

Thermoacoustic instabilities in combustion processes have received considerable of attention in recent years. Coupling between heat release from the flame and acoustic, causes large high frequency pressure oscillations that are unwanted. The most promising way to stabilize such a system, is to perturb the system by injecting small amounts of gas close to the flame. To allow the injected gas to mix well with the main flow before burning, the injector must be placed upstream of the flame. This introduces an unwanted time delay due to transport of injected gas to the flame, and because of the high frequency of the unstable oscillations, even small time delays can be a problem. In this paper we focus on control of a low order oxy-fuel combustion model with a time delay. We apply a procedure that can calculate

the intervals of time-delays for which the system can be stabilized. This is useful during design of the combustion chamber, as it allows us to place the injector at an optimal location. For the low order model, it also gives us exact knowledge about how much operating conditions of the combustion chamber can change, before the controller becomes unable to stabilize the system. Further it allows us to find controller tunings that can handle a wide range of time-delays, and are robust toward modeling errors.

6.1 Introduction

The motivation of this paper is stabilization of an oxy-fuel combustion process. Oxy-fuel means that the fuel is burnt in a CO_2/O_2 mixture instead of air. The use of oxy-fuel is central in several suggested future power plants to achieve zero CO_2 emissions. More details about oxy-fuel can be found in Bolland and Saether (1998), Snarheim et al. (2007). While we choose to focus on an oxy-fuel process in this paper, the results will also be of interest for a conventional combustion process, as the dynamics of the two processes are similar.

Thermodynamic instabilities have been recognized as a problem in combustion processes for a long time. These instabilities take the form of large pressure oscillations in the combustion chamber. The fact that the coupling between heat release oscillations and acoustic pressure can be a driving mechanism for thermodynamic instabilities was identified as early as 1878 (Rayleigh, 1878). The heat release and acoustics are coupled in a feedback loop, and depending on the phase difference between the signals, the heat release either remove from or add energy to the pressure oscillations, the latter case making the system unstable. Obvious implications of these instabilities are vibrations and mechanical stress that may lead to structural damage and system failure. Alleviating the oscillations might allow for better energy utilization and less pollutant emissions.

Modern (conventional) premixed gas turbines have to operate at very lean conditions due stringent requirements on NO_x emissions. These operating conditions make the gas turbines prone to instabilities (Annaswamy

and Ghoniem, 2002), and is an important reason for the attention active control of thermoacoustic instabilities has received recently. This is also reflected in the numerous publications within the field in recent years. Reviews on thermoacoustic instabilities and active control can be found in Annaswamy and Ghoniem (2002), Candel (2002), Dowling and Morgans (2005).

The goal when using active control for a combustion process, is to reduce the amplitude of the pressure oscillations. This can be done by modulating the system such that the phase relation between heat release from the flame and acoustics, removes energy from the system. To modulate the system, one can use either a loudspeaker or injection of gas. While loudspeakers have been used successfully on laboratory scale combustors, they are not sufficiently robust for industrial use, and their power consumption may become to large for an industrial application (Dowling and Morgans, 2005). We therefore choose to focus on injection.

There are two possibilities for injection; one can inject directly into the flame, or upstream of the flame. Injecting directly into the flame will not allow the injected gas to mix with the main flow before burning. This can cause hot spots on the flame surface, and secondary diffusion flames (Hathout et al., 2000). Injection upstream of the flame gives better mixing, but will cause a time delay due to transport of the injected gas to the flame (see Figure 6.1).

Because of the high frequency (typically several hundred Hz) of the pressure oscillation, even small time delays can be a problem. However, if the time delay is taken into account during controller design, it is still possible to stabilize the system. In conventional combustion processes, it is common to use fuel as the injected gas. For oxy-fuel processes, there is an alternative in CO_2. In Snarheim et al. (2007) it was found that CO_2-injection is a promising actuator for oxy-fuel processes. The main benefits are that it is free (because CO_2 is captured in the process), and as it is an inert substance, it does not manipulate the equivalence (air/fuel) ratio. For oxy-fuel processes it is important (from an economical perspective) to operate at near stoichiometric operating conditions to avoid oxygen in the exhaust. Therefore, we choose to use CO_2 injection to control the system.

In this paper we focus on robustness analysis of the system shown in Figure 6.1, using a linear controller. This means studying the following problems;

1. Find the set of controller tunings that stabilize the system, and the associated time delay margins for which the system remains stable.

2. Find how much model parameters can change, before the system becomes unstable.

The solution to these problems helps addressing several questions. The most important is where to place the injector. One wants the injector to be placed as far from the flame as possible, to ensure good mixing of the reactants before burning. However, the injector must be placed such that the system can be stabilized. As the time delay is a function of both injector location (L) and operating conditions ($\bar{U}$, see Figure 6.1), the injector should be placed in such a way that it is robust toward changes in $\bar{U}$. Solving 1) and 2) also lets us quantify how much $\bar{U}$ can change before the system becomes unstable. It will also give us the possibility to tune the controller such that it maximizes robustness toward changes in $\bar{U}$ and modeling errors.

We choose to focus on robustness rather than nominal performance in this paper. A usual performance measures for a combustion process is how fast the system is stabilized (i.e bandwidth). In practice nominal bandwidth is not critical as the dynamics are fast. Hence robustness, i.e the ability to stabilize the system for a variety of disturbances and operating conditions is the critical measure.

For control, we will use a linear controller that is simple to analyze. A natural choice is then to use a PID-controller. However, as the control goal is only to reduce the amplitude of the pressure oscillations in the combustion chamber, integral action is not necessary. This leaves us with a PD controller.

The paper is briefly outlined as follows: In Section 6.2 we present the model for which we will do the control analysis. Then we present the method we will use to analyse the controlled system in Section 6.3. The results of

the analysis are presented in Section 6.4 and discussed in Section 6.5. We end the paper with some concluding remarks.

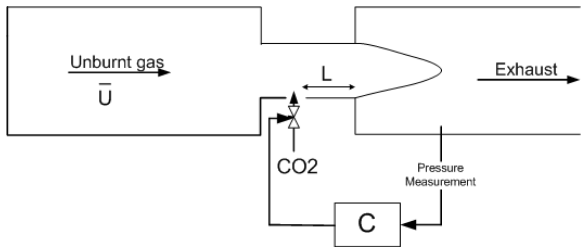

Figure 6.1: Sketch of combustion chamber controlled with CO_2-injection. Unburnt gas enters the combustion chamber with a mean velocity $\bar{U}$. To stabilize the system, CO_2 is injected at a distance L from the flame. The time delay due to transport from injector to flame is given by $\tau = L/\bar{U}$.

6.2 Model

A common way to model combustion processes is to model the heat-release from the flame, the acoustics and the coupling between them. For the heat-release we will use a thin wrinkled flame model, first presented in Fleifil et al. (1996). The acoustics are modeled using a one-dimensional wave-equation, which is discretized using a Galerkin expansion. Due to page-limitations we will not present the modeling here, but details can be found in Snarheim et al. (2007) where a linear model for oxy-fuel combustion is presented. We will use a slightly modified version of this model,

$$\ddot{\eta}_i + 2\zeta\omega_i\dot{\eta}_i + \omega_i^2\eta_i = \frac{\tilde{b}_i}{\pi R^2}\left(\bar{\kappa}\left(R\sum_{i=1}^{n}\tilde{c}_i\dot{\eta}_i + Ru_c + d_6\lambda'_{O_2}\right) + d_2\dot{\lambda}_{O_2}\right), \tag{6.1}$$

where η_i is the dynamics for the i'th acoustic mode and ω_i is the oscillation frequency associated with the mode, and ζ is damping. Further, $\tilde{b}_i$, $\tilde{c}$, κ,

R, d_1 and d_2 are constants depending on the geometry of the combustion chamber and composition of the gas mixture entering the flame. The inputs to the system are perturbations in the injected gas mass flow rate (u_c), and perturbations in the O_2/CO_2 composition due to injection of CO_2 (λ'_{O_2}). For analysis, we will use a model containing only one acoustic mode ($n = 1$), the unstable one. Moreover, we will also assume that perturbations in λ_{O_2} are small and can be neglected. We will also add a time-delay $\tau = L/\bar{U}$, where L is the distance between the injector and flame, and $\bar{U}$ is the mean velocity of the gas at the injector location. Injector dynamics are not considered. With the assumptions above, we can model the combustion process as a second order transfer function

$$G(s) = \frac{K}{s^2 - 2\zeta\omega_0 s + \omega_0^2} e^{-\tau s}, \qquad \zeta > 0, \tag{6.2}$$

where K is the process gain and ω_0 is the unstable frequency. The output of the model is pressure fluctuations around the mean pressure, and the input is the flow rate of injected CO_2.

6.3 Control and stability

In this section we will focus on how a combustion process with one unstable acoustic mode can be controlled using a pre-flame CO_2 injector. Active control using pre-flame injection was also considered in Hathout et al. (2000). They used a controller based on the Smith predictor. In Morgans and Dowling (2007) a combustion model with a time delay was controlled using a PD controller. However, the time-delay considered was due to the modeling of flame dynamics. Stability was proved using a Nyquist plot. The PD controller has a clear motivation as it can provide a much needed phase lift around the unstable frequency. We will therefore use a filtered PD-controller to control the system (6.2)

$$C(s) = K_p \frac{1 + T_d s}{1 + \alpha T_d s}.$$

We now get the following transfer function for the controlled combustor

$$G(s) = \frac{K}{s^2 - 2\zeta\omega_0 s + \omega_0^2} \frac{K_p(1 + T_d s)}{1 + \alpha T_d s} e^{-\tau s}. \tag{6.3}$$

Our goal is now to find for which ranges of time-delays this controller is stable. Further, we want to investigate robustness toward modeling errors in the process parameters ζ, ω_0 and K. To do this, it is convenient to express the closed loop system as a differential-difference equation

$$\dot{x}(t) = A_0 x(t) + \sum_{k=1}^{q} A_k x(t - k\tau), \qquad \tau > 0, \tag{6.4}$$

where q is the number of time delays. For the model (6.3), we get the following matrices

$$A_0 = \begin{bmatrix} 0 & 1 & 0 \\ -\omega_0^2 & 2\zeta\omega_0 & 0 \\ \frac{1-\frac{1}{\alpha}}{\alpha T_d} & 0 & -\frac{1}{\alpha T_d} \end{bmatrix}, \; A_1 = \begin{bmatrix} 0 & 0 & 0 \\ -\frac{KK_p}{\alpha} & 0 & -KK_p \\ 0 & 0 & 0 \end{bmatrix}.$$

Stability of processes with time delay is a problem that has been studied much. The review articles Richard (2003) and Gu and Niculescu (2003) are good starting points for the literature in this field. A linear time invariant time-delayed system is stable if all the roots of the characteristic equation have negative real parts. The problem with time-delayed systems is that the characteristic equations are transcendental equations with infinite number of solutions, making this a challenging condition to check (Gu and Niculescu, 2003).

The simplest way to check stability of a time-delayed system is probably to use a Nyquist plot together with the Nyquist stability criterion. However, this must usually be done manually, and it can be a cumbersome task to check for different model or controller parameters. Methods that allows for automatic calculation are better suited for such a task. For small systems, it can be possible to find analytical bounds on parameters which results in a stable process. For instance in Silva et al. (2002) they find the complete set of stabilizing PID parameters for a first order plant. More general methods

exist, for instance methods based on Lyapunov-Krasovskii functionals or the Razumikhin theorem. It was shown in Gu (2001) that the Lyapunov-Krasovskii functionals based method could be formulated as a Linear Matrix Inequality (LMI) problem. We have tested the LMI formulations proposed in Jia and Hideki (2003) and He et al. (2007) on the system in equation (6.3), but they were both too conservative to find a stability region at all for the parameters of interest to us.

An alternative to the methods above is based on the frequency domain. The main drawback of these methods are that certain conditions will need to be checked for a large amount of frequencies, making them computationally demanding. We have chosen to focus on a method from Chen (1995). This method finds an interval for the time delay (τ^-, τ^+) for which the system is stable. An advantage with this method is that it can also find delay-intervals for systems that are unstable for $\tau = 0$. A requirement of the method is that the system is on a differential difference form (6.4). This system is stable if

$$\det\left(sI - \sum_{k=0}^{q} A_k e^{-k\tau s}\right) \neq 0, \qquad \forall s \in \bar{C}^+,$$

where $\bar{C}^+$ is the closed complex right half plane. If there exist an $\tau^* \geq 0$ for which the system is stable, then there must be a neighbourhood around τ^* where the system remains stable. The goal is now to find a τ^+ and τ^- such that the system remains stable for all values of τ in the interval $(\tau^* - \tau^-, \tau^* + \tau^+)$, and becomes unstable for $\tau = \tau^* - \tau^-$ and $\tau = \tau^* + \tau^+$.

As we will use only one injector for control, we will only focus on the special case of one delay ($q = 1$). For this case the following theorem is given in Chen (1995);

Theorem 1. *Let $q = 1$ and $\text{rank}(A_1) = m$. Suppose the system (6.4) is stable for some $0 < \tau^* < \infty$. Furthermore, define*

$$\tau_i^+ := \begin{cases} \min_{1\le k\le n} \frac{\alpha_k^i}{\omega_k^i} & \text{if } \lambda_i(j\omega_k^i I - A_0, A_1 e^{-j\tau^*\omega_k^i}) = e^{-j\alpha_k^i} \\ & \text{for some } \omega_k^i \in (0,\infty),\ \alpha_k^i \in [0,2\pi]. \\ \infty & \text{if } \rho_m(j\omega I - A_0, A_1 e^{-j\tau^*\omega}) > 1 \quad \forall \omega \in (0,\infty). \end{cases}$$

$$\tau^+ := \min_{1\le i\le m} \tau_i^+.$$

$$\tau_i^- := \begin{cases} \min_{1\le k\le n} \frac{2\pi-\alpha_k^i}{\omega_k^i} & \text{if } \lambda_i(j\omega_k^i I - A_0, A_1 e^{-j\tau^*\omega_k^i}) = e^{-j\alpha_k^i} \\ & \text{for some } \omega_k^i \in (0,\infty),\ \alpha_k^i \in [0,2\pi]. \\ \infty & \text{if } \rho_m(j\omega I - A_0, A_1 e^{-j\tau^*\omega}) > 1 \quad \forall \omega \in (0,\infty). \end{cases}$$

$$\tau^- := \min_{1\le i\le m} \tau_i^-. \tag{6.5}$$

Then, the following statements hold:

i) System (6.4) is stable for any $\tau \in [\tau^*, \tau^* + \tau^+)$. If $\tau^+ < \infty$, the system becomes unstable at $\tau = \tau^* + \tau^+$.

ii) If $\tau^* > \tau^-$, then the system is stable for any $\tau \in (\tau^* - \tau^-, \tau^* + \tau^+)$ and is unstable at $\tau = \tau^* - \tau^-$.

iii) If $\tau^* \le \tau^-$, then the system is stable for any $\tau \in [0, \tau^* + \tau^+)$.

In equation (6.5) $\lambda_i(A, B)$ is the ith generalized eigenvalue of the matrix pair (A,B), and ρ_m is a spectral radius defined as

$$\rho_m(A, B) = \min\{|\lambda| : \det(A - \lambda B) = 0\}.$$

Proofs and more details about the theorem can be found in Chen (1995). To find the delay margins, one starts by calculating the generalized eigenvalues $\lambda_i(j\omega_k^i I - A_0, A_1 e^{-j\tau^*\omega_k^i})$ over a large enough frequency range (the moduli of the generalized eigenvalue will exceed one beyond a certain frequency). If the spectral radius $\rho_m\left(j\omega I - A_0, A_1 e^{-j\tau^* k}\right) > 1$ for all $\omega \in (0,\infty)$, then the system is stable for all $\tau \ge 0$. If not, find all ω_k^i where $|\lambda_i| = 1$. From these frequencies one can now calculate α_k^i and find τ^+ and τ^-. Note that the results for τ^+ and τ^- are exact. However, to find ω_k^i it is necessary to

do a frequency search, and the accuracy of the algorithm thus depends on how well this search is done.

The procedure requires that a stable τ^* is known. This might not always be the case. One can then use $\tau^* = 0$ as a starting point. We will assume that at least one $\lambda_i(A_0+A_1)$ is in the right half plane (if not, one knows that τ^* is stable). The procedure will now return a value τ^+, and the procedure can be run once more, now with $\tau^* = \tau^+ + \varepsilon$, where $\varepsilon \ll \tau^+$, and the new τ^+ and τ^- will give a stable interval. To summarize, we propose the following algorithm based on Theorem 1 to find the stability margins for a linear system with a single time delay;

Step-1 Set $\tau^* = 0$

Step-2 Calculate $\rho_m\left(j\omega I - A_0, A_1\right)$ for each ω. If $\rho_m > 1$ for all ω, the system is stable for all τ.

Step-3 Find all ω_k^i where $|\lambda|$ crosses 1. If no ω_k^i where found, the system is unstable for all τ.

Step-4 For each ω_k^i, find α_k^i such that $\lambda_i(j\omega_k^i I - A_0, A_1 e^{-j\tau^*\omega_k^i}) = e^{-j\alpha_k^i}$.

Step-5 Find τ^+ and τ^- as in equation (6.5).

Step-6 If $A_0 + A_1$ have a positive eigenvalue, set $\tau^* = \tau^+ + \epsilon$ where $\epsilon \ll \tau^+$. Repeat Step 3-5.

6.4 Results

6.4.1 Controller parameters

In this Section we will focus on stability analysis of (6.3). As τ depends on injector placement and mean velocity of the gas (operating conditions), it is important to know how much τ can change before the system becomes unstable. We will also find the controller parameters that are most robust toward changes in τ (i.e has the widest time-delay margins). The following

parameters are used in the model (6.2); $K = 1$, $\omega_0 = 1200$ ($\approx$ 190Hz), $\zeta = 10/\omega_0$. We will now use the procedure from Section 6.3 to find time-delay intervals for a large set of controller parameters. This is done using a brute force method. For a large set of values for K_p and T_d (α is kept constant at 0.1), the delay margins were computed. The results are shown in Figure 6.2. For a given set of controller parameters (K_p, T_d), the system will be stable for all time-delays between the two surfaces. From the figure it is quite clear that the tuning of the controller has an impact on how wide the time-delay margins are. The most important parameter seems to be the derivative time T_d. The widest time-delay margins are found for $T_d = 0.0025$. Using this value, the controller will increase the phase margins for frequencies $\omega = 400$rad/s to 4000rad/s, probably with a maximum increase around the unstable frequency.

When it comes to the controller gain K_p, the impact on the time-delay margins are lower than for T_d. However, large gains tends to reduce the time-delay margins.

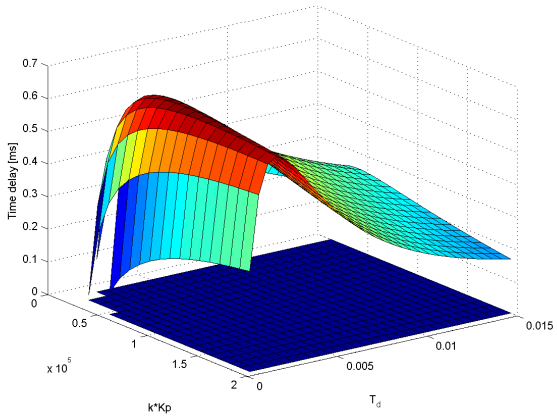

Figure 6.2: Time-delay margins for a set of controller parameters. The system is stable for time-delays between the two surfaces.

In general, the delay margins found are quite small. The maximum time-delay that can be stabilized is close to $\tau = 0.65$ms. If the unburnt gas is entering the flame with a velocity $\bar{U} = 10$m/s, the injector has to be placed within 6.5mm of the flame. However, if we change the sign of the controller, we can stabilize the system for larger time-delays. Figure 6.3 shows time-delay margins for negative values of K_p.

With a negative gain, the system can be stabilized for delays up to 3.1ms. In the case of $\bar{U} = 10$m/s, the injector can be up to 3.1cm upstream of the flame. The time-delay margins are also much wider in this case. While the derivative time T_d still is important to achieve maximum delay margins, the magnitude of the gain K_p is more important for this case.

The time-delay margins spans from 0.5ms to 3.1ms. It is interesting to note that this span is 2.6ms wide, exactly half a period of a 1200rad/s signal.

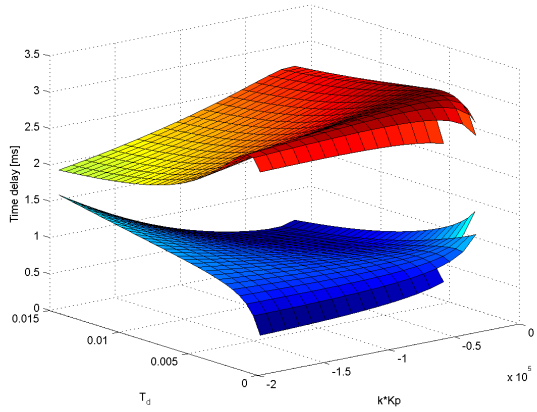

Figure 6.3: Time-delay margins for a set of controller parameters using negative gain. The system is stable for time-delays between the two surfaces.

It might seem strange that by use of positive feedback, one can stabilize the system and increase the time-delay margins. The reason for this is that

the system is oscillatory, and for such systems a time-delay can stabilize an unstable process (see for instance Abdallah et al. (1993)). Figure 6.4 shows an unstable system oscillating with a frequency of $\omega = 1200$rad/s. To see why a negative gain can stabilize the system, consider a pressure measurement taken at time $t = 0$. For time-delay values marked by the arrow A ($\tau = 1.3$ms to 3.8ms), the sign of the pressure signal will have changed by the time the output of the controller manipulates the system. Thus a negative gain can stabilize the system for these time-delays. If the time-delays are even larger, the arrow marked B ($\tau = 4$ms to 6.5ms), a positive gain must be used to stabilize the system. This indicates that there will exist a new layer of time-delay margins that can be stabilized with use of positive feedback. Note that these analysis are just to illustrate why a negative gain can stabilize the system. However, they do not take into account the dynamics of the PD controller, and thus the indicated delay margins do not correspond to the ones found in Figure 6.3.

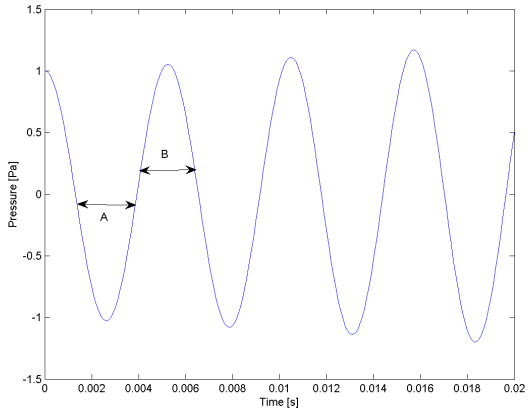

Figure 6.4: An unstable system oscillating with a frequency of $\omega = 1200$rad/s.

6.4.2 Robustness

In this section we will focus on a single controller tuning, and check how robust it is toward changes in oscillation frequency (ω_0), damping (ζ) and time-delay. We have omitted the process gain K, as its influence on the time-delay can be found by looking at KK_p in Figure 6.2 and 6.3. For the controller, we use $K_p = -40000$, $T_d = 0.002$ and $\alpha = 0.1$. We used the same procedure as in the previous section, but now with perturbations in model parameters instead of controller parameters. The parameter perturbations are around $\omega_0 = 1200\text{rad/s}$ and $\zeta = \frac{10}{\omega_0}$. The results are shown in Figure 6.5. We see that the time-delay margins are very dependent on the oscillation frequency (ω_0). If we have designed the system to operate at a time-delay of 2ms, then a 40% increase in oscillation frequency will cause the system to go unstable. This can be a problem, if the oscillations shift from a low frequency mode, to a high frequency mode. It is natural that the time-delay margins shrink as the frequency is increased. An increased frequency means that the period of the oscillations decrease, making the interval where the controller signal has the appropriate phase smaller. From the figure we can also see that the damping factor ζ is not very important for the time-delay margin.

6.5 Discussion

6.5.1 Application of results

The control design is based on a simple combustion model. A possible use of the results herein, is to adjust the model parameters in (6.2) to data from a real combustor, and do the control design based on the simple model. The oscillation frequency and the growth rate of the oscillations can be found using pressure measurements. As the process is unstable, it might be difficult to find the process gain (K). Thus, some tuning of the controller parameters might be necessary to maximize the time-delay margins.

The time-delay margins give a good measure for where the injector should be placed. It seems natural to place the injector close to the up-

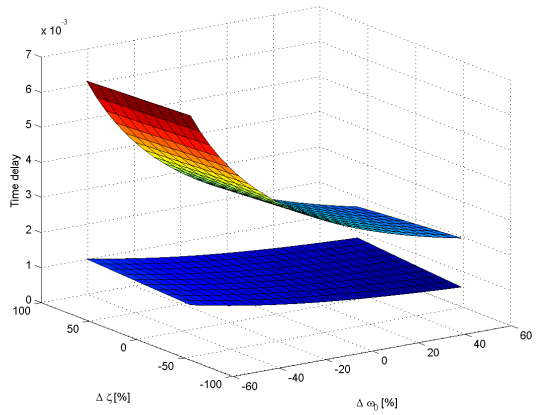

Figure 6.5: Robustness toward changes in ζ and ω_0. The system is stable for time-delays between the two surfaces.

per time-delay margin, as this will ensure better mixing of the reactants. However, to allow for changes in operating conditions ($\bar{U}$), some distance to the delay margin is needed. If large changes in $\bar{U}$ are expected, a solution could be to do a gain scheduling controller design. The controller parameters will then be a function of $\bar{U}$.

6.5.2 Modeling assumptions

We have used a linearized model based on coupling between heat release from the flame and acoustics to represent a combustion process. This means that we have neglected linear and nonlinear dynamics. However, when considering the time-delay's impact on controllability of the system, it seems that the oscillation frequency is the most important model parameter. This is indicated in Figure 6.5. Injector dynamics are not included in the analysis. Usually, they are modeled as an additional time constant. A first approximation of the impact of the injector dynamics is to reduce the time delay margin with the value of the injector time constant.

A crucial modeling assumption is that we have included only one acoustic mode. When stabilizing the unstable mode, the amplitude of other modes may increase. The results indicate that one can stabilize a wider range of time-delays using a negative gain in the controller, but one should be careful to use this on a real plant. If another acoustic mode is triggered, the negative gain in the controller can amplify the signal, causing the normally stable mode to become unstable. Whether this happens or not, depends on the relationship between the controller gain and the natural damping of the relevant acoustic mode.

The analysis will not detect effects of coupling between acoustic modes. In addition, we ignored the impact of changes in the oxidizer ratio λ_{O_2}. These will both change the dynamics of the process slightly.

We have only considered a constant time-delay τ. When the system is unstable, the velocity of the unburnt gas will oscillate. In this case, the time-delay will be time varying, and oscillate with the frequency of the unstable mode. While no guarantees for stability can be given based on the results herein, it seems natural that the time-delay margins give an indication of how large the amplitude of the velocity U can grow, before the controller becomes unable to stabilize the system.

6.5.3 Frequency search

An important step in the algorithm used to find the time-delay margins is to detect all frequencies where $|\lambda_i|$ crosses 1. As long as these can be found accurately, the time-delay margins returned are exact. This is also the part of the algorithm that is time consuming. It is important to make sure that the algorithm checks for large enough frequencies to detect all crossings. This can be seen quite easily by plotting the eigenvalue as a function of frequency. We choose to do the search in two steps. First we find all crossings on a widely spaced frequency grid. Then we do a new search on a much smoother frequency grid, close to all frequencies where the eigenvalue crosses one, to increase the accuracy of the algorithm. For the model studied here, the crossing point has a quite sharp v-shape, crossing 1 from above, and then from below at a slightly larger frequency. This means

that if the first search is too widely spaced, there will be crossings that are not detected. A possible improvement is to make a frequency search that detects sharp changes, and adjust the frequency step itself. This would probably make the algorithm more efficient and reliable.

6.6 Conclusions and future work

We have presented a method to analyze stabilization of an oxy-fuel combustion process with time-delay, using a PD controller. The method allows us to find exact time-delay margins, for which the controller remains stabilizing. This can be useful during design, to find the best injector position. During operation, it gives us knowledge about how much operating conditions can change before the controller becomes unable to stabilize the plant. The method also allows us to find controller tunings that maximize the time-delay margins, and quantify robustness toward modeling errors.

We have focused on a simple (one acoustic mode) combustion model. However, as long as the model is linear, much more advanced models can be analyzed.

In ongoing work we are testing the control design on an advanced oxy-fuel combustion simulator.

Chapter 7

Control design and stability analysis of oxy-fuel thermoacoustic instabilities

This chapter is based on Snarheim et al. (2009a), as submitted to IEEE Trans. Control System Technology, 2009.

Abstract

Thermoacoustic instabilities may cause large high frequency pressure oscillations in continuous combustion, which in a worst case can lead to structural damage or system failure. Previous research have proven that for conventional combustion, perturbing the system by injecting small amounts of gas close to the flame may reduce or stabilize the oscillations if the injection rate is chosen appropriately by feedback control. To allow the injected gas to mix well with the main flow before burning, the injector must be placed upstream of the flame. This introduces a time delay in the control loop. In this paper we apply a frequency domain method to analyze stability and control of a low order linear oxy-fuel combustion model with a time delay. We propose an extension to the method, which makes it possible to identify

time delay margins for a large set of controller- and/or model-parameters. Based on this we can find robust controller parameters, along with useful knowledge about how much operating conditions can change while retaining stability. To test the chosen control design, we performed a simulation study on a nonlinear CFD model of oxy-fuel combustion. It was found that when sampling time is not limiting the controller performance, the time delay margins found from simulations compare well to the margins found in the linear analysis. However, as sampling rate was not included in the analysis, the results were less accurate when sampling rate limited the controller performance.

7.1 Introduction

Gas turbines are widely used for power production from gaseous fossil fuels. Although gas turbine engines are relatively clean burning, there is inevitably emissions of CO_2 from combustion of fossil fuels. Thus, with today's increasing concern about global warming and climate change, there is an incentive to investigate gas turbine processes with CO_2 capture.

One attractive concept for this is the semi-closed gas turbine cycles using CO_2 as working medium. This process has been studied in e.g Bolland and Saether (1998), Ulizar and Pilidis (1997), Ulfsnes et al. (2003). The concept is based on combustion of natural gas with O_2 in an (inert) CO_2 atmosphere. Hence, the gas leaving the combustion chamber contains (almost) pure CO_2 and steam. The steam can be removed using a condenser, and we are left with (almost) pure CO_2, of which most is recycled for use as working medium, while to avoid accumulation, some must be removed from the cycle. The removed CO_2 must be compressed for long term safe storage to have the desired positive effect on the global warming (carbon sequestration).

While overall process dynamics has been studied in Snarheim et al. (2005), Imsland et al. (2005), in this paper, we concentrate on the dynamics of the combustion chamber. It is known that conventional gas turbine combustion chambers might exhibit detrimental instabilities under some operating conditions (Annaswamy and Ghoniem, 2002). Recent experimen-

tal work (Ditaranto and Hals, 2006) indicates that similar instabilities also occur in oxy-fuel combustion, possibly even more severe than in the conventional case.

This gives a clear motivation for studying if it is possible to use active feedback control for alleviating these instabilities for oxy-fuel combustion, as has been successfully done for conventional combustion (Annaswamy and Ghoniem, 2002). The actuator that is used for stabilization is secondary injection of CO_2 upstream of the flame. This means that there will be a time-delay due to transport of the injected gas to the flame. To analyze the dynamics of such a system we use a simple second order linear model with a time-delay. A frequency search method from Chen (1995) is used to analyze stability, control design and robustness of the linear time-delay system. The results from the analysis are validated by use of an advanced oxy-fuel combustion simulator.

The paper is briefly outlined as follows: In Section 7.2 we give some background on combustion instabilities in general, then we proceed to discuss the special case oxy-fuel combustion. The simulation model and the control relevant model are presented in Section 7.3, while Section 7.4 looks at the control design. The control design is tested on an advanced combustion simulator in Section 7.5. We end the paper with a discussion and some concluding remarks.

7.2 Thermodynamic instabilities in oxy-fuel combustion

Thermodynamic instabilities have been recognized as a problem in combustion processes for a long time. These instabilities take the form of large pressure oscillations in the combustion chamber. The fact that the coupling between heat release oscillations and acoustic pressure can be a driving mechanism for thermodynamic instabilities was identified as early as 1878 (Rayleigh, 1878). The heat release and acoustics are coupled in a feedback loop, and depending on the phase difference between the signals, the heat release either remove from or add energy to the pressure oscilla-

tions, the latter case making the system unstable. Obvious implications of these instabilities are vibrations and mechanical stress that may lead to structural damage and system failure. Alleviating the oscillations might allow for better energy utilization and less pollutant emissions.

Modern (conventional) premixed gas turbines have to operate at very lean conditions due to stringent requirements on NO_x emissions. These operating conditions make the gas turbines prone to instabilities, and is an important reason for the attention active control of thermoacoustic instabilities has received recently. This is also reflected in the numerous publications within the field in recent years. Reviews on thermoacoustic instabilities and active control can be found in Annaswamy and Ghoniem (2002), Candel (2002), Dowling and Morgans (2005).

However, when it comes to oxy-fuel, the literature on instabilities is scarce. Experimental results on a laboratory scale combustor are published in Ditaranto and Hals (2006). They show that up to a certain threshold in oxidizer composition (the ratio between oxygen and carbon dioxide in the oxy-fuel mixture), the instability patterns are similar to what is found when burning fuel with air. Above this threshold, however, the instabilities tend to grow even stronger. The composition of the unburnt gas in oxy-fuel combustion can be described by equivalence ratio (ϕ) and oxidizer ratio (λ_{O_2}), defined as

$$\lambda_{O_2} = \frac{n_{O_2}}{n_{O_2} + n_{CO_2}}, \quad \phi = \frac{(n_{\text{fuel}}/n_{O_2})_{\text{actual}}}{(n_{\text{fuel}}/n_{O_2})_{\text{stoichiometric}}}, \tag{7.1}$$

where n_x refers to the number of moles of component x. Figure 7.1 shows sound pressure level plots from the experiments in Ditaranto and Hals (2006). The main oscillation frequencies are easy to identify by the peaks. Due to the geometry of the combustion chamber, there exists several acoustic modes that can be triggered, depending on operating conditions. This gives a clear incentive to investigate active control strategies for this type of combustion. Moreover, it also indicates that a good controller must be able to reduce pressure oscillations over a broad frequency range, possibly broader than for conventional combustion instabilities.

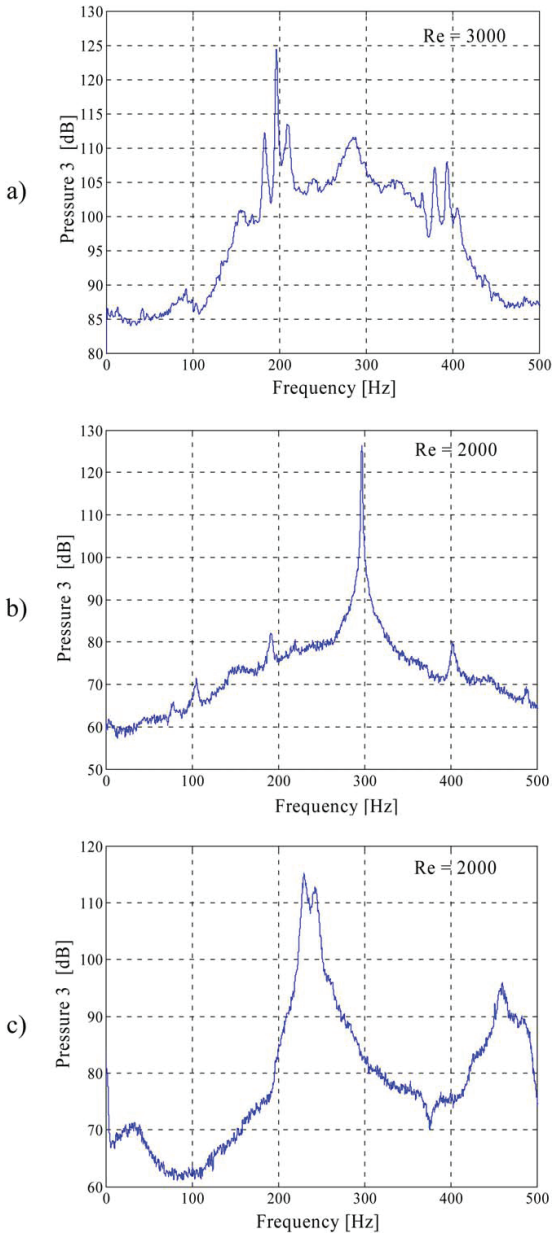

Figure 7.1: Experimental results from oxy-fuel combustor. The triggered frequency and instability peak depend on operating conditions: a) $\lambda_{O_2} = 0.42$, $\phi = 0.9$, Re $= 3000$; b) $\lambda_{O_2} = 0.41$, $\phi = 0.9$, Re $= 2000$; c) $\lambda_{O_2} = 0.42$, Re $= 2000$, $\phi = 0.9$. λ_{O_2} and ϕ are defined in 7.1. From Ditaranto and Hals (2006).

In oxy-fuel combustion it is possible to change the composition of the oxidizer (the ratio between O_2 and CO_2). Compared to conventional combustion in air, this is the equivalent of changing the ratio between nitrogen and oxygen, which generally is hard and expensive. The difference between plot b) and c) in Figure 7.1 indicates that the oxidizer composition is very important. The difference is only 1% in oxidizer ratio. From a control point of view, this means that for oxy-fuel there exists a new degree of freedom that can be used to stabilize the system. One focus of this paper is to model the effect of perturbations in oxidizer composition, and investigate the use of this variable for control. The extra degree of freedom is illustrated in Figure 7.2.

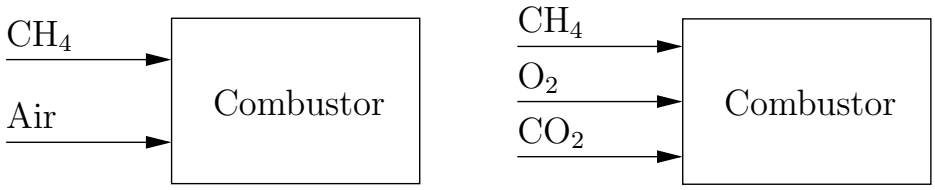

(a) Conventional combustion chamber (b) Oxy-fuel combustion chamber

Figure 7.2: Conceptual difference between a conventional combustion chamber and an oxy-fuel combustion chamber from a control point of view.

7.3 Modeling

In this section we will present two models; a simulation model and a model for control analysis. The simulation model is based on solving the Navier-Stokes equations combined with a flame model. We will give a short introduction to this model, but a complete presentation can be found in Haugen et al. (2009). The model for control analysis is a linear model based on the wave equation.

7.3.1 Simulation model

Historically, combustion instabilities have been investigated by linearizing the Navier-Stokes and energy equations in order to obtain a wave equation in frequency space. The linearization method has gained its great popularity due to its simplicity and the possibility to use it in order to obtain both analytical and numerical solutions. Linear models will however not be able to predict the dominating frequency and the level of the (non-linear) statistically stationary state, i.e the amplitude of the limit cycle. Leaving the linearized wave equation and instead solving the non-linear Navier-Stokes equations together with the energy equation, gives us the ability to predict the shape and the level of the acoustic frequency spectrum both during the exponential growth phase and during the statistically stationary state. For numerical testing of models for active control it is for these reasons a necessity to use non-linear simulation models, i.e. the classical linear models will no longer do.

Solving the full 3D Navier-Stokes equations in a direct numerical simulation (DNS) is however a formidable task, and can be done only for relatively small domains even on todays largest computer clusters.

In this work we will use a Navier-Stokes solver which has been designed to simulate combustion instabilities in relatively simple geometries, where the flow can be assumed to be quasi one-dimensional. Quasi one-dimensional means that one solves the governing equations only in one dimension, but variable cross sections are incorporated into the equations, making the solution a simple three dimensional solution.

The one-dimensional variable cross section continuity, momentum, temperature and species equations are

$$\frac{\partial \rho}{\partial t} = -\frac{1}{A}\frac{\partial \rho A u}{\partial x} + S_\rho, \tag{7.2}$$

$$\frac{\partial u}{\partial t} = -u\frac{\partial u}{\partial x} - \frac{1}{\rho}\frac{\partial p}{\partial x} + \frac{4}{3}\nu\left(\frac{\partial^2 u}{\partial x^2} + \frac{1}{\rho}\frac{\partial u}{\partial x}\frac{\partial \rho}{\partial x}\right), \tag{7.3}$$

$$\frac{\partial T}{\partial t} = -u\frac{\partial T}{\partial x} + \frac{1}{\rho c_v}\left(-\frac{p}{A}\frac{\partial uA}{\partial x} + k\frac{\partial^2 T}{\partial x^2} + \dot{q}_v + \dot{q}_c\right), \tag{7.4}$$

$$\frac{\partial Y_k}{\partial t} = -u\frac{\partial Y_k}{\partial x} + D\frac{\partial^2 Y_k}{\partial x^2} + w_k + S_k, \tag{7.5}$$

where A is the cross sectional area. Here ρ is the mass density, u is the fluid velocity, $p = \rho r T$ is the pressure, T is the temperature, $r = R/\bar{m}$, R is the universal gas constant, $\bar{m}$ is the mean molar mass, ν is the kinematic viscosity, k is the conductivity, c_v is the heat capacity at constant volume, w_k is the reaction rate of species k, Y_k is the mass fraction of species k, $\dot{q}_c$ is the heating due to chemical reactions and D is the mass diffusivity. The extra source terms in the continuity and mass fraction equations, S_ρ and S_k, represent the injectors used for the active control, and they are non-zero only at the position of the injectors. In the 1D approximation the viscous heating $\dot{q}_v$ reduces to

$$\dot{q}_v = 2\mu \mathbf{S}^2 = \frac{4}{3}\nu\rho\left(\frac{\partial u}{\partial x}\right)^2, \tag{7.6}$$

when $\mathbf{S}$ is the traceless rate of strain tensor. One should note the non-obvious 4/3 term in front of the viscosity in (7.6) which is due to the 1D approximation.

For a description of the flame model, boundary conditions, viscous wall damping and similar details, see Haugen et al. (2009) where a detailed description of the full simulation tool is given. From here on we will use the name SINMA when we refer to the simulation model.

7.3.2 Simulation case

We have chosen to use the experimental setup in Ditaranto and Hals (2006) as a simulation case. A sketch of the combustor is shown in Figure 7.3. The combustion chamber consists of a 0.8 m long premixing section, before the combustor enters a 0.05 m long flame arrestor and a 0.1 m slot that leads to the 0.48 m long combustion chamber. The height in the premixing and combustion zone is 5.4 cm, while the height of the slot is 5 mm. To control the system we will inject CO_2 somewhere in the slot (between the flame arrestor and the combustion chamber, see Figure 7.4). The main gas flow

has a composition of $\phi = 0.9$ and $\lambda_{O_2} = 0.41$. The velocity at the inlet is 0.80 m/s and increases to 8.64 m/s in the slot. Without control the process is unstable with an oscillation frequency of 293 Hz.

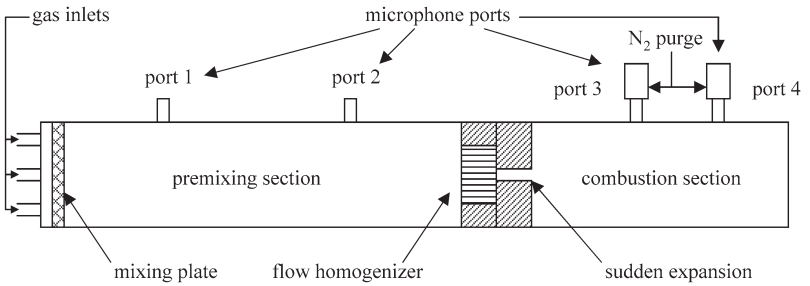

Figure 7.3: Sketch of the experimental setup in Ditaranto and Hals (2006). The parameters in SINMA are set to represent this setup.

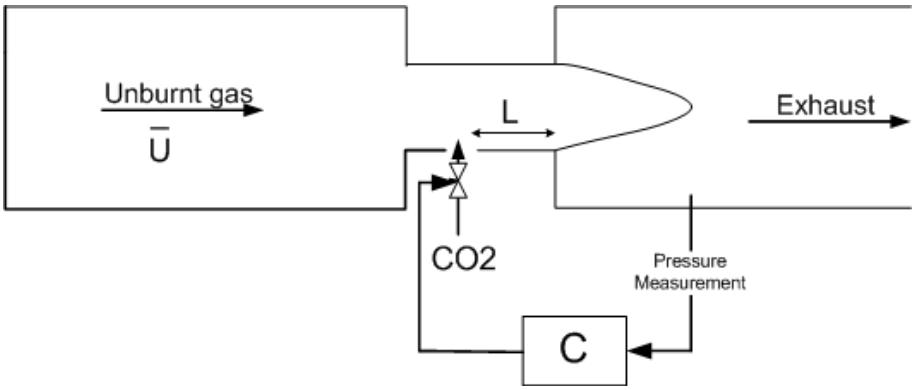

Figure 7.4: Injection of CO_2 close to the burning zone. The time-delay due to transport of the injected CO_2 to the burning zone is given by $\tau = L/\bar{U}$.

7.3.3 Control relevant model

To be able to design a controller and analyze stability of the controlled combustion process, we need a simple model that captures the most important dynamics. A common way to model combustion processes is to consider the coupling between heat release from the flame and acoustics. A linear combustion model based on this principle was developed in Annaswamy et al. (1997), and was extended for perturbations in the equivalence (air/fuel) ratio in Hathout et al. (2000). Inspired by these an extension for oxy-fuel combustion was developed in Snarheim et al. (2007). All these models have in common that they are based on the linear wave equation

$$\frac{\partial^2 p'}{\partial t^2} - c^2 \frac{\partial^2 p'}{\partial x^2} = (\gamma - 1)\frac{\partial q'}{\partial t}(x,t),$$

where p' is a perturbation in the pressure ($p = \bar{p} + p'$), c is the speed of sound, γ is the specific heat ratio, and the heat release q, enters the equation as an energy source. It was shown in Annaswamy et al. (1997) how this equation can be discretized using a modal expansion

$$p'(x,t) = \bar{p}\sum_{i=1}^{n} \psi_i(x)\eta_i(t),$$

where $\psi_i(x)$ and $\eta_i(t)$ are modal shape and amplitude, $\psi_i(x) = \cos(k_i x + \theta)$. The phase-shift θ depends on the geometry of the chamber. Using this expansion within the wave equation and integrating over the combustor length gives

$$\ddot{\eta}_i + 2\zeta\omega_i\dot{\eta}_o + \omega_i^2\eta_i = \tilde{b}_i\dot{q}'_f.$$

The damping factor ζ is added to account for heat and friction losses, $\tilde{b}_i$ is a constant and $\dot{q}'_f$ is the heat release rate at the flame location. To keep the model simple, we will consider only one acoustic mode ($n = 1$), the one that is unstable. Using the assumption that the heat release rate is a function of velocity and composition of the unburnt gas, the combustion model can be formulated as a second order transfer function

$$G(s) = \frac{k}{s^2 - 2\zeta\omega_0 s + \omega_0^2} e^{-\tau s}, \qquad \zeta > 0, \tag{7.7}$$

that maps pressure at the flame zone to injected CO_2. The time-delay is due to transport of the injected CO_2 from injector to the flame zone and is given by $\tau = L/\bar{U}$, where L is the distance between flame and injector, and $\bar{U}$ is the mean velocity of the unburnt gas. The parameters in the model are found by fitting the model to simulation data from SINMA. The frequency (ω_0) can be found from a Fourier transform of the pressure data, and ζ can be found from the growth rate in the data. The process gain (k) is more difficult to find since the system is unstable. There is no simple way to match the initial conditions between SINMA and the linear model. Figure 7.5 shows a comparison between an impulse response for the linear model and a simulation using SINMA. For the linear model, the following parameters are used; $\omega_0 = 1841$ rad/s, $k = 50 \cdot 10^3 \cdot \omega_0^2$ and $\zeta = 5 \cdot 10^{-3}$. The fit between the models are good in the beginning of the time history. Note that the limit cycle SINMA approaches is large, about 15000 Pa.

7.4 Control and Stability

In this section we will study how an oxy-fuel combustion process can be controlled using a pre-flame CO_2 injector. Active control using pre-flame injection was also considered in Hathout et al. (2000), where they used a controller based on the Smith predictor. In Morgans and Dowling (2007) a combustion model with a time delay was controlled using a PD controller. However, the time-delay considered was due to the modeling of flame dynamics. A Nyquist plot was used to prove stability of the controlled system. The PD controller has a clear motivation as it can provide a much needed phase lift around the unstable frequency. Therefore, we will use a filtered PD-controller to control the system (7.7)

$$K(s) = K_p \frac{1 + T_d s}{1 + \alpha T_d s}.$$

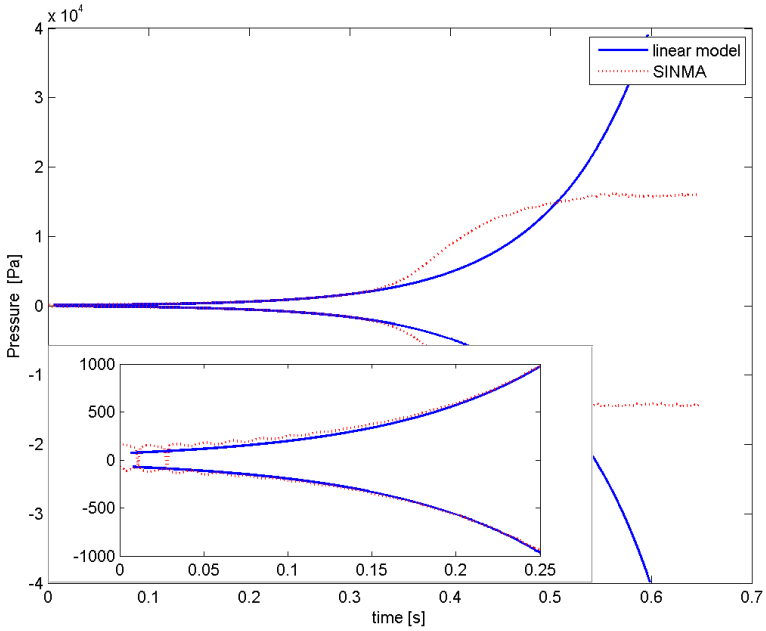

Figure 7.5: Envelopes of the pressure signal of the linear model (-) and simulation data (.).

Based on the model presented in the previous section, we want to find controller parameters that can stabilize the system. We also want to find for which time-delays the system can be stabilized and to investigate robustness toward modeling errors and changes in operating conditions.

The controlled process can be formulated as a differential difference equation

$$\dot{x}(t) = A_0 x(t) + A_1 x(t-\tau), \qquad \tau > 0, \tag{7.8}$$

where

$$A_0 = \begin{bmatrix} 0 & 1 & 0 \\ -\omega_0^2 & 2\zeta\omega_0 & 0 \\ \frac{1-\frac{1}{\alpha}}{\alpha T_d} & 0 & -\frac{1}{\alpha T_d} \end{bmatrix}, \; A_1 = \begin{bmatrix} 0 & 0 & 0 \\ -\frac{kK_p}{\alpha} & 0 & -kK_p \\ 0 & 0 & 0 \end{bmatrix}.$$

7.4.1 Stability of time-delay systems

Stability of dynamic systems with time delay is a problem which has received considerable attention. The review articles Richard (2003) and Gu and Niculescu (2003) are good starting points for the literature in this field. A linear time invariant time-delayed system is stable only if all the roots of the characteristic equation have negative real parts. The problem with time-delayed systems is that the characteristic equations are transcendental equations with infinite number of solutions, making this a challenging condition to check (Gu and Niculescu, 2003).

The simplest way to check stability of a time-delayed system is probably to use a Nyquist plot in combination with the Nyquist stability criterion. However, this must usually be done manually, and it can be a cumbersome task to check for different model or controller parameters. Methods that allow for automatic calculation are better suited for such a task. For small systems, it can be possible to find analytical bounds on parameters which results in a stable process. For instance in Silva et al. (2002) they find the complete set of stabilizing PID parameters for a first order plant. More general methods exist, for instance methods based on Lyapunov-Krasovskii functionals or the Razumikhin theorem. It was shown in Gu (2001) that the Lyapunov-Krasovskii functionals based method could conservatively be formulated as a Linear Matrix Inequality (LMI) problem. We have tested the less conservative LMI formulations proposed in Jia and Hideki (2003) and He et al. (2007) on the system in equation (7.8), but they were both still too conservative to find a stability region at all for the parameters of interest to us.

An alternative to the state-space methods above is to use frequency domain methods. These are non-conservative, but on the other hand, certain

conditions will need to be checked for a large range of frequencies, making them computationally demanding. We have chosen to use a method from Chen (1995), which was also used on a similar system as herein in Snarheim et al. (2009b). This method finds an interval for the time delay, (τ^-, τ^+) for which the system is stable. An advantage with this method is that it can also find delay-intervals for systems that are unstable for $\tau = 0$. A requirement of the method is that the system is on a differential difference form,

$$\dot{x}(t) = A_0 x(t) + \sum_{k=1}^{q} A_k x(t - k\tau), \qquad \tau > 0. \tag{7.9}$$

This system is only stable if

$$\det\left(sI - \sum_{k=0}^{q} A_k e^{-k\tau s}\right) \neq 0, \qquad \forall s \in \bar{C}^+,$$

where I is the identity matrix and $\bar{C}^+$ is the closed complex right half plane. If there exist a $\tau^* \geq 0$ for which the system is stable, then there must be a neighborhood including τ^* where the system remains stable. The goal is now to find a τ^+ and τ^- such that the system remains stable for all values of τ in the interval $(\tau^* - \tau^-, \tau^* + \tau^+)$, and becomes unstable for $\tau = \tau^* - \tau^-$ and $\tau = \tau^* + \tau^+$.

As we will use one injector for control, only the special case of a single delay ($q = 1$) is of interest to us. For this case the following theorem is given in Chen (1995):

Theorem 2. *Let $q = 1$ and $\mathrm{rank}(A_1) = m$. Suppose the system (7.9) is stable for some $0 < \tau^* < \infty$. Furthermore, define*

$$\tau_i^+ := \begin{cases} \min_{1\le k\le n} \frac{\alpha_k^i}{\omega_k^i} & \text{if } \lambda_i(j\omega_k^i I - A_0, A_1 e^{-j\tau^*\omega_k^i}) = e^{-j\alpha_k^i} \\ & \text{for some } \omega_k^i \in (0,\infty),\ \alpha_k^i \in [0,2\pi]. \\ \infty & \text{if } \rho_m(j\omega I - A_0, A_1 e^{-j\tau^*\omega}) > 1 \quad \forall \omega \in (0,\infty). \end{cases}$$

$$\tau^+ := \min_{1\le i\le m} \tau_i^+.$$

$$\tau_i^- := \begin{cases} \min_{1\le k\le n} \frac{2\pi-\alpha_k^i}{\omega_k^i} & \text{if } \lambda_i(j\omega_k^i I - A_0, A_1 e^{-j\tau^*\omega_k^i}) = e^{-j\alpha_k^i} \\ & \text{for some } \omega_k^i \in (0,\infty),\ \alpha_k^i \in [0,2\pi]. \\ \infty & \text{if } \rho_m(j\omega I - A_0, A_1 e^{-j\tau^*\omega}) > 1 \quad \forall \omega \in (0,\infty). \end{cases}$$

$$\tau^- := \min_{1\le i\le m} \tau_i^-. \tag{7.10}$$

Then, the following statements hold:

i) System (7.9) is stable for any $\tau \in [\tau^*, \tau^* + \tau^+)$. If $\tau^+ < \infty$, the system becomes unstable at $\tau = \tau^* + \tau^+$.

ii) If $\tau^* > \tau^-$, then the system is stable for any $\tau \in (\tau^* - \tau^-, \tau^* + \tau^+)$ and is unstable at $\tau = \tau^* - \tau^-$.

iii) If $\tau^* \le \tau^-$, then the system is stable for any $\tau \in [0, \tau^* + \tau^+)$.

Proofs and further details about the theorem can be found in Chen (1995). To find the delay margins, one starts by calculating the generalized eigenvalues $\lambda_i(j\omega_k^i I - A_0, A_1 e^{-j\tau^*\omega_k^i})$ over a large enough frequency range (the moduli of the generalized eigenvalues will exceed one beyond a certain frequency). If the spectral radius $\rho_m\left(j\omega I - A_0, A_1 e^{-j\tau^* k}\right) > 1$ for all $\omega \in (0,\infty)$, then the system is stable for all $\tau \ge 0$. If not, find all ω_k^i where $|\lambda_i| = 1$. From these frequencies one can now calculate α_k^i and find τ^+ and τ^-. Note that the results for τ^+ and τ^- are exact. However, to find ω_k^i it is necessary to do a frequency search, and the accuracy of the algorithm thus depends on how well this search is done.

The procedure requires that a stable τ^* is known. This might not always be the case. In Chen (1995), the following procedure is suggested to create

a set of disjoint delay intervals over which the system is stable. Suppose that $\rho_m\left(j\omega I - A_0, A_1\right) \leq 1$ for some $\omega \in (0, \infty)$. Let $\lambda_i\left(j\omega_k^i I - A_0, A_1\right) = e^{-j\beta_k^i}$, where $\beta_k^i \in [0, 2\pi]$ for all $i = 1, 2, \cdots, m$ and $k = 1, 2, \cdots, n$. Now rearrange the quantities β_k^i/ω_k^i as ν_j, $j = 1, 2, \cdots, nm$ in such a way that $0 \leq \nu_1 < \nu_2 < \cdots < \nu_{nm}$. Then it follows that $\det(j\omega_j I - A_0 - A_1 e^{-j\tau\omega_j}) = 0$ for $\tau = \nu_j + (2p\pi/\omega_j)$ where $p = 0, 1, 2, \cdots$.

As a result, one can find a full range of delay values for which the system is stable by examining each of the intervals $\left(\nu_j + \frac{2p\pi}{\omega_j}, \nu_{j+1} + \frac{2p\pi}{\omega_{j+1}}\right)$ and $\left(\nu_{nm} + \frac{2p\pi}{\omega_{mn}}, \nu_1 + \frac{2(p+1)\pi}{\omega_1}\right)$ where $j = 1, 2, \cdots, mn - 1$ and $p = 0, 1, 2, \cdots$.

To summarize, we use the following algorithm based on Theorem 2 to find the stability margins for a linear system with a single time delay that is stable for τ^*:

Algorithm 1.

Step-1 *Calculate $\rho_m\left(j\omega I - A_0, A_1\right)$ for each ω. If $\rho_m > 1$ for all ω, the system is stable for all τ.*

Step-2 *Find all ω_k^i where $|\lambda|$ crosses 1. If no ω_k^i where found, the system is unstable for all τ.*

Step-3 *For each ω_k^i, find α_k^i such that $\lambda_i(j\omega_k^i I - A_0, A_1 e^{-j\tau^*\omega_k^i}) = e^{-j\alpha_k^i}$.*

Step-4 *Find τ^+ and τ^- as in equation (7.10).*

7.4.2 Time delay margins for perturbations in model parameters

In this section we will outline a procedure to allow us to automatically find the time delay margins for perturbations in the system matrices A_0 and A_1. This is relevant as it gives us the opportunity to identify how the time delay margins vary as a function of controller parameters and/or model parameters.

A shortcoming of the procedure based on Theorem 2 is that it requires knowledge of a stable τ^* for the system of interest. In the special case when the system is stable for $\tau^* = 0$, we have shown how to find a set of disjoint delay intervals in which the system is either stable or unstable. However, for each delay interval of interest, it is necessary to determine whether the interval is stable or not. This can for instance be done by use of a Nyquist plot. To do this for every perturbation (ΔA_0,ΔA_1) of interest, would be overly time consuming. Fortunately, it is not necessary, as the time delay margins are continuous functions of parameters in A_0 and A_1.

Proposition 1. *If* (τ^-, τ^+) *is a stable delay interval for the delay system given by* (A_0, A_1)*, then* $\tau^* = \frac{\tau^+ - \tau^-}{2}$ *is stable for the delay system* $(A_0 + \Delta A_0, A_1 + \Delta A_1)$ *if* ΔA_0 *and* ΔA_1 *are small enough.*

Proof. The eigenvalues of a square complex matrix depends continuously on its entries (Horn and Johnson, 1985). If ΔA_0 and ΔA_1 are small (as measured by some matrix norm), the condition

$$\lambda_i(j(\omega_k^i + \Delta\omega_k^i)I - (A_0 + \Delta A_0), (A_1 + \Delta A_1)e^{-j\tau^*(\omega_k^i + \Delta\omega_k^i)}) = e^{-j(\alpha_k^i + \Delta\alpha_k^i)},$$

to be checked in (7.10) will be fulfilled for a small $\Delta\omega_k^i$ and $\Delta\alpha_k^i$. Thus, the time delay margins are continuous functions of parameters in (A_0, A_1). Hence, $\tau^* = (\tau^+ + \tau^-)/2$, where τ^+ and τ^- are margins for the original system (A_0, A_1), will be stable for the system $(A_0 + \Delta A_0, A_1 + \Delta A_1)$, as long as the perturbation $(\Delta A_0, \Delta A_1)$, is small enough. ■

To find the delay-margins as a function of process parameters we then start with the original system (A_0, A_1), and find the disjoint delay intervals. For the intervals of interest, investigate whether they are stable or not, for instance by use of the Nyquist stability criterion. Then make a small perturbation in process parameters. For each stable interval, use $\tau^* = (\tau^+ + \tau^-)/2$ and identify the new stable delay intervals for the perturbed system. The stable delay margins for the perturbed system can be used to find a stable τ^* for larger perturbations in the same direction. This can easily be implemented as an algorithm, but a problem is how to quantify a

small perturbation. We chose to perturb the system in constant intervals and then stop perturbing the system in one direction when the width of the margins were less than a threshold (i.e $\tau^+ - \tau^- < \epsilon$ for a given ϵ). At some point, the width of the time delay margins will approach zero, and we use ϵ to avoid stepping past this point. A consequence is that we loose some information about the system, but at the same time, solutions in this part of the parameter space are not robust, and are thus of low interest to us.

If we for instance want to find time delay margins for perturbations in one parameter (θ) in A_0 and/or A_1, we create a vector with m parameter values of interest, such that $|\theta_1| < |\theta_2| < \cdots < |\theta_m|$. For the original system (A_0, A_1) we have found n stable time delay regions of interest, where $\tau_1^*, \cdots \tau_n^*$ is in the middle of its respective time delay region. We can then apply the following algorithm to find the stable time delay regions for the m parameter values.

Algorithm 2.

Step-1 *set $i = 1$ (iterates over τ_i^*).*

Step-2 *set $j = 1$ (iterates over θ_j).*

Step-3 *Use Algorithm 1 with $\tau^* = \tau_i^*$ on the system $(A_0(\theta_j), A_1(\theta_j))$ to find $\tau_{i,j}^+$ and $\tau_{i,j}^-$.*

Step-4 *If $j < m$ and $\tau_{i,j}^+ - \tau_{i,j}^- > \epsilon$, set $\tau_i^* = (\tau_{i,j}^+ + \tau_{i,j}^-)/2$ and $j = j + 1$ and repeat from step 3.*

Step-5 *If $i < n$ set $i = i + 1$ and repeat from step 2.*

After applying the algorithm for the m perturbations in one direction, we can apply the algorithm again for parameters in the opposite direction. Note that we in principle can use this algorithm to investigate as many parameters (dimensions) as we want. For instance, once we have established the time delay margins for $(A_0(\theta_1), A_1(\theta_1))$, we can apply Algorithm 2 for a new parameter, with $(A_0(\theta_1), A_1(\theta_1))$ as the original system.

7.4.3 Analysis on one acoustic mode model

In this section we will perform stability analysis of (7.8) by use of the procedure from the previous section. As τ depends on injector placement and mean velocity of the gas (operating conditions), it is important to know how much τ can change before the system becomes unstable. We will also find the controller parameters that are most robust toward changes in τ (i.e has the widest time delay margins). When we have chosen controller parameters, we will study robustness. The model parameters found in Section 7.3.3 will be used.

Controller parameters

We use Algorithm 2 to find time delay intervals for a large set of controller parameters. This is done using a brute force method. For a large set of values for K_p and T_d (α is kept constant at 0.1), the delay margins were computed. For a single controller tuning, there may exist several bands of time delay margins for which the controller is stable. Figure 7.6 shows the time delay margins for the first band (i.e for injector locations closest to the flame). For a given set of controller parameters (K_p, T_d), the system will be stable for all time delays between the two surfaces. From the figure it is quite clear that the tuning of the controller has an impact on how wide the time delay margins are. The derivate time seems to be most important, and $T_d = 1.6 \cdot 10^{-3}$ gives the widest time delay margin. However, the time delay margins are narrow with a maximum of about 0.4ms.

The analysis reveals that for larger time delays, the margins are wider. Figure 7.7 shows time delay margins for the next two bands. In these regions the time delay margins can be up to 1.5ms wide. However, it turns out that the set of controller parameters that stabilize the system is smaller for these bands. As the process gain (k) is the model parameter with most uncertainty, it seems wise to choose controller tunings that are robust towards errors in this parameter. Thus the tuning $K_p = 1.0 \cdot 10^{-6}$, $T_d = 1.6 \cdot 10^{-3}$, $\alpha = 0.1$, (marked with a line in the figure) seems to balance wide time delay margins with robustness toward the process gain.

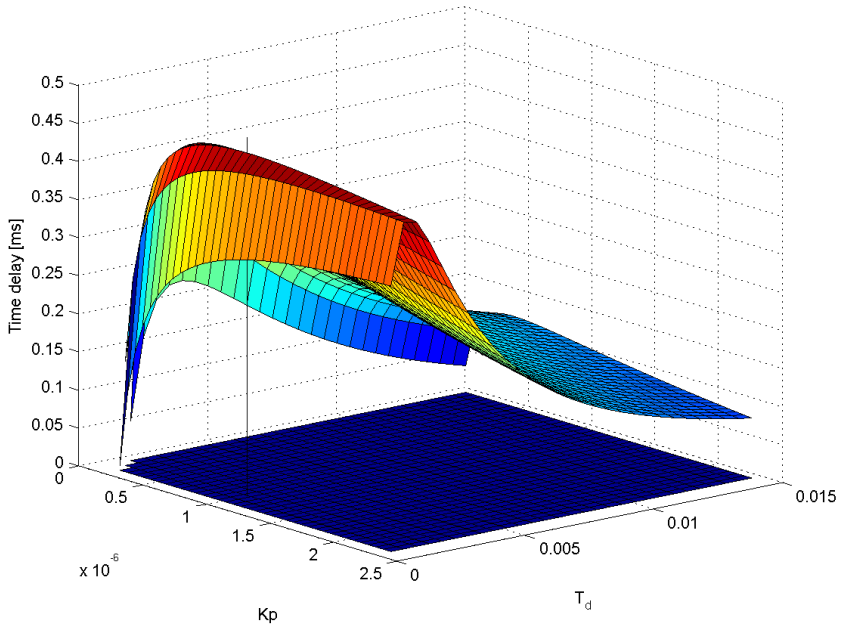

Figure 7.6: Time delay margins as a function of controller parameters. The system is stable for time delays between the two surfaces.

Robustness

In this section we will check how robust the controller tuning found in the previous section is towards changes in oscillation frequency (ω_0), damping (ζ) and time delay. We have omitted the process gain k as its influence on the time delay can be found by looking at K_p in Figure 7.6 and 7.7. We use the same procedure as in the previous section, but now with perturbations in model parameters instead of controller parameters. The parameters are perturbed from nominal values $\omega_0 = 1841\text{rad/s}$ and $\zeta = 5 \cdot 10^{-3}$. The results are shown in Figure 7.8, where we have chosen to show the results for the second time delay layer only. We see that the time delay margins

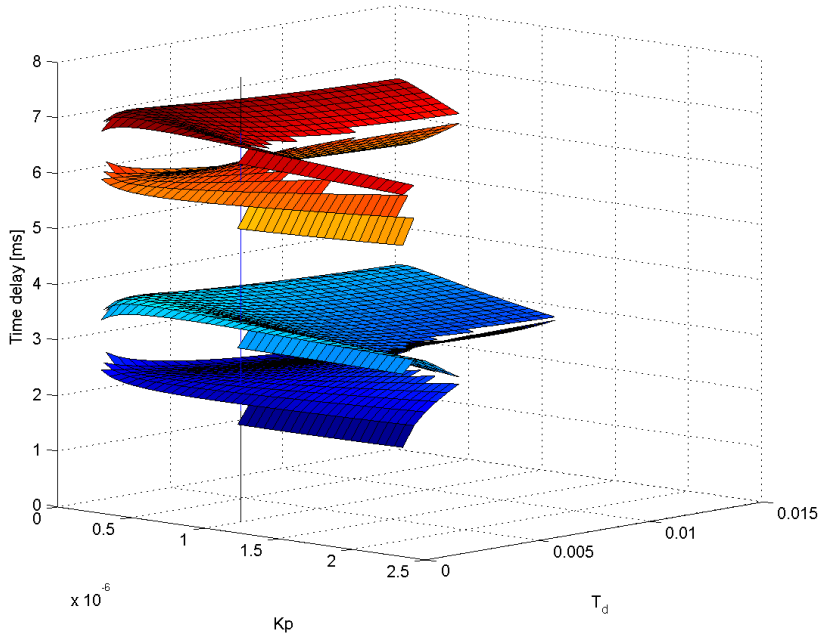

Figure 7.7: Time delay margins as a function of controller parameters. The system is stable for time delays between the two pairs of surfaces.

are very dependent on the oscillation frequency (ω_0). It is not easy to see from the figure, but for high oscillation frequencies the two surfaces are closer. For the highest oscillation frequency shown, the distance between the surfaces is 0.8ms, while it is 1.4ms for the lowest oscillation frequency. This is natural, as a higher oscillation frequency means that the period of the signal is smaller. The damping factor ζ does not have much impact on whether we can stabilize the system or not. However, it has an impact on how fast we can stabilize it. This can however not be discerned from the figure.

If we now consider the original model and controller, it is found that

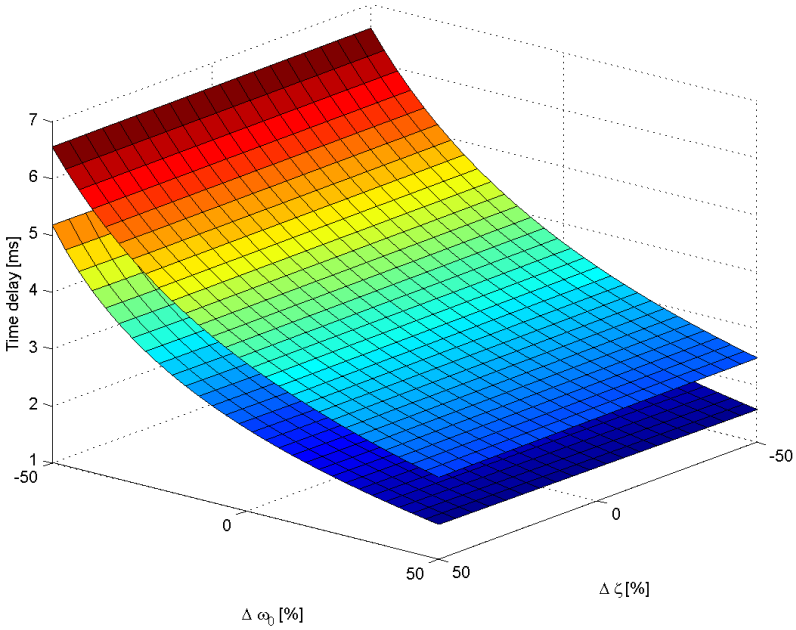

Figure 7.8: Robustness toward changes in ζ and ω_0. The system is stable for time delays between the two surfaces.

the system is stable for time delays in the range 2.4-3.6ms. Then, assume that the injector is positioned such that the time delay is 3ms under normal operating conditions. Figure 7.9 shows how much ω_0 and ζ can change before the system becomes unstable.

7.5 Simulations on Sinma

In this section we implement the controller found in Section 7.4 in the simulation model SINMA (see Section 7.3.1). The goal is to identify the time delay margins for the simulation model, and compare them to the ones found

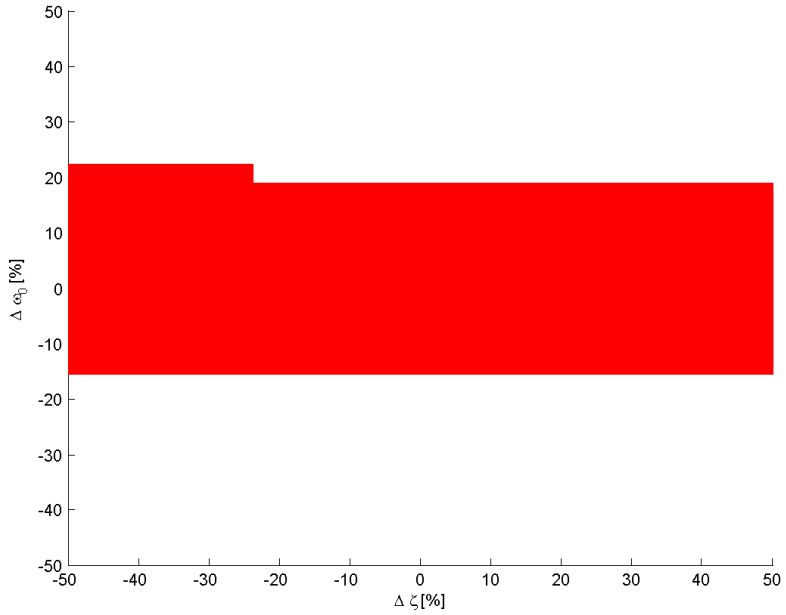

Figure 7.9: Robustness toward changes in ζ and ω_0 when the time delay is fixed at 3ms. The system is stable for model parameters inside the colored box.

in the previous section. As the area where we inject CO_2 seems to matter for the controller performance, we have used two cases for the slot length. The controller sampling time is a limiting factor for the performance, and to be able to stabilize the process, it was found that 1kHz was a minimum. However, we have also run a series of simulations where the sampling time is 10kHz, to test the performance when the sampling time is not limiting the performance.

7.5.1 Controller implementation

A discrete PD controller was implemented in the SINMA code. Based on the analysis in Section 7.4.3 we have chosen to use $K_p = 1.0 \cdot 10^{-6}$ and $T_d = 1.6 \cdot 10^{-3}$, as these parameters seemed to give wide time delay margins and are robust to errors in the process gain. The controller input is a pressure measurement at the flame location. The amount of injected CO_2 is limited to reducing the oxidizer ratio from $\lambda_{O_2} = 0.41$ to $\lambda_{O_2} = 0.39$.

7.5.2 Time delay margins

In the simulations the injector location has been varied in the range 0cm to 10cm from the flame. We have also used two different slot lengths for the injector, 1cm and 2mm. By slot length we mean the line section in the longitudinal direction where gas is injected. By running a large set of simulations, we identified the injector locations that stabilized the process. These are compared to the time delay margins found in the linear analysis, in Figure 7.10. For each of the four different cases, the injector locations that give a stable response is marked with a colored box. The distance from the flame is measured from the middle of the injector. The injector position is shifted 5mm between each simulation. A consequence of this is that the stable regions found might be a bit conservative.

The first thing to notice is that for injector locations very close to the flame, we were not able to stabilize SINMA. For all simulation cases we recognize a pattern with stable and unstable regions. How well they match the analysis differs between the simulation cases.

In the case where sampling time is not limiting the performance, the stable regions are wider than what we found in the analysis. The intervals are however shifted a bit to the left (closer to the flame). However, if we had based the control design on the second or third region found in the analysis, we would be able to stabilize SINMA. Two important effects not considered in the analysis, is that the injector has an extent, and that the time delay is time-varying (because the velocity in the combustion chamber is oscillating with the unstable frequency). This might be the reason for the

shift to the left.

When the sampling time is reduced to 1kHz, we are still able to stabilize the process. However, the time delay margins are reduced significantly. The regions for stable injector locations are shifted even more to the left. We believe that this is mostly a sampling phenomenon. The effect of a sample hold element can be approximated with a time delay of half the sampling time. In this case, this adds a time delay of about 0.5ms to the system. With this sampling rate we can only change injection about three times during a cycle, and cannot expect the controller to perform that well.

Although the response is stable in the regions marked in Figure 7.10, the controller performance is better in the middle of the intervals. For these injector locations, the pressure amplitude decays faster and the final amplitude is smaller.

7.5.3 Controller performance

In Figure 7.11 we show the controller performance for an injector located at a distance 4cm from the flame with a slot length of 1cm. The sampling time is 1kHz and the injector is limited to reduce λ_{O_2} with 0.02. Control is switched on after 0.14 seconds in the simulation. It is clear that the controller successfully reduces the amplitude of the pressure oscillations. The performance when we reduce the slot width to 2mm is shown in Figure 7.12. In this case the controller responds faster.

The frequency of the instability is 293Hz, which gives a cycle time of about 3.5ms. The mean velocity in the slot is $\bar{U} = 8.7$m/s, which means that one cycle covers about 3cm in the longitudinal direction of the combustion chamber. When we use a 1cm slot, we inject gas into about a third of a complete cycle. It seems like this is too much, and that the performance becomes better when the slot length is reduced.

In Figure 7.13 sound pressure levels are compared for the uncontrolled, 1cm and 2mm slot length case. The injector is placed 4 cm upstream of the flame, and the sound pressure level is measured based on the resulting limit cycle. Indications of the amplitude of the pressure can be seen at the end (with respect to time) of Figure 7.5, 7.11 and 7.12. The unstable frequency

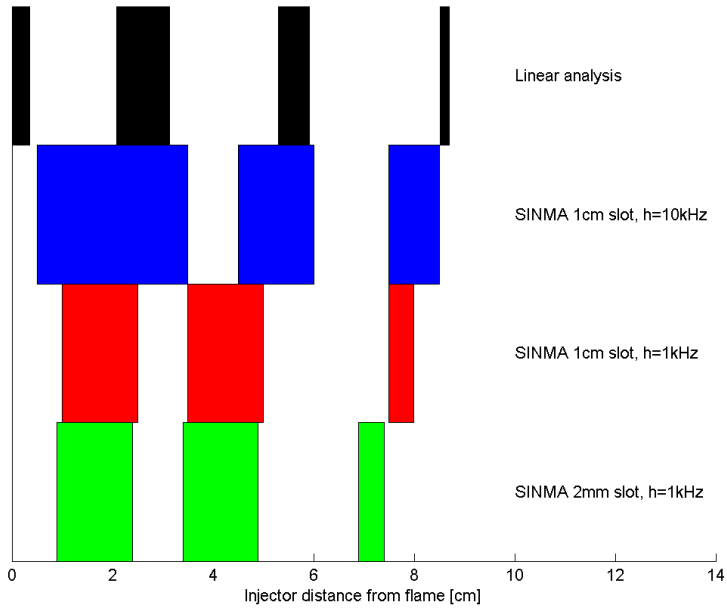

Figure 7.10: Comparison between time delay margins found from analysis on linear model and simulations in SINMA.

peak is reduced by 60 dB with a 1 cm slot, and an additional 10 dB with a 2 mm slot length. Among the experiments reported in Annaswamy and Ghoniem (2002), reductions varied between 12-50 dB. Thus, the reductions we achieved might be unrealistic, probably due to too low damping parameters in SINMA and the lack of disturbances. However, the results shows that an extra reduction of 10 dB can be achieved by using a small slot length.

In the simulations the amplitude of the unstable pressure has grown to 300 Pa. This is about the maximum amplitude we are able to stabilize. If we need to stabilize larger pressure oscillations, we must give the controller

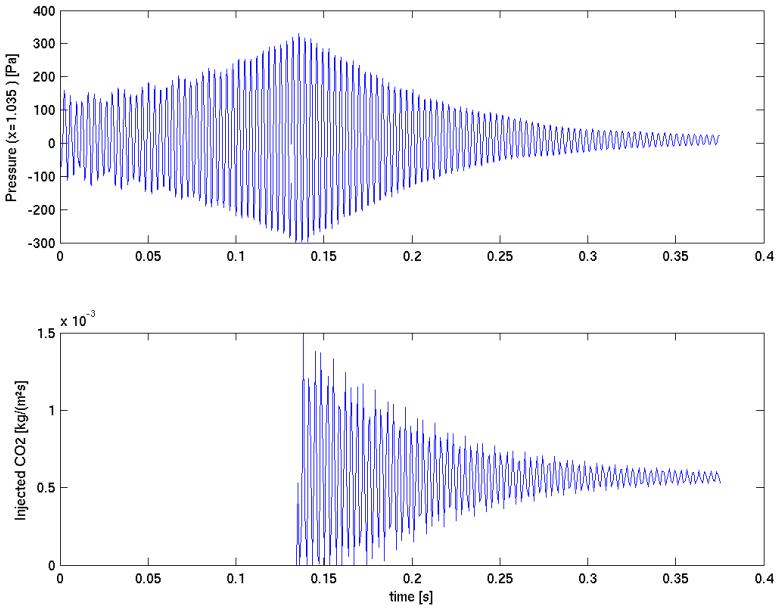

Figure 7.11: Controller performance using a secondary injector at a distance 4cm from the flame with a slot-width of 1cm.

more authority (i.e increase the capacity of the CO_2 injector).

7.6 Discussion

7.6.1 Acoustic modes

In the linear analysis we considered a model with only one acoustic mode. We have also analysed linear models containing several acoustic modes. For such models, there was only a small region of injector locations very close to the flame, for which the model could be stabilized. This is because the

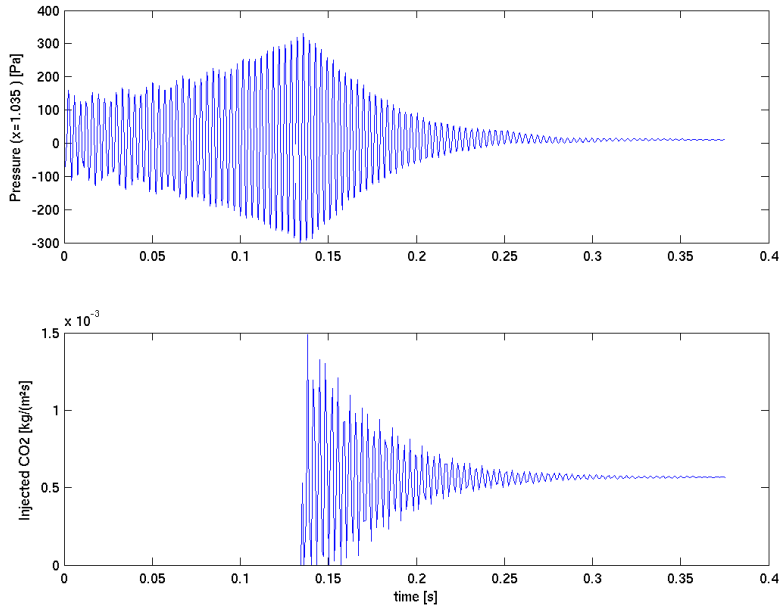

Figure 7.12: Controller performance using a secondary injector at a distance 4cm from the flame with a slot-width of 2mm.

time delay must be stable for all the frequencies contained in the model. In a real plant there exists non-linear dynamics (for instance friction and heat losses) not captured in the linear model, that will cause the process to reach a limit cycle. As the control goal is to reduce the amplitude of the pressure oscillations, such a limit cycle is acceptable as long as its amplitude is significantly lower than for the uncontrolled process. The use of a one-mode model gave results that coincided with the results found from simulations in SINMA, and it seems better to use only the unstable mode in the analysis.

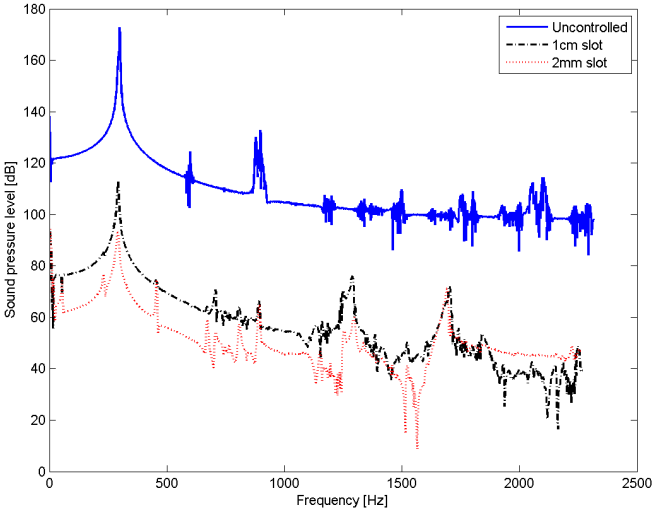

Figure 7.13: A comparison of sound pressure levels between the uncontrolled, 1cm and 2mm slot length case.

7.6.2 Control design

Based on the results herein, it is clear that control of combustion processes using pre-flame injection is a challenging task. Especially if one expects changes in the velocity of the feed (i.e the process is operated at different loads) and/or changes in the unstable frequency. The first will directly change the time delay and the latter will change the phase relation between the actuator and the flame. By fitting combustor data to a simple second order model, we are able to gain insight into how large changes in these parameters we can handle. A possible way to improve robustness toward changes in frequency and load might be to use several injectors (at different distances from the flame). As the operator of the plant should have knowledge of the load of the combustion process, and the unstable frequency is easy to measure, one should have good knowledge about the current oper-

ating conditions. One could then identify which injector that can stabilize the system under the current operating conditions and use this one. Such a control system would however be both complex and expensive.

In the simulations for this specific system, we needed a minimum sampling time of about 1kHz (slightly more than three times the unstable frequency) to be able to stabilize the system. This is somewhat larger than what is realistic with todays technology. According to Candel (2002) a direct-drive valve can modulate gaseous fuels with a bandwidth limited to about 400Hz. The unstable frequency is however dependent on the geometry of the combustion chamber, and there exists many combustion processes that can be stabilized with todays technology.

The best controller performance was achieved when injecting over a small area. How large pressure oscillations we could handle depended on how much CO_2 we could inject. It was also found that when using a realistic (lower sampling time and actuator limitations) controller, the third region had the widest time delay margins. As this will also give good mixing of the gases before burning, it seems like the best region to put the injector.

7.6.3 Robustness towards changes in the unstable frequency

In the experimental results in Ditaranto and Hals (2006), they experienced that the unstable frequency changed for perturbations in the gas-composition (see Figure 7.1). The robustness towards changes in frequency for the controller parameters used in SINMA are shown in Figure 7.9, for a single injector location. It is clear that the frequency changes in the experimental results are larger than what we can expect to handle based on the linear analysis. For the three different cases shown in Figure 7.1 they observed that the flame dynamics changed significantly. Unfortunately, the flame model used in SINMA can not capture these frequency changes, and we were not able to test if similar frequency changes would happen in the presence of control.

7.6.4 Actuator dynamics

Both in the linear analysis and in the simulations using SINMA the actuator dynamics where neglected. However, due to the high frequencies in the process, they are important. A common way to model the actuator dynamics is to add a new time constant, which will make stabilization of the process more difficult. Nevertheless, if actuator dynamics were included in both analysis and simulations, the analysis would probably still be able to predict stabilizing injector locations.

7.7 Conclusions

A frequency domain based method to identify stable time delay margins for linear time delay systems, was applied to a linear oxy-fuel combustion model. We proposed an extension to the method, making it possible to find time delay margins for perturbations in model and/or controller parameters. This procedure makes it possible to find controller parameters which have wide time delay margins, and are robust towards changes in operating conditions and modelling errors. Further, it provides useful information about where we should place the injector.

To validate the results from the linear analysis, we used a simulation study on a nonlinear CFD model of oxy-fuel combustion. A PD controller with parameters based on the linear analysis, was sufficient to stabilize the system. However, a minimum sampling rate of about 1kHz was necessary. It was found that using a small slot length for the injector improved the controller performance. When the sampling time does not limit the controller performance, it was found that the time delay margins compared well to the margins found in the analysis. However, when the controller sampling rate limits performance, the prediction of the stable time delay margins was less accurate.

Chapter 8

Conclusions and further work

In Chapter 3 we investigated control design for a proposed oxy-fuel gas turbine cycle. With an emphasis on efficiency during part load operation, different control strategies were compared. It was found that if the power plant was designed such that the pressure in the low-pressure part of the plant could vary, the plant could be operated at part load with a small loss in efficiency. In addition, because the gas turbine cycle is semiclosed, load changes could take place faster than for a conventional gas turbine cycle.

Experimental investigation of the use of air injection using microjets to stabilize a step combustor, was the topic in Chapter 4. It was found that depending on the fuel bar location, the use of microjet was either better or worse than using a air slot. The results also showed that the effectiveness of air injection is very sensitive to the amount of air injected. Using a wrong flowrate could result in either bad performance or blowout. This gives a clear motivation to investigate the use of feedback control, which would probably increase performance and robustness. Better performance can probably also be achieved if the air flowrate is modulated at a high frequency.

The last part of the thesis was concerned with thermoacoustic instabilities in oxy-fuel combustion. A linear low order model of oxy-fuel combustion was developed in Chapter 5. Control analysis on the model showed

that CO_2 injection is a promising actuator to stabilize oxy-fuel combustion processes. For the CO_2 to mix well with the reactants before burning, the CO_2 must be injected upstream of the flame. This, however, introduces a time-delay in the control loop. Chapter 6 presented a frequency domain based method, targeted at including this time-delay in the control design analysis, for a linear combustion model. Based on the method, one can find good injector locations, and controller parameters that are robust toward changes in operational conditions and modelling errors. The method was further refined in Chapter 7 to be able to automatically calculate all time-delay margin bands of interest, for perturbations in model and/or controller parameters. Further, simulations on a nonlinear CFD model of oxy-fuel combustion showed that the method is a useful tool to analyze stability and control of combustion processes. When sampling rate was not limiting the controller performance, the time delay margins found from analysis compared well to the simulation results. However, as sampling rate was not included in the linear analysis, the results were less accurate when using a practical controller implementation with low sampling rate and actuator limitations.

A natural continuation of this work is to obtain experimental results of control of oxy-fuel combustion. A test rig could be used to validate the linear model, and to confirm that CO_2-injection can be used to stabilize such a process. The experimental setup should be designed in such a way that one can investigate the impact of the time-delay, for instance by having several spots where the injector could be located. Further, one should test if a control design based on identifying the unstable frequency, the systems growth rate and gain, and analysis of the time delay, is sufficient to stabilize a real system.

The method to analyze stability and robustness of time-delay systems can be of interest for other applications. It might be possible to achieve similar results for systems with several time-delays. Also, the algorithms in the method could be improved. A better frequency search and a method that change the size of the step in system parameters, based on distance to stability margins, would increase the accuracy of the method.

Appendix A

Control issues in the design of a gas turbine cycle for CO_2 capture

This Appendix is a copy of Imsland et al. (2005), as published in Journal of Green Energy (2005). The paper contains the model used in Chapter 3.

International Journal of Green Energy, 2: 217–231, 2005

ISSN: 1543-5075 print / 1543-5083 online
DOI: 10.1081/GE-200058983

Taylor & Francis
Taylor & Francis Group

CONTROL ISSUES IN THE DESIGN OF A GAS TURBINE CYCLE FOR CO_2 CAPTURE

Lars Imsland, Dagfinn Snarheim, and Bjarne A. Foss
Department of Engineering Cybernetics, Norwegian University of Science and Technology, Trondheim, Norway

Ragnhild Ulfsnes and Olav Bolland
Department of Energy and Process Engineering, Norwegian University of Science and Technology, Trondheim, Norway

This article is concerned with control issues related to the design of a semi-closed O_2/CO_2 gas turbine cycle for CO_2 capture. Some control strategies and their interaction with the process design are discussed. One control structure is implemented on a dynamic simulation model using a predictive controller, and simulations assess the performance and compare its merits with a conventional PI structure. The results indicate that it can be advantageous for operability to allow a varying (as opposed to fixed) compressor inlet pressure, at the cost of a more expensive design. Furthermore, the results show that a predictive controller has some advantages with respect to the simpler conventional PI control structure, in particular in terms of constraint handling.

Keywords: ***CO_2 capture; Control design; Control-integrated process design; Semi-closed gas turbine cycle; Predictive control***

INTRODUCTION

Gas turbines are widely used for power production from gaseous fossil fuels. Although gas turbine engines are relatively clean burning, there is inevitably a production of CO_2 from combustion of fossil fuels. Thus, with today's increasing concern about global warming and climate change, there is an incentive to investigate gas turbine processes with CO_2 capture.

Focusing on gas turbines, it is generally acknowledged (see e.g. Bolland and Undrum (2003)) that there are three main concepts for CO_2 capture:

(a) Conventional power cycles where CO_2 is removed from the exhaust (post-combustion removal),
(b) Removal of carbon from fuel (pre-combustion removal), and
(c) Combustion with pure oxygen (instead of air), which leaves the exhaust consisting of CO_2 and water (easily condensed to obtain pure CO_2).

Received 10 October 2004, accepted 15 December 2005.
Address correspondence to Lars Imsland, Department of Engineering Cybernetics, Norwegian University of Science and Technology, 7491 Trondheim, Norway. E-mail: lars.imsland@itk.ntnu.no.

While all these concepts have their pros and cons, we will in this paper concentrate on a process based on concept c).

The process we study (described in more detail later) recycles the exhaust gas, consisting mainly of CO_2 after water is removed, as working fluid in the gas turbine. CO_2 capture is achieved since some CO_2 must be removed from the cycle to avoid accumulation. The scope of the paper is to provide a limited assessment of the operational capabilities of this gas turbine cycle. In particular, we look at the design of control strategies to achieve close-to-optimal load control operation, despite disturbances that inevitably will excite the system. Therefore, we study both a conventional approach, as well as an approach based on online optimization (often denoted predictive control).

The process is studied in e.g. Bolland and Saether (1992), Bolland and Mathieu (1998), and Ulizar and Pilidis (1997, 2000), but must still be considered to be at the design stage. Apparently, the only analysis of transient performance is reported in Ulfsnes et al. (2003). On conventional (open) gas turbine processes, there is considerably more, for instance Rowen (1983) and Ordys et al. (1994). Predictive control of conventional gas turbines is suggested in Vroemen et al. (1999) with experiments in van Essen and de Lange (2001).

The first sections of the paper provide some background as well as motivation for the integrated process design approach taken in this paper. Thereafter, the process is described, and a dynamic model is developed. The main challenges for a control system are discussed, and two different control methods are assessed. This is done by simulations of the dynamic model of the gas turbine cycle as well as its control system. A brief discussion and some conclusions end the paper.

A RATIONALE FOR INTEGRATED PROCESS DESIGN

As the focus of this paper is a process that has not been built yet, one might question why it is appropriate to look at dynamics, operability and control at this stage. We argue that for new process designs, it is advantageous to address issues related to operations at an early stage, even though this might not be usual in "traditional" sequential process design practice. The obvious reason is that an integrated process design practice—letting operational concerns have an early influence on the chosen process design—may lead to designs that are easier to operate than otherwise (van Schijndel and Pistikopoulos, 1999). The price to pay for this advantage is increased design complexity by the need to include dynamics at an early design stage.

Another (related) reason stems from the fact that power processes with CO_2 separation/capture thermodynamically has a disadvantage compared to processes without capture capabilities. A 10 percentage point efficiency loss is typical (Bolland and Undrum, 2003). Thus, to compete, it is imperative that these processes are optimized with respect to efficiency. This inevitably results in a strong focus on energy (and mass) recycle. Such designs generally lead to strong dynamic interaction between sub-processes, which typically is a challenge when it comes to operability and control. Therefore, it is important that there is a strong focus on dynamics already at early design stages, to avoid process layouts that are unnecessarily hard to operate.

To elaborate further on dynamic behavior, a power plant that delivers power to a grid needs to respond to changes in load demand in an acceptable manner, quickly and without too much overshoot. Good transient performance is more important than earlier since deregulated power markets implies more frequent power demand changes. Other

situations where dynamics come into play are startup and shutdown of a plant, and different fault conditions. The latter may include the loss of sensor signals or an error in some auxiliary system.

CONTROL DESIGN

Control design amounts to two critical choices. First, it is necessary to define the input and output signals of the controller. The inputs are mainly online measurements, e.g., a frequency signal or a fuel flow measurement in a power plant. These input signals may include variables that are controlled as well as auxiliary measurements used to infer non-measurable variables. Input signals may, however, also be generated by plant operators, for instance a request for a load change. The output signals of the controller define the value of the plant's manipulated variables such as the position of a fuel valve. Second, the control algorithm itself must be defined. In general the controller will have several input signals and several manipulated variables, thus it is a multivariable controller.

In this work we will base the choice of control inputs and outputs (manipulated variables) on inspection of the semi-closed CO_2/O_2 gas turbine cycle and on the performance specifications of the controlled cycle. The latter implies that if for instance there are limits on the turbine inlet temperature (TIT) the controller needs some input signal that is related to the TIT.

Two control design methods are applied in this work. First, we design a conventional controller using single input single output PID-controllers. Second, we apply a model predictive control strategy implying that the controller at each sampling instant solves an optimization problem to compute the output signal. This method, which has gained a high reputation in the process industries, is briefly explained in the following section.

Predictive Control

Linear MPC (Model Predictive Control) refers to an online optimization where, at each sample instant, the control is determined by optimizing future behavior as predicted by a linear process model, subject to constraints on states (or controlled variables) and manipulated variables, then applying the first part of the computed control on the process (Maciejowski, 2002).

The linear discrete-time process model used for prediction is on standard state-space form,

$$x(k+1) = Ax(k) + Bu(k) + Ed(k),$$
$$z(k) = C_z x(k) + D_z u(k) + F_z d(k)$$

where $z(k)$ are the controlled variables. A standard linear Kalman filter (Gelb, 1974) is used to estimate the state ($x(k)$) from the measured variables and the manipulated variables ($u(k)$). The $d(k)$ is a disturbance state used in the Kalman filter to compensate steady state error in the controlled variables (i.e., integral control). Symbol k denotes the discrete time index.

We assume linear constraints on states (or controlled variables), manipulated variables and rate of variation on manipulated variables,

$$G_x x(k) \le g_x, \quad G_u u(k) \le g_u, \quad G_{\Delta u}(u(k) - u(k-1)) \le g_{\Delta u}.$$

The most important constraints that are imposed here, are the upper limit on turbine inlet temperature (1598K) and the constraint on valve operation (opening between 0 and 1, stroke time 15s).

We choose to minimize a quadratic objective function of the following form, which optimizes future behavior[1],

$$V(k) = \sum_{i=1}^{H_p} \left\| \hat{z}(k+i \mid k) - r(k+i) \right\|_Q^2 + \sum_{i=0}^{H_u} \left\| \hat{u}(k+i \mid k) - \hat{u}(k+i-1 \mid k) \right\|_R^2$$

where $\hat{z}(k+i \mid k)$ and $\hat{u}(k+i \mid k)$ are predicted variables at future time $k+i$, given information at time k (with $\hat{u}(k-1 \mid k) = u(k-1)$), and $r(k)$ is the reference (desired) trajectory for the controlled variables. We use $H_p = H_u = 50$, with sample time 0.5s, which means that we predict and optimize behavior over a horizon of 25s. The quadratic objective function together with the linear process model and linear constraints, imply that the problem can be formulated as a convex quadratic program, which can be solved efficiently.

PROCESS DESCRIPTION

A sketch of the process is shown in Figure 1. In the combustion chamber, methane (CH_4) and oxygen (O_2) react at a ratio slightly above the stoichiometric ratio. Recycled gas, mainly consisting of (CO_2), is compressed and used as an inert in the combustion to

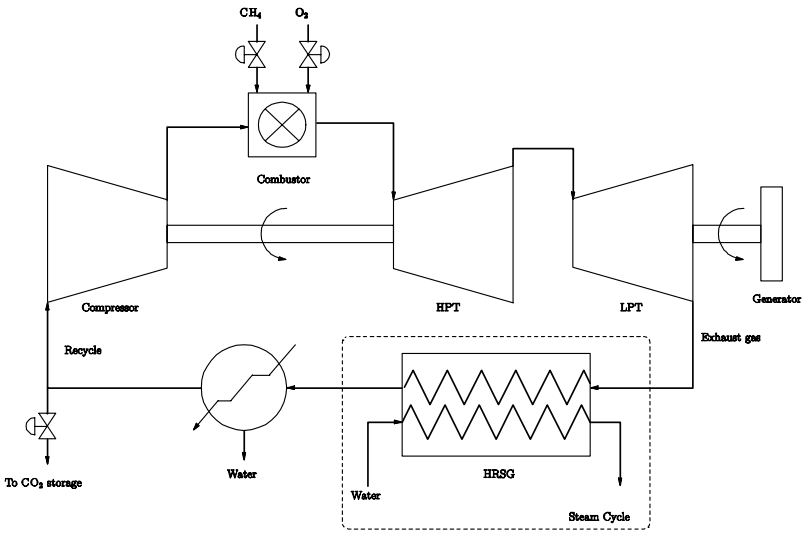

Figure 1 Semi-closed CO_2/O_2 gas turbine cycle – process layout.

[1]The norm $\|\cdot\|_H$ is defined by $\|z\|_H = \sqrt{z^T H z}$, $H > 0$.

Table 1 Typical values for some key variables.

Variable	*Symbol*	*Typical value*
LPT power output	$\dot{W}_{LPT}$	100MW
Turbine inlet temperature	TIT	1597K
Compressor mass flow	$\dot{m}_c$	173kg/s
Exhaust gas temperature	TET	1095K
Mass flow CO_2 to storage	$\dot{m}_{CO_2}$	16kg/s
Fuel mass flow	$\dot{m}_{CH_4}$	6.1kg/s
O_2 mass flow	$\dot{m}_{O_2}$	25kg/s
Compressor inlet temp.	T_{in}	290K
Compressor pressure ratio		19.3

limit temperatures in the combustion chamber and turbine inlet. The gas leaving the combustor is expanded in two turbines. The high pressure turbine (HPT) drives the compressor, while the low pressure turbine (LPT) is connected to a generator. The exhaust gas leaves the power turbine with a temperature well suited to deliver heat to a steam bottoming cycle. After the heat recovery steam generator (HRSG) the gas has to be cooled in a condenser, and condensed water is removed from the cycle. The exhaust gas, now mainly consisting of CO_2 is split into two streams; one stream is recycled to the compressor and the other stream is removed from the cycle for storage. We have tried to keep the notation standard; see also the nomenclature of Ulfsnes et al. (2003). Some typical design values for key variables are given in the Table 1.

MODELING

Choosing an Appropriate Model

In order to make decisions related to control and operability, it is crucial to have a dynamic model that represents the relevant dynamics well. It is important to be aware that these models have a different focus than the steady state models usually used for process design. The dynamic models used for developing and analyzing control structures do not need to be accurate when it comes to steady state, but needs to capture the dominant dynamic phenomena (as for instance dynamic interaction between different process parts). In the following we try to separate, conceptually, the different types of models that might be used towards commissioning of a plant:

1. Steady-state models. These are used for evaluation of "thermodynamic feasibility" and efficiency of a design, and optimization of steady state efficiency.
2. Advanced dynamic models. These are used for detailed study of the process. The complexity is high. The models may be defined by nonlinear partial differential equations.
3. Simplified dynamic models for control analysis and design. They may also be used for online purposes such as in a predictive controller.

As a side remark, an integrated process design procedure will usually imply the use of both a steady state model and a dynamic model in parallel.

The dynamic process model used in this work is based on Ulfsnes et al. (2003), and can be categorized as a simplified dynamic model, cf. the numbered list above. Some simplifications are made, mainly for computational efficiency reasons. The modeling is performed using the modeling environment gPROMS (Process Systems Enterprise Ltd., 2003). Thermodynamic properties have been determined with the physical property package Multiflash. A brief presentation of the model is given below.

Compressor

The power required for compression is equal to the increase in enthalpy,

$$\dot{W}_c = \dot{m}_c \Delta h_c$$

The increase in specific enthalpy will be calculated by assuming it being somewhat larger (given by the efficiency) than the isentropic enthalpy increase $\Delta h_{c,s}$,

$$\Delta h_c \eta_{c,s} = \Delta h_{c,s}$$

We have assumed a constant isentropic efficiency $\eta_{c,s}$.

For a given compressor, the static relation between (dimensionless) compressor speed, compressor mass flow and compressor pressure ratio is usually called the *compressor map*. The "reduced" quantities are the standard quantities used for compressors with air as the working fluid (Saravanamuttoo et al., 2001):

$$N_{red} = \frac{N}{\sqrt{T_1}}, \qquad N_{\dim} = \frac{N_{red}}{N_{red,design}} .$$

$$\dot{m}_{red} = \frac{\dot{m}_c \sqrt{T_1}}{p_1} \sqrt{\frac{R}{\gamma_1}}, \qquad \dot{m}_{\dim} = \frac{\dot{m}_{red}}{\dot{m}_{red,design}}.$$

The gas constant R is dependent on the molar weight M_c of the working fluid, $R = \bar{R}/M_c$. In our case, we will assume that the compressor map given by that dimensionless "reduced speed" $N_{\dim}$ is proportional to dimensionless "reduced mass flow" $\dot{m}_{\dim}$:

$$N_{\dim} = K \dot{m}_{\dim}$$

This corresponds to having vertical lines in the compressor map. This can be a good approximation in the normal operating range of a gas turbine cycle.

Combustion

Due to the rapid response of the combustion process, we have assumed an instantaneous mass balance, which gives the following mass flow leaving the combustion chamber,

$$\dot{m}_{out} = \dot{m}_c + \dot{m}_{CH_4} + \dot{m}_{CO_2}$$

Similarly, the energy balance is given by

$$\dot{m}_{CH_4}\Delta h_{CH_4} + \dot{m}_{O_2}\Delta h_{O_2} + \dot{m}_c\Delta h_{cc} + m_{out}\Delta h_{rx} = 0$$

where Δh_{rx} is the enthalpy of reaction, assuming all fuel reacts according to

$$CH_4 + 2O_2 \rightarrow CO_2 + 2H_2O$$

Compared to using an equilibrium reactor as in Ulfsnes et al. (2003), this is a good approximation assuming that the oxygen excess ratio

$$\lambda_{O_2} = \frac{\dot{n}_{O_2}}{2\dot{n}_{CH_4}}$$

is large enough to achieve complete combustion. Furthermore, we assume a fixed percentage pressure drop over the combustion chamber.

The fuel (CH_4) and O_2 streams enter the combustion chamber through two valves. We assume both of these are controlled with flow controllers, and we assume that a perfect ratio controller controls the inflow of O_2, such that a constant oxygen excess ratio is maintained. The reference $\dot{m}_{CH_4,ref}$ to the flow controller for the CH_4 stream is the manipulated variable for the controller to be designed. If we assume that this flow controller is well tuned, then we can write

$$\frac{d\dot{m}_{CH_4}}{dt} = \frac{1}{\tau_{CH_4}}(\dot{m}_{CH_4,ref} - \dot{m}_{CH_4})$$

where τ_{CH_4} is given by the bandwidth of the flow controller. Further, $\dot{m}_{O_2}$ is set to a fixed ratio of $\dot{m}_{CH_4}$ given by λ_{O_2} and the molar masses.

Turbine

The power generated by the high pressure turbine is

$$W_{HPT} = \dot{m}_{HPT}\Delta h_{HPT}$$

where the enthalpy drop is less than the isentropic enthalpy drop,

$$\Delta h_{HPT} = \eta_{HPT,s}\Delta h_{HPT,s}$$

given by the (assumed constant) isentropic turbine efficiency $\eta_{HPT,s}$. The same relations are used for the low pressure turbine (exchange HPT with LPT).

Moreover, we assume that both turbines can be regarded as "choked nozzles", which is used to calculate the relationship between pressure drop, temperature and mass flow (and molar weight), when these differ from the design values ("off-design calculations"). The choked nozzle equation used here is given as,

$$\tilde{p}_{in} = \tilde{\dot{m}}\sqrt{\frac{\tilde{T}_{in}}{\tilde{M}}},$$

where ~ indicates the ratio to the design value, e.g. for the molar weight, $\tilde{M} = M/M_{design}$.

Rotating Shaft

The high pressure turbine drives the compressor via a rotating shaft. Newton's second law gives

$$I\frac{d\omega}{dt} = \frac{\dot{W}_{HPT} - \dot{W}_c}{\omega}$$

where $\omega = \pi N/30$.

The low pressure turbine drives the generator via another rotating shaft. We assume that the generator delivers its power to an infinite bus, thus the rotating speed of the low pressure turbine will be fixed.

Heat Recovery Steam Generator and Condenser

In this work, we look at the heat recovery steam generator and condenser as a single counter flow heat exchanger. We do not model in any detail anything on the cold side of the heat exchanger. However, as the load of the plant varies, the amount of removed heat varies. For instance, a load increase will give a heat exchanger inlet mass flow with higher heat content. If the additional heat is not removed, then the compressor inlet temperature will inevitably increase, which will have a severe effect on the overall efficiency of the cycle. Thus, in a real plant, the steam bottoming cycle and condenser must be operated such that the changes in the compressor inlet temperature are suppressed. We have chosen to model this by letting a PI-controller decide the flow on the cold side of the heat exchanger such that the outlet temperature is kept constant. A suitable tuning of this controller represents the dynamics of the change in operating point for the steam cycle and condenser.

The heat transferred in the heat exchanger is modeled as proportional to the difference in average temperature between cold and hot side,

$$\dot{Q} = U_{wall}A_{wall}(T_{cold,avg} - T_{hot,avg})$$

where $U_{wall}A_{wall}$ is the heat transfer coefficient for the whole wall. We have used the arithmetic mean when calculating average temperature, since the (more correct) logarithmic mean proved to have a significant impact on computational performance, and because it is not important to have accurate temperatures on the cold side.

The heat exchanger will not react instantly to changes in the inflow. We thus model the "real" outlet temperature as a first order lag of the outlet temperature given from the above equation. For the hot side, this is

$$\frac{dT_{hot,out}}{dt} = \frac{1}{\tau_{HX}}\left(\frac{\dot{Q}}{\dot{m}_{hot}c_{p,hot}} + T_{hot,in} - T_{hot,out}\right)$$

and accordingly on the cold side.

In order to model pressure variations, a dynamic "overall" mass balance together with the ideal gas law is used. The outlet composition is set equal to inlet composition at all times.

Valve and Splitter

After most of the water is removed in the condenser, some of the CO_2 leaves the cycle through a valve. The flow through this valve is mainly determined by the pressure difference over the valve, using the valve equation

$$\dot{m}_{CO_2} = K_v\sqrt{\Delta p}u_v$$

where $0 \le u_v \le 1$ is the (rate constrained) valve opening, a control manipulated variable.

CONTROL STRUCTURE AND CLOSED LOOP SIMULATIONS

The control problem we consider is that of load control, i.e., operate the process so it supplies a specified load to the grid. As the process is open loop stable, the control objective is to operate the process as efficiently as possible, under varying disturbances. The major disturbances that affect the operation and are considered herein are load changes and disturbances affecting the heat transfer in the HRSG.

The first part of this section is devoted to the choice of the variables used for affecting process behavior (the manipulated variables), the variables the controller will try to influence (the controlled variables) and the variables used to get information about the state of the process (the measured variables). Thereafter, simulations show the performance of the chosen control structure, for both a simple PI controller, and a MPC controller.

Manipulated Variables

Possible manipulated variables are fuel valve, O_2 valve, CO_2 valve, compressor variable guiding vanes (VGV), and a number of variables affecting the operation of the HRSG and the condenser.

As explained above, we assume a perfect ratio controller to manipulate the O_2 valve to obtain a constant ratio of inflow of CH_4 and O_2. We also assume a well-tuned controller controlling the fuel valve, leaving us with the reference value as a manipulated variable. Furthermore, we have chosen to not include compressor VGVs. This is a limitation that will be mentioned in the Discussion.

We have not developed a detailed model of the cold side of the HRSG and the condenser, thus any manipulated variables related to these systems are not available to us. However, according to Kehlhofer et al. (1999), these are not normally used for load control in a conventional combined cycle. Thus, for the steam bottoming cycle, these manipulated variables should be used to operate the steam cycle as efficiently as possible for varying loads, removing as much heat as possible from the turbine exhaust.

This leaves us with opening of CO_2 valve and fuel inflow controller reference as manipulated variables (u) for this study.

Controlled Variables

With two manipulated variables, we can have two controlled variables. However, there are three natural selections of controlled variables.

Power: As this study considers the load control problem, the obvious controlled variable is the power output. The overall power output is the sum of the LPT power output, $\dot{W}_{LPT}$, and the steam turbine power output. Since the response in LPT power output is much faster than the steam turbine power output, we assume the LPT power output is controlled to achieve the total desired power output. In effect, this is not very different from how power control for the overall plant would work.

Temperature: For the semi-closed gas turbine cycle considered alone (without the steam cycle), the efficiency is mainly decided by pressure and temperature ratios. The pressure ratio is mainly decided from the design stage, but temperatures are subject to online variations. The closed cycle Carnot efficiency is maximized by keeping the turbine inlet temperature (TIT) as high as possible (limited by turbine material temperature constraints), and keeping the compressor inlet temperature as low as possible. Combined cycle considerations clutter the picture slightly, since the efficiency of the steam cycle must also be considered. However, Ordys et al. (1994) recommends for conventional combined cycles to keep the turbine exhaust temperature (TET) as high as possible (subject to constraints on TIT) to maximize energy flow to the HRSG, and we have adopted this philosophy in this paper and choose to control TET[2]. Note that for a given load, maximizing TET is close to maximizing TIT.

Pressure: The third variable, which is natural to consider for control, is the pressure at the low pressure side. In contrast to the conventional open gas turbine cycle, the semi-closed gas turbine cycle is not dependent on atmospheric conditions. Thus, the pressure at the compressor inlet may be different from the atmospheric pressure. An important design issue is whether this pressure should be allowed to vary (and in that case, how much it can vary), as this has a major impact on the physical design of the HRSG. If it is allowed to vary, the HRSG must be built with wall thickness that can handle the allowed pressure variations. On the other hand, if this pressure is specified to remain at atmospheric pressure,

[2]Nevertheless, we would like to note that several aspects also points in favor of controlling TIT, as recommended by Kehlhofer et al. (1999).

then conventional HRSGs can be used. A varying pressure can be beneficial both from an efficiency point of view, but also for handling disturbances.

In our simulations, we have chosen to not control the pressure, and hence let the pressure "float".

For optimum part load efficiency, the optimum TET (and if pressure is controlled, the optimum pressure) may vary with load changes, but for simplicity we have chosen to keep the desired TET fixed in this study.

In summary, the controlled variables (z) will be LPT power output ($\dot{W}_{LPT}$) and turbine exhaust temperature (TET).

Measured Variables

Although the TIT imposes an important constraint, it is not possible to measure this variable, and the TIT must be inferred from other measurements. In our case, this is done through a Kalman filter, which is also needed to obtain the states for MPC prediction. We have used TET, N , $\dot{W}_{LPT}$ and the state of the steam cycle (the integral error of the PI controller controlling mass flow on cold side of HRSG) as measured variables (y) for the Kalman filter.

Closed Loop Simulations

The simulations are performed in gPROMS, while the controller calculations are done in Matlab. gPROMS communicates with Matlab via gPROMS' Foreign Process Interface. The QP-problem is solved using quadprog from the Optimization Toolbox in Matlab. At each sample instant, the measurements are transferred from gPROMS to Matlab, where an optimal control trajectory is computed, and the manipulated variables for the next sample interval are returned to gPROMS. The linear models used in the MPC (cf. the Control Design Section) were obtained from gPROMS, using the LINEARIZE-function in the full-load operating point.

The MPC closed loop trajectories are compared to trajectories from a well-tuned PI control structure (with anti-windup) where the turbine exhaust temperature is controlled by the CO_2 valve controller, while the flow of fuel controls the power output[3]. In a conventional gas turbine, the power loop would incorporate logic to avoid too high TIT, but this is not implemented here. A conventional process would also reduce mass flow by using VGV to keep high TIT/TET at part-load, but this is obtained in this process since the controller changes the total mass in the loop when operating the CO_2 valve.

A simulation of the closed loop is shown in Figures 1-3. The first disturbance (at 20s) is a change in power reference from 100MW to 80MW, and at 150s the reference returns to 100MW. At 300s, an "event" in the HRSG/condenser causes an increase in compressor inlet temperature from 290K to 310K in less than 10s. Note that both these disturbances are rather large considering how fast they happen.

We see that the PI controller obtains good control of power, at the cost of TIT constraint violations. Less deviation can be obtained by detuning the power controller. The MPC-controller obtains better control of temperature, at the cost of having a dip in power output at the last disturbance. How large this dip must be, is a matter of tuning – if a higher

[3]The reference to this controller is filtered to allow tighter control of the power subject to other disturbances.

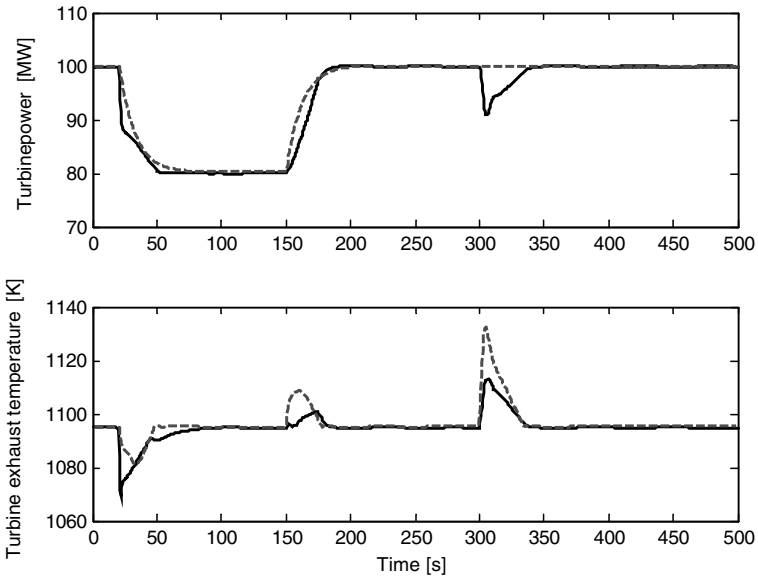

Figure 2 Controlled variables, using MPC (solid) and PI (dashed).

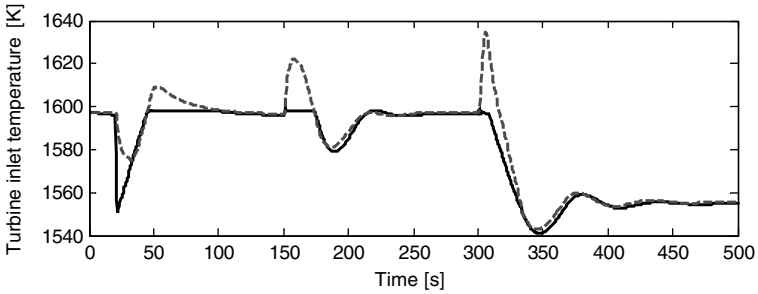

Figure 3 Turbine inlet temperature, using MPC (solid) and PI (dashed).

temperature limit is used (or the hard TIT constraint is replaced with a soft constraint), then better power control can be achieved.

DISCUSSION

Control structure: Since we have not considered compressor VGV as a manipulated variable, we have only two degrees of freedom for control. The power output has to be controlled, thus we must choose to use the second degree for controlling either temperature

or pressure[4]. In this paper we have chosen to control temperature, which means that the pressure in the cycle will float, and the process equipment must hence be designed to tolerate this. However, a varying pressure has advantages both with respect to part load efficiency and disturbance handling, for instance, the CO_2-valve can be used for varying compressor mass flow during load changes.

If the HRSG pressure is constrained to be at atmospheric pressure, then the CO_2-valve is more or less assigned to this task, and there is no degree of freedom left for varying the compressor mass flow with this variable. Therefore, in this case, the use of compressor VGV is required for good part load performance.

Thus, our results show that for this process it is possible to vary compressor massflow using the CO_2-valve, and hence if the pressure is allowed to vary, it is viable to operate the cycle at part-load without using VGV. Nevertheless, in future work, we aim at including VGV as a manipulated variable, to obtain more control flexibility as well as possibly better part-load performance.

There are also some important constraints that are not taken into account in this paper, which might to some degree necessitate including VGV:

- Compressor surge constraints (operate the compressor to avoid surge).
- Pressure constraints, especially related to the HRSG.
- Constraints related to processing (compressing) downstream the CO_2-valve.

Some of these issues are addressed in Snarheim (2004a, 2004b). In particular, Snarheim (2004b) discusses optimal part-load operation using VGVs, for both fixed and varying HRSG pressure.

Control performance trade-off: As can be suspected, there is a trade-off between good control of temperature and good power control. The PI-controller can have considerably smaller maximum turbine inlet temperature if the power controller is detuned. As we can see in Figure 4, the PI power controller actually contributes to the temperature rise after the last disturbance. For the MPC controller, we see that the fuel manipulated variable is used to keep the temperature below the limit, but we must pay with a dip in power output. If we can allow a higher temperature limit (or allow the temperature limit to be a soft constraint), this dip can be considerably reduced.

Control complexity trade-off: There is a considerable difference in complexity between the PI control structure, implemented by simple algorithms, and the MPC control structure, consisting of online mathematical programming as well as a Kalman filter. The increase in complexity is rewarded by better control, and in particular better handling of constraints. As mentioned above, the PI-controller implemented in the simulations does not take constraints (apart from the constraints on manipulated variables) into consideration. In a real implementation, the PI-controller would have to be augmented with logic to achieve this, which in practice can be a tedious procedure involving tuning and iterations. On the other hand, constraints in MPC are specified in a straightforward manner, and handled in a structured way. There is also the possibility to include “soft constraints” (constraints that may be broken), and prioritize between different constraints.

[4]Note that even if we control pressure, we must make sure that the turbine inlet temperature constraint is not violated.

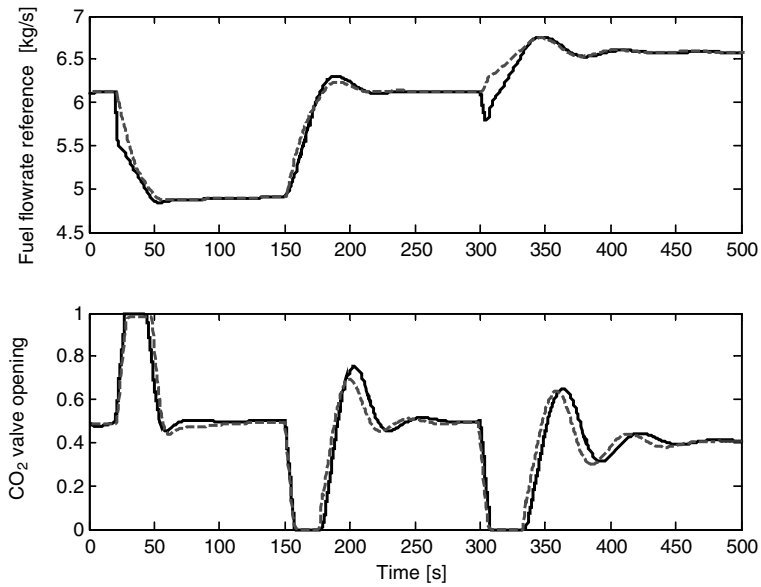

Figure 4 Manipulated variables, using MPC (solid) and PI (dashed).

CONCLUSION

In this paper we have argued that it is beneficial to integrate control issues early in design procedures. In particular, for the process considered in this paper, we claim that allowing pressure variations in the cycle allows better process control. These advantages must be weighed against the increased design complexity of a semi-closed gas turbine cycle without fixed pressure at the compressor inlet.

Furthermore, we show that using a rather complex control algorithm has several advantages, especially related to handling of process constraints. Again, these advantages must be weighed against the cost of implementation. However, as such controllers are becoming standard in other parts of industry, the cost and uncertainty of implementation of such controllers should be manageable.

ACKNOWLEDGEMENTS

The Gas Technology Center NTNU-SINTEF and NFR are acknowledged for financial support.

REFERENCES

1. Bolland, O., Mathieu, P. (1998). Comparison of Two Removal Options in Combined Cycle Power Plants. *Energy Conversion & Management* 39(16-18):1653–1663.
2. Bolland, O., Saether, S. (1992). New Concepts for Natural Gas Fired Power Plants which Simplify the Recovery of Carbon Dioxide. *Energy Conversion & Management* 33(5-8):467–475.

3. Bolland, O., Undrum, H. (2003). A novel methodology for comparing CO2 capture options for natural gas-fired combined cycle plants. *Advances in Environmental Research* 7(4):901–911.
4. Gelb, A. (1974). *Applied Optimal Estimation;* MIT Press: Cambridge, MA, USA.
5. Kehlhofer, R. H., Warner, J., Nielsen, H., Bachmann, R. (1999). *Combined-Cycle Gas Steam Turbine Power Plants*, 2nd Ed., PennWell: Tulsa, USA.
6. Maciejowski, J. M. (2002). *Predictive Control with Constraints*. Prentice Hall: Harlow, England.
7. Ordys, A. W., Pike, A. E., Johnson, M. A., Katebi, R. M., Grimble, M. J. (1994). *Modelling and Simulation of Power Generation Plants*. Springer-Verlag: London, England.
8. Process Systems Enterprise Ltd. (2003). *gPROMS Introductory User Guide*. Process Systems Enterprise Ltd, UK.
9. Rowen, W. I. (1983). Simplified mathematical representations of heavy-duty gas turbines, ASME. *J. Eng. Power* 105:865–869.
10. Saravanamuttoo, H. I. H., Rogers, G. F. C., Cohen, H. (2001). *Gas Turbine Theory*, 5th Ed., Prentice Hall: Upper Saddle River, NJ.
11. van Schijndel, J., Pistikopoulos, E.N. (1999). Towards the Integration of Process Design, Process Control, and Process Operability: Current Status and Future Trends. *In Proceedings of Foundations of Computer-Aided Process Design 99*, Breckenridge, Colorado, USA.
12. Snarheim, D. (2004a). *Modeling, simulation and control of the semiclosed O2/CO2 gas turbine cycle*. Master's thesis at Department of Engineering Cybernetics, NTNU.
13. Snarheim, D., Imsland, L, Ulfsnes, R., Bolland, O., Foss, B. A. (2005b). Control design for a gas turbine cycle with CO2 capture capabilities. Submitted to IFAC World Congress, Prague, Czech Republic.
14. Ulfsnes, R.E., Bolland, O., Jordal, K. (2003). Modelling and simulation of transient performance of the semi-closed O2/CO2 gas turbine cycle for CO2-capture. In *Proceedings of ASME TURBO EXPO 2003*, Atlanta, Georgia, USA, GT2003-38068.
15. Ulizar, I., Pilidis, P. A. (1997). Semiclosed-Cycle Gas Turbine With Carbon Dioxide-Argon as Working Fluid. *Journal of Engineering for Gas Turbines and Power* 119:612–616.
16. Ulizar, I., Pilidis, P. (2000). Handling of Semiclosed Cycle Gas Turbine With a Carbon Dioxide-Argon Working Fluid. *Journal of Engineering for Gas Turbines and Power* 122:437–441.
17. van Essen, H.A., de Lange, R. (2001). Nonlinear model predictive control experiments on a laboratory gas turbine installation. *ASME J. Eng. Gas Turbines Power* 123:347–352.
18. Vroemen, B.G., van Essen, H.A., van Steenhoven, A.A., Kok, J.J. (1999). Nonlinear model predictive control of a laboratory gas turbine installation. *ASME J. Eng. Gas Turbines Power* 121:629–634.

Bibliography

C. Abdallah, P. Dorato, J. Benites-Read, and R. Byrne. Delayed positive feedback can stabilize oscillatory systems. In *Proc of the American Control Conf.*, 1993.

N. Aimard, C. Prebende, D. Cieutat, S.M. Ivan, and T. Remi. The Integrated CO2 Pilot in the SW of France (Oxycombustion and Geological Storage): A Potential Answer to CO2 Mitigation in Bitumen Production. In *International Thermal Operations and Heavy Oil Symposium*, 2008.

M. Altay, R. Speth, D. Snarheim, D. Hudgins, A. F. Ghoniem, and A. M. Annaswamy. Impact of microjet actuation on stability of a backward-facing step combustor. *Proceedings of 45th AIAA Aerospace Sciences Meeting and Exhibit*, 2007.

A. M. Annaswamy and A. F. Ghoniem. Active control of combustion instability: Theory and practice. *IEEE Control Systems Magazine*, 22:37–54, 2002.

A.M. Annaswamy, M. Fleifil, J.P. Hathout, and A.F Ghoniem. Impact of linear coupling on the design of active controllers for the thermoacoustic instability. *Combustion, Science and Technology*, 128:131–180, 1997.

A.M. Annaswamy, O. E. Rifai, M. Fleifil, J.P. Hathout, and A.F Ghoniem. A model-based self-tuning controller for thermoacoustic instability. *Combustion, Science and Technology*, 135:213–240, 1998.

A.M. Annaswamy, M. Fleifil, J. W. Rumsey, R. Prasanth, J.P. Hathout, and A.F Ghoniem. Thermmoacoustic instability: model-based optimal control designs and experimental validation. *IEEE Trans. Control. Syst. Tech*, 8(6):905–918, 2000.

J.B. Bell, M.S. Day, J.F. Grcar, M.J. Lijewski, J.F. Driscoll, and S.A. Filatyev. Numerical simulation of a laboratory-scale turbulent slot flame. *Proceedings of the Combustion Institute*, 31(1):1299–1307, 2007.

D. Bernier, S. Ducruix, F. Lacas, and S. Candel. Transfer function measurements in a model combustor: Application to adaptive instability control. *Combustion, Science and Technology*, 175:993–1013, 2003.

G. Billoud, M. A. Galland, C. H. Huu, and S. Candel. Adaptive contol of combustion instabilities. *Combustion, Science and Technology*, 81:257–283, 1992.

O. Bolland and S. Saether. Comparison of two removal options in combined cycle power plants. *Energy Conversion and Management*, 39:1653–1663, 1998.

O. Bolland and H. Undrum. A novel methodology for comparing CO_2 capture options for natural gas-fired combined cycle plants. *Advances in Environmental Research*, 7:907–911, 2003.

M. Bryngelsson and M. Westermark. CO2 capture pilot test at a pressurized coal fired CHP plant. *Energy Procedia*, 1(1):1403–1410, 2009.

D. U. Campos-Delgado, B. B. H. Schuermanns, K. M. Zhou, C.O Paschereit, E. A. Gallestey, and A. Poncet. Thermoacoustic instabilities: modeling and control. *IEEE Trans. Control Syst. Tech.*, 11(4):429–447, 2003.

S. Candel. Combustion dynamics and control: Progress and challanges. *Proceedings of the Combustion Institute*, 29:1–28, 2002.

J. Chen. On computing the maximal delay intervals for stability of linear delay systems. *IEEE Trans. Aut. Control*, 40:1087–1093, 1995.

P.J. Cook. Demonstration and Deployment of Carbon Dioxide Capture and Storage in Australia. *Energy Procedia*, 1(1):3859–3866, 2009.

FEC Culick. Combustion Instabilities In Propulsion Systems. *Unsteady Combustion*, 306:173–241, 1996.

L.B. Davis and S.H. Black. Dry low NO_x combustion systems for GE heavy-duty gas turbines. *GE Power Systems*, 10, 2000.

P. J. Dines. *Active control of flame noise*. PhD thesis, University of Cambridge, 1983.

M. Ditaranto and J. Hals. Combustion instabilities in sudden expansion oxy-fuel flames. *Combustion and Flame*, 146:439–512, 2006.

N. Docquier and S. Candel. Combustion control and sensors: a review. *Progress In Energy And Combustion Science*, 28(2):107–150, 2002.

A. P. Dowling and A. S. Morgans. Feedback control of combustion oscillations. *Annual review of Fluid Mechanics*, 37:151–182, 2005.

S. Ducruix, T. Schuller, D. Durox, and S. Candel. Combustion Dynamics and Instabilities: Elementary Coupling and Driving Mechanisms. *Journal of Propulsion and Power*, 19(5):722–734, 2003.

I.S. Ertesvåg. *Turbulent strøyming og forbrenning*. Tapir akademisk forlag, Trondheim, 2000.

S. Evesque, A. P. Dowling, and A. Annaswamy. Self-tuning regulators for combustion oscillations. In *Proc. R. Soc. Lond. A*, 2003.

M. Fleifil, A.M. Annaswamy, Z.A. Ghoniem, and A.F. Ghoniem. Response of a laminar premixed flame to flow oscillations: A kinematic model and thermoacoustic instability results. *Combustion and Flame*, 106:487–510, 1996.

M. Fleifil, J. P. Hathout A.M. Annaswamy, and A.F. Ghoniem. The origin of secondary peaks with active control of thermoacoustic instability. *Combustion, Science and Technology*, 133:227–265, 1998.

A. F. Ghoniem, S. Park, H. M. Altay, and A. M. Annaswamy. Novel hydrocarbon-flame anchoring strategies using highly reactive fuels. In *Proceedings of the 18th ONR Propulsion Meeting*, 2005a.

A.F. Ghoniem, A. Annaswamy, S. Park, and Z.C. Sobhani. Stability and emissions control using air injection and H_2 addition in premixed combustion. *Proceedings of the Combustion Institute*, 30(2):1765–1773, 2005b.

gPROMS. gPROMS Introductory User Guide. Process Systems Enterprise Ltd., January 2003.

GreenGen. Development plan. `http://www.greengen.com.cn/en/developmentplan.htm`, 2009. Accessed 22 July 2009.

K. Gu. A further refinement of discretized Lyapunov functional method for the stability of time-delay systems. *International Journal of Control*, 74 (10):967–976, 2001.

K. Gu and S.I. Niculescu. Survey on Recent Results in the Stability and Control of Time-Delay Systems. *Journal of Dynamic Systems, Measurement, and Control*, 125:158, 2003.

J. P. Hathout, M. Fleifil, A. M. Annaswamy, and A. F. Ghoniem. Active control using fuel-injection of time-delay induced combustion instability. *AIAA Journal of Propulsion and Power*, 18:390–399, 2002.

J.P. Hathout, A.M. Annaswamy, and A.F Ghoniem. Modeling and control of combustion instability using fuel injection. In *Meeting on Active Control Technology*, 2000.

N. E. L. Haugen, Ø. Langørgen, and S. Sannan. Non-linear simulations of combustion instabilities with a quasi-1d Navier-Stokes code. *Submitted to Journal of Sound and Vibration*, 2009.

Y. He, Q.G. Wang, C. Lin, and M. Wu. Delay-range-dependent stability for systems with time-varying delay. *Automatica*, 43(2):371–376, 2007.

R. A. Horn and C. R. Johnson. *Matrix Analysis*. Cambridge University Press, Cambride, UK, 1985.

IEA. *International energy agency, key world statistics*. Stedia Media, France, 2007a.

IEA. *International energy agency, CO_2 emissions from fuel combustion*. Stedia Media, France, 2007b.

L. Imsland, D. Snarheim, R. Ulfsnes, O. Bolland, and B. A. Foss. Modeling and control of a O2/CO2 gas turbine cycle for CO2 capture. *Proceedings of DYCOPS 2004*, 2004.

L. Imsland, D. Snarheim, B. A. Foss, R. Ulfsnes, and O. Bolland. Control issues in the design of a gas turbine cycle for CO_2 capture. *International Journal of Green Energy*, 2(2), 2005.

IPCC. *Intergovernmental Panel on Climate Change Special Report on Carbon Dioxide Capture and Storage*. Cambridge univerity press, Cambridge, UK, 2005.

Y Jia and K Hideki. Improved LMI representations for delayindependent and delay-dependent stability conditions. *Journal of Control Theory and Applications*, 1:70–76, 2003.

Y. Kaya. The role of CO_2 removal and disposal. *Energy conversion and management*, 36:375–380, 1995.

R. Kehlhofer, J. Warner, H. Nielsen, and R. Bachmann. *Combined-Cycle Gas and Steam Turbine Plants*. PennWell Publishing Company, 2nd edition, 1999.

A. Kemal and C. Bowman. Real time adaptive feedback control of combustion instability. In *26th. Symp. Int. Combust*, 1996.

F. Kozak, F. Petig, R. Morris, E.and Rhudy, and D Thimsen. Chilled ammonia process for CO2 capture. *Energy Procedia*, 1(1):1419–1426, 2009.

M. Krstic, A. Krupadanam, and C. Jacobsen. Self-tuning control of a nonlinear model of combustion instabilities. *IEEE Trans. Control Sys. Tech*, 7(4):424–436, 1999.

P. J. Langhorne, A. P. Dowling, and N. Hooper. A practical active control system for combustion oscillations. *AIAA Journal of Propulsion and Power*, 6:324–333, 1990.

G. Lartigue, U. Meier, and C. Berat. Experimental and numerical investigation of self-excited combustion oscillations in a scaled gas turbine combustor. *Applied Thermal Engineering*, 24(11-12):1583–1592, 2004.

T. Lieuwen. Modeling Premixed Combustion-Acoustic Wave Interactions: A Review. *Journal Of Propulsion And Power*, 19(5):765–781, 2003.

T. Lieuwen, H. Torres, C. Johnson, and BT Zinn. A Mechanism of Combustion Instability in Lean Premixed Gas Turbine Combustors. *Journal of Engineering for Gas Turbines and Power*, 123:182, 2001.

GP Liu and S. Daley. Output-model-based predictive control of unstable combustion systems using neural networks. *Control Engineering Practice*, 7(5):591–600, 1999.

J: M. Maciejowski. *Predictive Control with Constraints*. Prentice Hall, 2002.

MIT. Carbon dioxide capture and storage projects database. `http://sequestration.mit.edu/tools/projects/index.html`, 2009. Accessed 22 July 2009.

A.S. Morgans and A.P Dowling. Model-based control of combustion instabilities. *Journal of Sound and Vibration*, 299:261–282, 2007.

S. Murugappan, S. Acharya, DC Allgood, S. Park, AM Annaswamy, and AF Ghoniem. Optimal control of a swirl-stabilized spray combustor using

system identification approach. *Combustion Science and Technology*, 175 (1):55–81, 2003.

H. A. Nilsen. Modelling and control of oxy-fuel combustion. Master's thesis, Norwegian university of science and technology, 2006.

AW Ordys, AW Rike, and MA Johnson. *Modelling and simulation of power generation plants*. Springer London etc, 1994.

C.O. Paschereit, P. Flohr, and E.J. Gutmark. Combustion Control by Vortex Breakdown Stabilization. *Journal of Turbomachinery*, 128:679, 2006.

Lord J.W.S Rayleigh. The explanation of certain acoustical phenomena. *Nature*, 18, 1878.

J.P. Richard. Time-delay systems: an overview of some recent advances and open problems. *Automatica*, 39(10):1667–1694, 2003.

W. I. Rowen. Simplified mathematical representations of heavy-duty gas turbines. *ASME J. Eng. Power*, 105:865–869, 1983.

S. S. Sattinger, Y. Neumeier, A. Nabi, B. T. Zinn, D. J. Amos, and D. D. Darling. Sub-scale demonstration of the active feedback control of gas-turbine combustion instabilities. *Journal for Engineering for Gas Turbines and power*, 122:262–268, 2000.

G. J. Silva, A. Datta, and S. P. Bhattacharyya. New results on the synthesis of PID controllers. *IEEE Trans. Aut. Control*, 47(2):241–252, 2002.

S. Skogestad and I. Postlethwaite. *Multivariable Feedback Control Analysis and Design*. Wiley, second edition, 2005.

GP. Smith, DM. Golden, M. Frenklach, NW. Moriarty, B. Eiteneer, M. Goldenberg, CT. Bowman, RK. Hanson, S. Song, WC. Gardiner, VV. Lissianski, and Z. Qin. GRI MECH 3.0. "`http://www.me.berkeley.edu/gri_mech/`", 2009.

D. Snarheim. Modeling, simulation and control of the semiclosed o_2/co_2 gas turbine cycle. Master's thesis, Norwegian university of science and technology, 2004.

D. Snarheim, L. Imsland, R. Ulfsnes, O. Bolland, and B. A. Foss. Control design for a gas turbine plant with CO_2 capture capabilities. In *Proc. 16th IFAC World Congress, Prague, Czech Republic*, 2005.

D. Snarheim, L. Imsland, and B. A. Foss. Control-relevant modelling and linear analysis of instabilities in oxy-fuel combustion. In *Proc. 9th European Control Conference ECC'07*, 2007.

D. Snarheim, N. E. Haugen, L. Imsland, , and B. A. Foss. Control design and stability analysis of oxy-fuel thermoacoustic instabilities. *Submitted to IEEE Trans. Control System Technology*, 2009a.

D. Snarheim, L. Imsland, and B. A. Foss. Active control of oxy-fuel combustion using preflame CO_2-injection. In *Accepted for European Control Conference ECC'09*, 2009b.

L. Strømberg, G. Lindgren, J. Jacoby, R. Giering, M. Anheden, U. Burchhardt, H. Altmann, F. Kluger, and G.N. Stamatelopoulos. Update on Vattenfall's 30 MWth oxyfuel pilot plant in Schwarze Pumpe. *Energy Procedia*, 1(1):581–589, 2009.

J. E. Tierno and J. C. Doyle. Multi mode active stabilization of a rijke tube. In *ASME Winter Annual Meet.: Active Control of Noise and Vib.*, 1992.

S. R. Turns. *An Introduction to Combustion, Concepts and Applications.* McGraw-Hill, Singapore, 2000.

J.H. Uhm and S. Acharya. Role of low-bandwidth open-loop control of combustion instability using a high-momentum air jet - mechanistic details. *Combustion and Flame*, 147(1-2):22–31, 2006.

R. E. Ulfsnes, O. Bolland, and K. Jordal. Modelling and simulation of transient performance of the semiclosed O_2/CO_2 gas turbine cycle for CO_2-capture. In *Proceedings of ASME Turbo Expo*, 2003.

I. Ulizar and P. Pilidis. A semiclosed-cycle gas turbine with carbon dioxide-argon as working fluid. *Journal of Engineering for Gas Turbines and Power*, 119:612–616, 1997.

HA Van Essen and HC De Lange. Nonlinear model predictive control experiments on a laboratory gas turbine installation. *Journal of Engineering for Gas Turbines and Power*, 123:347, 2001.

B. G. Vroemen, H. A. van Essen, A. A. van Steenhoven, and J. J. Kok. Nonlinear model predictive control of a laboratory gas turbine installation. *ASME J. Eng. Gas Turbines Power*, 121:629–634, October 1999.

B. Zinn. Pulsating combustion. *Advanced combustion methods(A 87-50643 22-25). London and Orlando, FL, Academic Press, 1986,*, pages 113–181, 1986.